LBL-28554

Lawrence Berkeley Laboratory
UNIVERSITY OF CALIFORNIA

Cell and Tissue Kinetics of the Subependymal Layer in Mouse Brain Following Heavy Charged Particle Irradiation

N.B. Manley,* J.I. Fabrikant, and E.L. Alpen
*(Ph.D. Thesis)

December 1988

Donner Laboratory
Biology & Medicine Division

Prepared for the U.S. Department of Energy under Contract Number DE-AC03-76SF00098.

LBL-28554

Cell and Tissue Kinetics of the Subependymal Layer in Mouse Brain Following Heavy Charged Particle Irradiation

Neela B. Manley,* Jacob I. Fabrikant, and Edward L. Alpen
*Ph.D. Thesis

Research Medicine and Radiation Biophysics
Lawrence Berkeley Laboratory
University of California
Berkeley, CA 94720

December 1988

This work was supported by the U.S. Department of Energy under Contract No. DE-AC03-76SF00098.

Dedications

This thesis is dedicated to my husband Bill and my son Gregory for their unconditional love and support

Acknowledgements

I would like to express my gratitude to Professor Jacob I Fabrikant for his guidance and patience throughout my stay at Berkeley and during the preparation of this thesis. I would also like to say a special thanks to Professor Ed Alpen for his encouragement and kindness all through this research and especially while preparing this thesis. Professors Timiras and Tobias provided many helpful suggestions in the writing of this document.

I would also like to thank Drs Frankel and Phillips for all their help with the irradiation procedures, their help with the computer analyses, and their sincere friendship.

Without Myrtle Foster's help at the microscope, with the experiments and with just about everything else that I did during my stay at the Donner Pavilion, I would never have made it.

I would also like to thank Kathy for her invaluable help in the preparation of this thesis, without her encouragement, I may have quit trying to befriend the computer. I would like to say a special thanks to Barbara for her friendship, her support and the use of her incredible typing skills.

Last, but not least I would like to thank my mother Nalini, my brothers Sunil and Anil, and my sisters-in-law Veronica and Rosalyn for their love and support through all my hard times. A sincere thanks to Ann, Karen, Mary, Pat and the rest of my Berkeley family for all their love and support.

Table of Contents

List of Figures

List of Tables

Abstract

The subependymal layer in the CB6F1 mouse brain is an actively proliferating cell population with a moderately high H^3-TdR labeling index (17.35%-26.35%), but a low mitotic index (0.5%-1.5%). It has a growth fraction of about 22% and a cell cycle time of about 37-39 hr. Analyses of the cell and tissue kinetics of this layer using high resolution autoradiography indicates: (1) this layer consists of 3 morphologically different types of cells which are in sequential stages of proliferation, differentiation and migration; (2) the subpopulations have varying cell cycle times and phase durations; and (3) the cell populations are continually proliferating with cell loss due to migration and cell death via pyknosis. The cell population is thus maintained in a steady-state of cell renewal.

The following studies investigate the cellular response and cell population kinetics of the subependymal layer in the mouse brain exposed to heavy charged particle irradiation. Partial brain irradiation with helium (230 MeV/amu) and neon ions (425 MeV/amu) was confined to one cortex of the brain (0.25 x 1.5 cm along the sagittal axis). Both the irradiated and the unirradiated contralateral cortex showed similar disturbances of the cell and tissue kinetics in the subependymal layers. The irradiated hemisphere exhibited histological damage, whereas the unirradiated side appeared normal histologically. The decrease in the values of the labeling indices 1 week after charged particle irradiation was dose- and ion- dependent. Mitotic indices 1 week after 10 and 25 Gy helium and after 10 Gy neon were the same as those seen in the control mice.

Analysis of cell cycle kinetics 1 week after 10 Gy helium and 10 Gy neon irradiation suggests the presence of a progenitor subpopulation that is proliferating with a shorter cell cycle (possibly a stem cell population). Comparison of the responses to the different charged particle beams indicates that neon ions are more effective in producing direct cellular damage than the helium ions, but the surviving proliferating cells several divisions later continue to maintain active cell renewal. Based on the 1 week post-irradiation H^3-TdR labeling indices, a rough estimate of the RBE for neon ions is at least 2.5 when compared to helium ions.

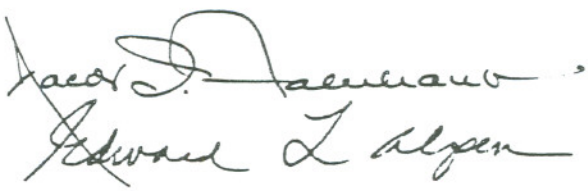

Introduction

This study concerns the cell population and cell cycle kinetics of the subependymal layer in the mouse brain, and the effects of charged particle irradiations on this cell population. Quantitative high resolution autoradiography was used to study the kinetic parameters in this cell layer. This study should help in understanding the effects of these high-energy heavy ions on normal mammalian brain tissue. The response of the mammalian brain exposure to charged particle ionizing radiation may be extremely variable. It varies from minimal physiological changes to overt tissue necrosis depending on a number of factors such as: the administered dose, dose-rate, the volume of the irradiated tissue, and the biological end-point being examined. The earlier radiation therapists believed that doses considerably higher than those normally used for the treatment of malignant tumors were needed to produce pathological damage to the central nervous system (CNS). This theory was later challenged when it was shown that the latency for radiation damage of nervous tissue is much longer than that for other organs (Lyman et al., 1983). Subsequently, interest in the mechanisms of "delayed radiation necrosis" continued with the development of clinical radiotherapy and, instances of radionecrosis in the human brain are recorded in the medical literature (O'Connel and Brunschwig, 1937; Scholtz, 1938; Pendergrass et al., 1940).

Doses up to 10 Gy have been reported to have no permanent effects on nervous tissue in animals (Haymaker, 1962; Hopewell and Wright, 1967). In

contrast, single doses of 100 Gy or more produce acute radiation necrosis (Hicks and Montgomery, 1952; Hicks et al., 1956; Vogel, 1958; Zeman, 1965). The irradiated tissue develops nonselective necrosis within hours or days of exposure. Exposure of the brain to a single dose greater than 15 Gy but less than 100 Gy causes a different phenomenon, viz., delayed radiation necrosis (Haymaker, 1961, mice; Kogel and Barendsen, 1974, rats). The delay in manifestation of the damage may be a few weeks or several months depending on the dose used, and the mammalian species studied. Delayed radionecrosis in the brain, in contrast to the acute form, displays selectivity. Damage to the blood vessels, white matter and the selective destruction of the brain stem have been observed (Bailey, 1962).

Apart from a few scattered nervous tissue cells that exhibit initial acute interphase death (Brownson, Suter and Diller, 1963) the exposed nervous tissue appears morphologically normal. Functional changes in the rat nervous system, i.e., hyperexcitability and increased nervous activity, have been shown to occur shortly after whole-body exposure to 5 Gy or less of X-rays (Rosenthal and Timiras, 1961). Changes in conditioned and learned behaviour have also been reported in rats, mice and cats with similar and lower doses of X-rays (Kimeldrof et al., 1960). These types of effects have often been reported following whole body X-irradiation. However, focal irradiation of the brain with doses below 5 Gy shows little overt functional damage in the early post-irradiation period. The delayed brain tissue damage develops and becomes manifest after a

latent period which is dependent on the dose and type of radiation.

At Lawrence Berkeley Laboratory, focal helium-ion irradiation is used for the radiosurgical treatment of deep-seated intracranial arteriovenous malformations (AVM). The dose range of 15 Gy to 45 Gy that has been used and, is delivered in 1 or 2 fractions, for these treatments is within the range in which delayed radiation necrosis has been reported. One of the advantages of helium-ion Bragg-peak irradiation is that the adjacent normal brain tissue receives only approximately 10% to 20% of the the dose to the intracranial target. This would mean that the normal brain tissue through which the plateau beam passes, usually does not receive more than 10 Gy of helium-ions and hence would be very unlikely to show much if any delayed radiation necrosis. Helium-ion irradiation is a high linear energy transfer (LET) radiation and the relative biological effectiveness (RBE) is expected to be higher than X-rays. The RBE value that is currently used for helium-ions is estimated to be approximately 1.3 in the spread Bragg peak.

The cell population hierarchy within the mammalian brain is extremely complex and quite heterogeneous. Most of the cell populations in the adult mammalian brain are either nonproliferating or proliferating very slowly. The only population in the adult mammalian brain that is known to be actively proliferating is the subependymal cell population. This layer of cells that lies just below the ependymal lining of the lateral ventricles is mitotically active and is made up of cells in various stages of their cell cycle. One of the precursor cell

populations is believed to be a stem cell population (Hubbard and Hopewell, 1980), and the other cells are presumed to be glial cell precursors.

The high rate of proliferation in this population is reflected by the rapid expression of radiation-induced damage, when this cell population is exposed to ionizing radiation. The subependymal layer, therefore, when included in the treatment volume for cancer treatments in the brain or, when in the vicinity of the treatment target for AVM's could very well be one of the normal cell populations that is affected by the ionizing radiation. Hence understanding the effects of charged particle irradiation on the subependymal cell population could prove to be of practical importance in the radiation treatment of the central nervous system.

Hopewell and Cavanagh (1972) evaluated the mitotic activity of the subependymal layer of rats at various time intervals after exposure to doses of 2, 8 , 20 and 40 Gy of X-rays. Following exposure to 20 Gy and less, the mitotic counts reached control levels by 3 months, but, after a dose of 40 Gy no recovery was seen and 6 months after irradiation mitotic counts were at zero level and the subependymal cell population was almost totally depleted. Similar observations on rats have been made on the cellularity of the subependymal layer following X-irradiation by Hubbard and Hopewell (1980).

An important question when considering the acute effects of brain irradiation on the subependymal layer is whether these effects are related to the irreversible delayed types of damage seen in the brain following irradiation. The

dose-response relationships obtained for cellular depletion in the subependymal layer following X-irradiation suggest that such a relation exists (Hopewell and Cavanagh, 1972; Chauser et al., 1977). The permanent loss of a source of new glial cells is thought to be at least contributory to the development of the specific white matter necrosis observed in rats as the delayed effects of radiation injury to the brain (Hopewell, 1980).

Little is known concerning the cellular response and the cell population kinetics of the proliferating cell populations in the mammalian brain following exposure to heavy charged particle radiation. The objectives of the research that follows are to examine in so far as possible, the cell cycle and cell population kinetics in the subependymal layer of the mouse brain in relation to the sites of cell proliferation, the size of the proliferating populations, and the duration of the components of the cell cycle. Cell population kinetic analysis is used to study the proliferating subpopulations, one of which is believed to be a stem cell population for the glial cells (Hubbard and Hopewell, 1980).

These data are then used to examine the cellular response and cell population kinetics in the subependymal cell populations after partial brain exposure to heavy charged particle radiation. The increased biological effectiveness of heavy charged particle irradiation as compared with X-rays, is examined with regard to the perturbations of the cell renewal kinetics in the subependymal layer. The dose and time-dependent cell and tissue kinetic parameters are determined during the early phases (ie., up to 1 week) of response to brain irradiation with 230

MeV/amu helium ions and 425 MeV/amu neon ions. The degree to which cell and tissue homeostasis can be maintained in this layer, and the capacity of recovery of these cells under the stress of charged particle radiation, are being studied in order to understand the underlying cellular mechanism that may lead to delayed white matter necrosis in brain. The altered patterns of cell proliferation, differentiation and migration of these glial cell precursors should help in understanding the pathogenesis of the delayed white matter necrosis. The relative biological effectiveness of neon ion vs. helium ion irradiation is examined using in vivo cell kinetic parameters in the mammalian brain. These values are important for practical application to improved treatment strategies for brain cancer and other life-threatening intracranial disorders in humans.

Chapter 1

The Subependymal Layer in the Mammalian Brain

1.0 Introduction

An essential step in the development of the human cerebral cortex is the formation of a distinct layer of an actively proliferating cell population between the ependymal and mantle layers of the forebrain in the region of the lateral ventricles. This layer is the subependymal layer (Fig. 1). This layer has been studied in humans during embryonic life (Rydberg, 1932; Kershman, 1938). The subependymal layer appears in the 14^{th} week of embryonic development, arising from the ependymal layer as a collection of undifferentiated neuroblasts and spongioblasts. The neuroblasts in this case do not have stainable neurofibrils and are sufficiently undifferentiated to be able to divide actively. The cells of the subependymal layer divide actively throughout the embryonic period. They are also capable of migration, and it is the migration of great numbers of the neuroblasts with attendant spongioblasts, outwards from this layer towards the periphery, that forms the mantle layer.

After birth, the human subependymal layer decreases in thickness, but persists in certain regions of the cortex as a thin layer of cells immediately below the ependyma. It is a distinct histological entity which seems to be found only in the part of the neural tube associated with the development of the cerebral cortex and not elsewhere in the spinal cord or the brain stem. The subepen-

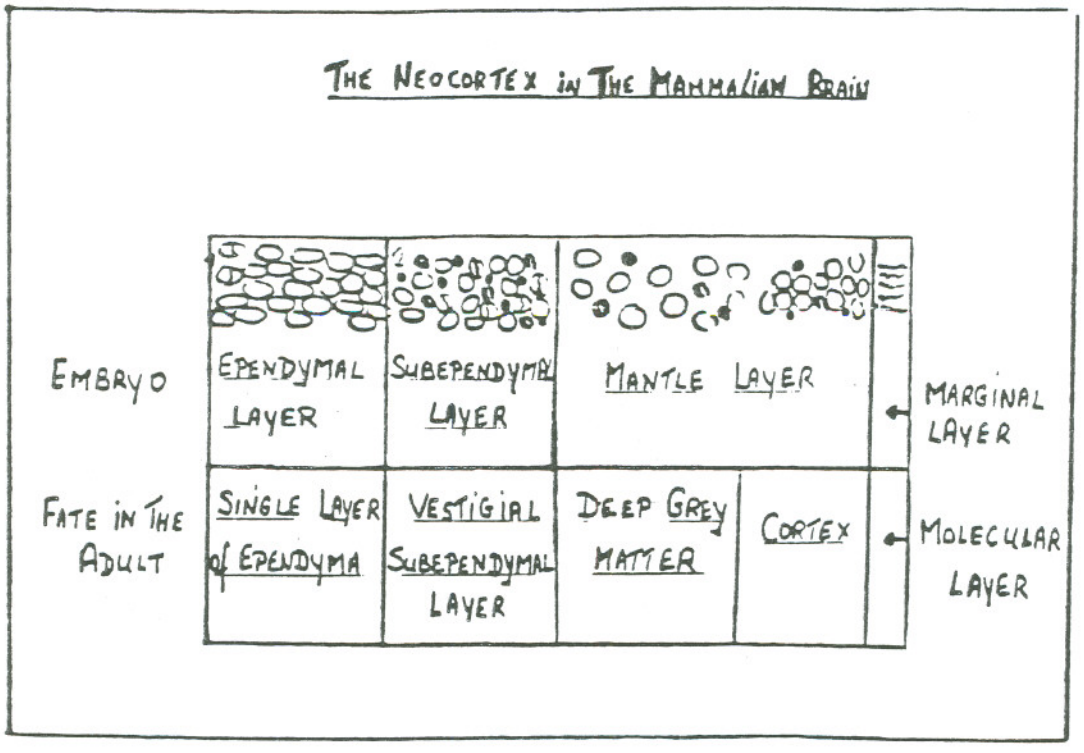

Figure.1 Histogenesis in the neocortex of the mouse brain according to Kershman (1938). The proportions of the various layers were taken from sections of 15 mm mouse embryos. The open circles represent neurons or neuron precursors and the solid black ovals depict neuroglial precursors (spongioblasts). Areas in which cell division by mitosis is known to occur are shown by cross-barring the nucleus to represent a cell in mitosis.

dymal layer is limited to those parts of the ventricles underlying the neocortex and the paleocortex and is not found in relation to the phylogenetically older archicortex or other parts of the brain stem. This layer is believed to persist indefinitely into adult life (Opalski, 1933; Globus and Kuhlenbeck, 1944). It is often referred to as the subependymal cell plate, and considered to remain a potential source of undifferentiated primitive cells which may on occasion give rise to neoplasms (Fig. 1).

A cell layer similar to the human subpendymal layer has also been described in laboratory animals such as the rat and the mouse. In the fetal, neonatal and young rat and mouse, the subependymal layer is an actively renewing cell population. The persistence of a high rate of mitotic activity even in the adult animal has made this layer an object of detailed investigation for developmental biology. The subependymal layer is now recognized as a population of undifferentiated, mitotically active progenitor cells that appears during embryonic life, and plays an important part in the production of neurons and neuroglial cells for the cerebral cortex in the embryo. The layer persists into adult life retaining its ability to produce glial cells (Smart, 1961; Hopewell, 1971).

This cell population is believed to consist of cells in various stages of proliferation, differentiation and migration. A stem cell population for the neuroglial cells has been postulated (Paterson et al., 1973; Hubbard and Hopewell, 1980). The young glial cells are believed to migrate from this layer to the cerebral cor-

tex at the level of the corpus callosum. Here they are identified as' free subependymal cells' (Paterson et al., 1973). These 'free cells' mature into light, medium and dark oligodendricytes, sucessively (Fig. 4).

Anatomical Location

In the adult mouse, the greater portion of the subependymal layer lies immediately under the ependyma of the lateral walls of the lateral ventricles (Figs. 2 and 3). It may be several cell layers thick in certain locations of the lateral ventricles. Anteriorly, it extends to the tip of the olfactory ventricle where the cells become crowded and a few cells extend medially to encircle the anterior extremity of the cavity (Fig. 2). Caudally, as the inferior horn of the ventricle is approached, the layer thins out and disappears. Towards the roof of the lateral ventrical the cells increase in number and extend laterally beyond the ventricle as a thin plate wedged between the upper surface of the caudate nucleus and the lower fibers of the corpus callosum. Extensions of this layer can be seen between the fibers of the corpus callosum and, occasional isolated groups of subependymal cells also occur in the corpus callosum. This is where the cells are believed to be migrating out of the subependymal layer, and into the cerebral cortex.

On the roof and the medial wall of the ventricle only small scattered groups of subependymal cells are seen. In certain parts of the anterior horn where the adjacent walls of the ventricles have fused together the subependymal layer still persists marking the position of the obliterated cavity. The position of the

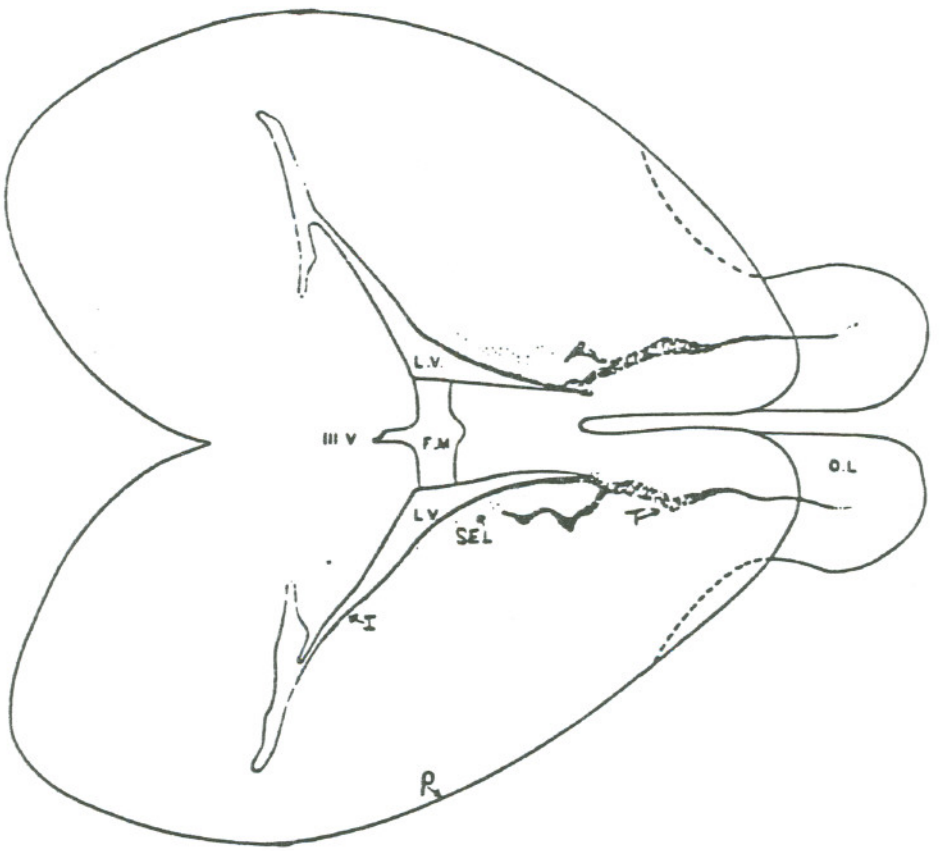

Figure.2 Plan view of the cerebral hemispheres of the adult mouse brain. The outer solid black line marks the periphery of the hemispheres (P). The inner solid black line line demarcates the lining of the ventricles (I). The stippled area represents the position of the subependymal layer (SEL). More heavily stippled areas mark where the layer is thicker (T). The largest accumulation of the subependymal layer in this view is in the frontoparietal region.

O.L.--- olfactory lobe, F.M.--- foramen of Munro, L.V.--- lateral ventricle, III V --- third ventricle.

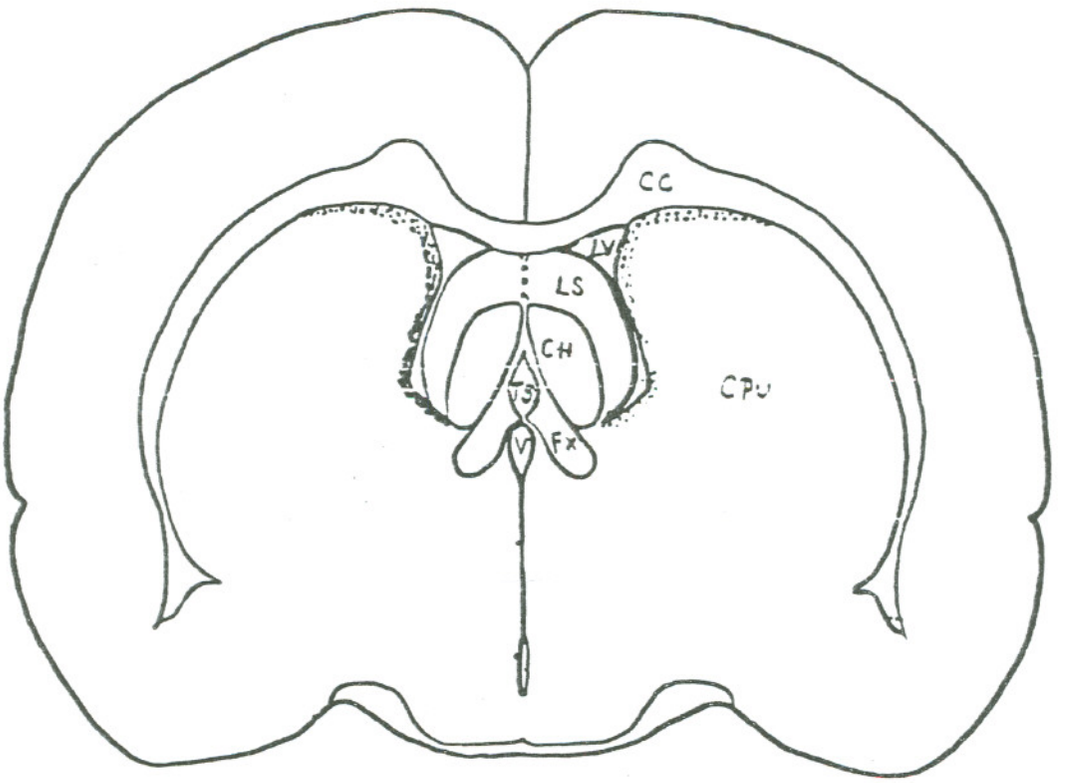

Figure.3 Coronal section at the level of the hippocampal commissure. The subepebdymal layer is seen lying under the lateral wall of the anterior horn of the lateral ventricle and extending laterally between the corpus callosum and the caudate nucleus. The stippled area represents the subependymal layer.

CC---corpus callosum, CH---hippocampal commissure, LV---lateral ventricle, FX---fornix, CPU---caudate nucleus, putamen, TS---nucleus triangularis septi, LS---lateral septal nucleus, V---third ventricle.

obliterated olfactory ventricle is also marked by a thin cord of subependymal cells. Hence, the subependymal cell population varies considerably in structure with the location in the brain. It is therefore necessary to study the layer at various locations in the brain to assess the response of these mitotically active cells to perturbing agents.

In the young mouse brain the subependymal layer is a much more prominent feature. At this stage it completely surrounds the anterior horn of the lateral ventricle and is many layers thick. In the inferior horn the subependymal cells are seen only along the lateral side of the ventricle but not on the medial side. As the mouse grows, the layer progressively diminishes and almost completely disappears from the inferior horn as well as the roof and medial wall of the anterior horn of the lateral ventricles.

Histological Characteristics

In mice the histological structure of the subependymal layer, examined in formalin-fixed tissue that is stained with hematoxylin and eosin, is characterized by three types of cells as shown in Figure 4.

The first cell type, referred to as the large light-nucleated subependymal cell (LL), has a light staining, irregularly oval or round nucleus ranging from 6-9 microns in diameter. The nuclear membrane is thin but clearly visible, with indentations and irregularly sized chromatin granules clumped against it. A small nucleolus is often seen against the nuclear membrane. The second cell type is the small light-nucleated subependymal cell (SL), it has a light staining

Figure.4 Photograph of a Hemetoxylin Eosin stained histological preparation of the subependymal layer, showing the 3 morphologically distinct types of cells in the cell populations. SD---cells with a small dark nucleus, SL---cells with a small light nucleus, LL---cells with a large light nucleus, N---neurons. (40 x magnification).

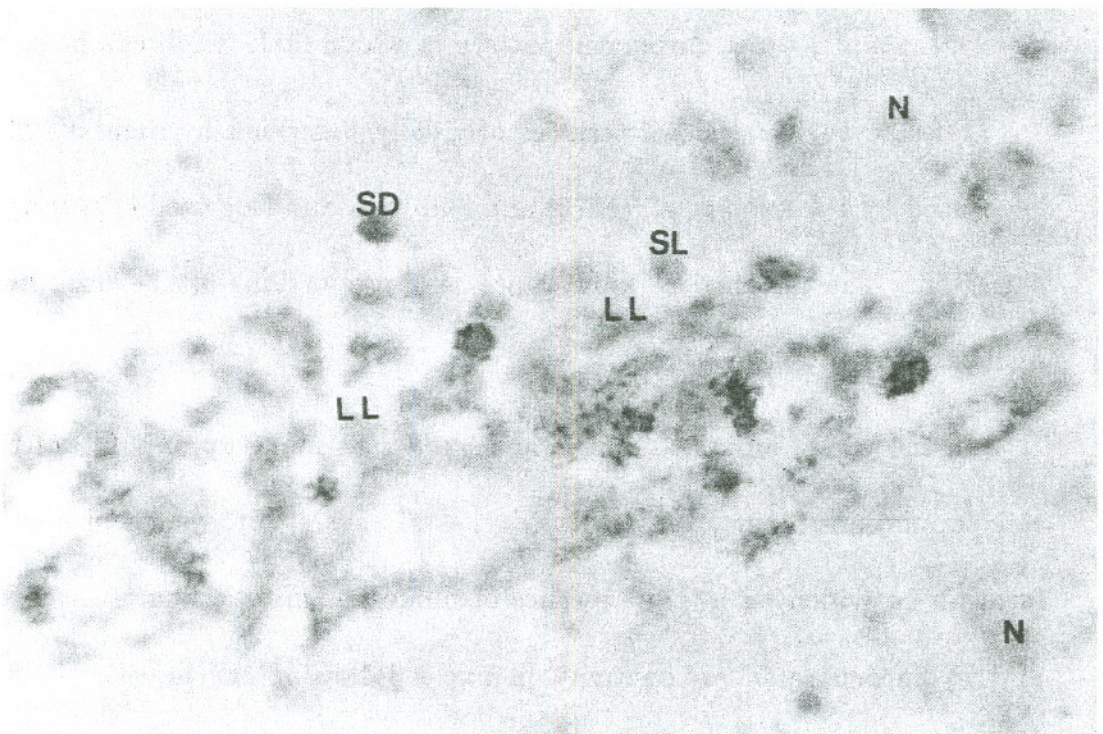

CBB 883-2532A

nucleus approximately 5 microns in diameter and is generally rounded with a granular appearance. The third type is the small dark-nucleated type and, it has a rounded nucleus approximately 4 microns in diameter with a thick nuclear membrane and a dense chromatin pattern in which little detail can be seen.

These cytological characteristics originally described by Smart (1961) have been used by Paterson et al. (1973) and Hubbard and Hopewell (1980) with little variation. The histological appearance and proportions of the dark and light nucleated cells varies with age.

In the young mouse, the light nucleated cells make up only 9% of the total cell population (Smart, 1961). Both types of cells are in a state of active proliferation as evidenced by the presence of numerous mitotic figures in both types, and by incorporated radioactivity in nuclei following the injection of tritiated thymidine (Paterson et al., 1973). At this stage the dark nuclei are irregular, almost lobed in appearance, suggesting that they are in the process of migrating away from the layer.

In the adult mouse, the proportion of light and nucleated cells rises to 46% (Smart, 1961). The mitotic activity is higher in the dark nucleated cells. Irregularity in their nuclear membrane suggests that these cells retain their ameboidism in the adult. Pyknotic nuclei are also found frequently in the subependymal layer of the adult mouse brain (Smart, 1961; Schultze and Korr, 1980). This is an indication that these cells undergo proliferation with concomitant cell loss through death.

The cells with the large light nuclei resemble the astrocyte histologically, while the cells with small dark nuclei resemble the oligodendrocyte. The histological characteristics of the subependymal layer are very similar to the various glial cells, and suggests a strong link between these two cell populations.

These descriptions have been used by Smart and Leblond (1961), Hopewell (1980) and all others who have examined the histological architecture of the subependymal layer. There is a tendency for similar cells to group together. The proportions of the various cells varies with the age of the animal. The young animal (few days old) shows fewer light nucleated cells (about 9%) as compared to the adult animal (about 49%), where the proportion of light nucleated to dark nucleated cells is about 1:1.

1.1 Cell Population Kinetics of the Subependymal Layer.*

Cell kinetic methods using labeled thymidine (TdR) and high resolution autoradiography, have been increasingly used to study the proliferative behavior of different cell types in the mammalian brain (Korr, 1980). These investigations provide quantitative histological data that cannot be obtained by histological methods alone. The site and time of cell proliferation of different kinds of cells as well as migration and differentiation of various neural cell types have been determined in this way (Schultze and Korr, 1980). Since most of the experimental studies on cell kinetics in the mammalian brain have been carried out in the

* The abbreviations used throughout this text are as follows: cell cycle time, T_c; cell cycle phases, G_1, S , G_2, M; durations of cell cycle phases, T_{G1}, T_S, T_{G2}, T_M; H^3-TdR labeling index, LI; growth fraction, GF; mitotic index, MI.

rat or the mouse, the data presented here will pertain to the parameters seen in these species. Considerable progress has been made concerning the knowledge of the cell proliferation kinetics of different cell types in the brain.

The subependymal cells proliferate actively throughout adult life in the rodent brain. This is shown by the high LI values obtained by different investigators. For the adult mouse, LI values of 19.3% (Korr, 1978, 1980), of 5% (Noetzel and Rox, 1964) or 6% (Shimada, 1966) have been reported, while in the rat, labeling indices of 16.6% (Lewis, 1968), 12.4% (Lewis, Patel and Balazs, 1977), 7.5% (Gracheva, 1969), and 2.6% (Wender et al., 1974) have been observed. The variations in the values may be due to different regions of the subependymal layer studied by the individual investigators. Mitoses are seen regularly in the subependymal layer and hence, percentage labeled mitoses (PLM) curves have been used to obtain cell cycle phase durations (Hubbard and Hopewell, 1980). These cell kinetic values in mice and rats range from: T_c = 18-21 hr, T_s = 8.5-12.3 hr, T_{G2+M} = 2-3.8 hr, T_{G1} = 4.3-7.5 hr (Lewis, 1968; Gracheva, 1969; Lewis et al., 1977). These phase durations are similar to those of the neural epithelial cells at the end of fetal development and also to those of the neuroglia and endothelial cells in the adult animal (Schultze and Korr, 1981). The Growth Fraction (GF), i.e., the proportion of cells in the cell population that is actively proliferating, estimated from the various cell kinetic parameters, varies between 0.16 and 0.4 (mice and rats).

Labeled and unlabeled pyknotic subependymal cells are seen very frequently throughout the subependymal layer; this is an indication of proliferation with concomitant cell loss. There is evidence that about 9% of the newborn subependymal cells in the mouse brain become pyknotic after mitosis (Korr, 1978a, 1980). Grain count decrements following a single injection of H^3-TdR indicate that there is continuous division of the labeled cells. Despite this continuous cell division, the number of cells in the subependymal layer does not increase with increasing age (Hopewell, 1971). It is now generally assumed that the majority of the newly-formed cells migrate out of the subependymal layer. Hubbard and Hopewell (1980) have carried out a detailed examination of the age-related changes in the numbers of both, the total, and component subpopulations of the subependymal layer in rats. These experiments provide evidence of transformation, differentiation, and cell migration in the subependymal layer. They observed a reduction in the SD nuclei and a similar rise in SL cells with no significant change in the nuclear density of the plate at 12 - 14 weeks of age, indicating that over this time period SD nuclei transform into SL nuclei. They also observed a subsequent decline in the number of SL nuclei in the subependymal layer of 14-18 week old animals, and a corresponding rise in the number of cells with LL nuclei; this suggests a further transformation of some SL nuclei into LL nuclei. Cell migration can also account for the subsequent decrease in SL and LL nuclei in the subependymal layer. Cells with LL nuclei have many characteristics of astrocytes (Smart and Leblond, 1961) and hence these nuclear

transformations could be seen as a differentiation process, which may in some cases be completed within the confines of the subependymal layer.

The implications of these observations is that the SD nucleated cells represent the proliferative or 'stem cell' population of the subependymal layer. In 14-week old rats, approximately 35% of the cells in this layer have SD nuclei. This is in close agreement with the calculated growth fraction of 30% for rats of the same age. Other investigators (Lewis, 1968; Smart and Leblond, 1961) have also suggested that SD nucleated cells are the 'stem' cells of the subependymal layer, as a result of observations on autoradiographic studies. On the basis of these findings, Hubbard and Hopewell (1980) have suggested a cell kinetic model to represent the production, differentiation, and migration of the cells of the subependymal layer of the adult rat (Fig. 5).

The "model" for the cell population kinetics of the subependymal layer is assumed to be one of a "steady-state growth" where the growth fraction (Mendelsohn, 1962) is constant but the proliferation of the cells follows an exponential pattern with a cell loss factor ϕ (Steel, 1977). Approximately 9% of the daughter cells become pyknotic (Korr, 1980), while others enter the nongrowth fraction by migrating out of the subependymal layer.

1.2 Radiation Effects on the Subependymal Layer

The high rate of cell proliferation seen in this layer permits the application of techniques of cell population kinetics for studying the early and late cell and tissue effects of radiation in the adult CNS. The role of the subependymal layer

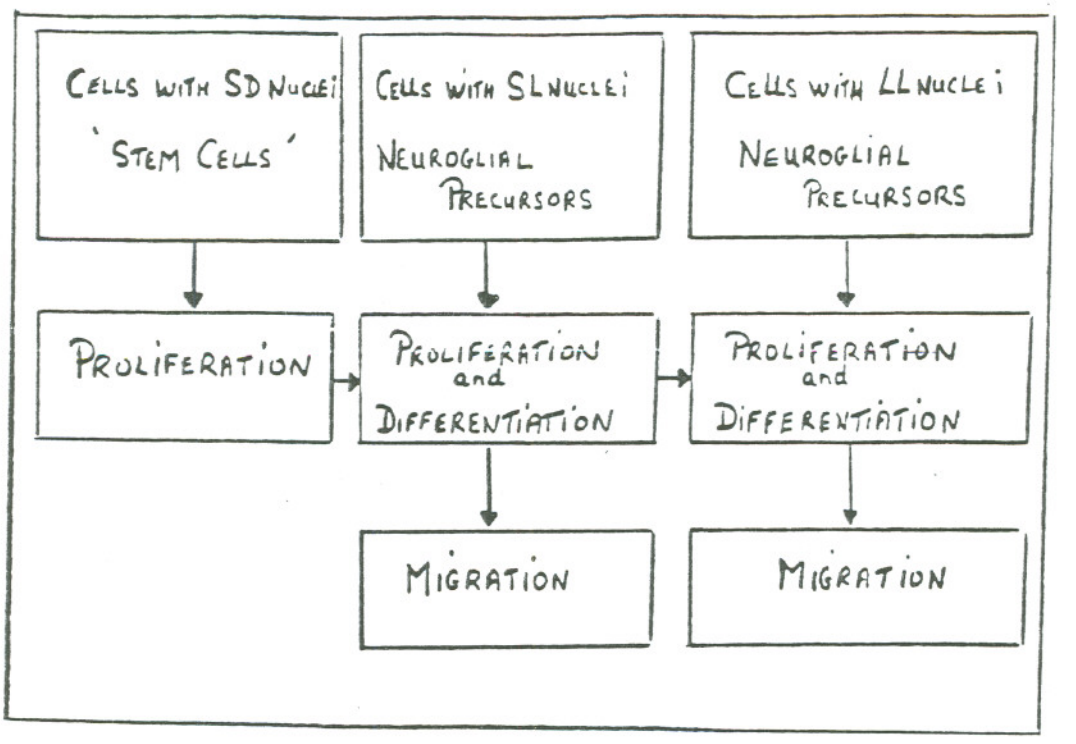

Figure.5 A schematic representation of a cell kinetic model of cell proliferation, differentiation and migration of the subependymal layer cell populations in the mammalian brain (Hubbard and Hopewell, 1980).

as the "stem cell" population for the glial cells is important when considering such cellular responses as the "delayed white matter necrosis" seen in the adult CNS following radiation. Hence, the subependymal layer is important when examining both, the "acute" as well as the "delayed" effects of radiation on the adult brain.

Acute effects of radiation on the subependymal layer cell populations.

Several quantitative histological studies have been performed to assess the effects of ionizing radiations on the cellularity of the subependymal layer. Hopewell and Cavanagh (1972) evaluated the mitotic activity in the subependymal layer of rats at various time intervals after doses of 2, 8, 20 and 40 Gy of X-rays. At 1 day after irradiation the number of mitoses was markedly reduced for all doses, followed by a rise at 7 days and again a reduction after 14 days. After doses of 20 Gy and less the mitotic counts had reached control levels by 3 months; after a dose of 40 Gy no recovery was seen and 6 months later mitotic counts were at zero level. The subependymal cell population was almost totally depleted 6 months after a dose of 40 Gy. The cell cycle time of the subependymal cells, 2 weeks after 8 Gy of X- irradiation was 22.4 hr; this was not significantly different from 22.6 hr found for control animals of the same age (Hubbard and Hopewell, 1980). The growth fraction for 14-week-old animals was 30 %. In X-irradiated animals of the same age this was found to be 16% two weeks after a dose of 8 Gy.

Hubbard and Hopewell (1980) carried out a detailed study of the cellular changes in the subpopulations of the subependymal layer following X-irradiation. In the irradiated brain of the young adult rat after a single dose of 8 Gy of 250 kVp X-rays they found the changes to be very similar to those found in other "stem cell" populations following radiation (Rubin and Casarett, 1968). When compared with the cells of the gastrointestinal crypts and bone marrow (Coggle, 1971) the time scale was greatly expanded. During the first 2 weeks after irradiation, the decline in the numbers of SD nuclei was significantly greater (approximately 20%) than the normal decline seen in age-matched control animals over this time period, this was consistent with the view that these cells represent the 'stem cell ' population of the subependymal plate. A similar decline in the mitotic activity of this layer and the lower growth fraction (16%) support the view of impaired cell proliferation after irradiation. Willis et al. (1976) report a 98% decrease in the proportion of SD nucleated cells in 6-week-old rats 24 hrs following X-irradiation of the brain with 6.5 Gy. Hubbard and Hopewell (1980) reported that the number of SL nucleated cells remained unchanged during the first 2 weeks after irradiation. This represents a decrease in the number of neuroglial precursors, since the numbers of this nuclear type had increased over the same time period in control rats. They reported no subsequent change in the numbers of LL nuclei following irradiation.

Assuming that the cell renewal in the subependymal layer does maintain the population size of the glial cells in the brain, the requirement for main-

tainence of the glial cell population should influence the proliferation rate of the SD nucleated cells. This renewal of glial cells is a gradual process and hence the depletion of the SD "stem cell" population by radiation does not result immediately in a deficit of new glial cells. However, over a period of time the smaller "stem cell" population would be unable to meet the demands for glial cells and would be stimulated into increased proliferation i.e., compensatory cell proliferation. This rise in the number of "stem cells" would be compromised by the need for partly differentiated neuroglial precursors. This was seen by Hubbard and Hopewell (1980) as a rise in the numbers of SL nuclei, 12 weeks after X-irradiation with 8 Gy. The "overshoot" in the proliferative cell compartment was seen 26 weeks after irradiation, when the SD population and the number of mitotic figures were significantly elevated as compared with the levels in age-matched controls (Hubbard and Hopewell, 1980). Should this response fail, there would be a gradual decline in the numbers of glial cells in the brain, with the inevitable development of delayed radiation injury leading to radiation necrosis. This response of the subependymal layer following a low dose of X-irradiation (8 Gy), which does not produce white matter necrosis, lasts for 39-52 weeks (Hubbard and Hopewell, 1980). The observation by Hopewell and Cavanagh (1972) that in the subependymal layer recovery occurred after 20 Gy or less of X-irradiation, but failed to do so after 40 Gy, is important for understanding the mechanism of late delayed CNS injury in general and white matter necrosis in particular.

These acute effects of X-irradiation have also been observed by other investigators. It has been observed that following irradiation, the dark-staining cells (SD cells) disappear rapidly, while the light-staining cells (SL and LL) do not (Chauser et al., 1977); this suggests that the dark-staining cells are the rapidly proliferating stem cells, while the light staining cells which are turning over more slowly are the glial precursors. These cellular responses following acute irradiation of the brain are the main effects that can be assessed at a cellular level. The important question is how they may be related, if at all, to the irreversible delayed types of damage seen following irradiation of the brain. The dose-response relationships obtained for cellular depletion in the subependymal layer suggests that such a relation exists (Hopewell and Cavanagh, 1972; Chauser et al., 1977). The permanent loss of a source of new glial cells is thought to be at least contributory to the development of the specific white matter necrosis observed as the early delayed effects of irradiation.

Importance of the subependymal layer in the development of white matter necrosis

It has been observed in the rat that for doses above 20 Gy of X-rays to the brain, the subependymal layer fails to recover and after a latent period of a few months, depending upon the dose, white matter necrosis develops (Hopewell and Cavanagh, 1972). No necrosis was observed in the brain exposed to 20 Gy or less; these brains demonstrated subsequent recovery of the subependymal layer. The sites at which white matter necrosis occurs are those to which cells of the

subependymal layer normally migrate, namely, the deeper parts of the cerebral hemispheres (Lewis, 1969). There is no cell migration to, and negligible local proliferation in, the cerebral cortex (Hopewell and Wright, 1970a; Holmes and Leblond, 1967) and this region displays little necrosis (Hopewell and Wright, 1970). These findings suggest that white matter necrosis may be a process developing independently of any vascular damage and, could occur as a result of radiation damage solely to the cell population of the subependymal layer. The reduction in the ability for extensive local neuroglial proliferation in the white matter following irradiation is also believed to be a contributory factor in developing white matter necrosis (Hopewell and Cavanagh, 1972).

The following study on the effects of helium and neon irradiation on the cell and tissue kinetics of the subependymal layer assesses quantitatively the effects of these high LET radiations as compared with the known effects of X-irradiation. The dose-response relationships of these charged particle radiations should give a measure of their effectiveness in disturbing the normal proliferation kinetics of the subependymal layer, as compared with X-rays. The effects of these charged particle irradiations on the histology of the mammalian brain have been described by various investigators. There are however, very few quantitative studies of the effects of charged particle irradiation on the mammalian brain. This study is aimed at obtaining quantitative values for the effects of charged particle radiations on the mouse brain.

Kraft et al. (1971) studied the effects of neon irradiation of the brain in pocket mice. Within 12 hours after irradiation with 10 Gy and 1 Gy they observed increased numbers of necrotic neuroglial cells, necrotic subependymal cells and necrotic microneurons of the dentate gyrus. They also observed necrotic neurons beginning about 2 weeks after exposure, with a peak incidence at 4-5 weeks and almost complete disappearance after 2 months. These histological changes have also been described by Haymaker (1969) following alpha particle irradiation of the of rat brains. Zeman (1968) reported similar changes in the mouse brain after X-irradiation and deuteron irradiations.

Chapter 2

The Kinetics of Proliferating Cell Populations

2.0 Mathematical Models

A model-based approach to the analysis of cell population kinetics is used to define and characterize the various kinetic parameters. A proliferating cell system can frequently be divided into various compartments of proliferation, maturation, and function (Fig. 6). Stem cells feed the proliferative compartment and are self-maintaining. The proliferative compartment normally amplifies the cell population through sequential divisions; cells leaving this compartment give rise to transitional or differentiated forms and ultimately enter a functional compartment or die.

The maintenance of a cell renewal system in vivo is dependent on the balance between the rate of cell production and the rate of cell loss. At the end of the intermitotic cell cycle, cells divide to produce two daughter cells. Howard and Pelc (1953) compartmentalized the intermitotic cell cycle into four phases: the pre-DNA synthesis phase (G_1); the DNA synthesis phase (S); the post-DNA synthesis phase (G_1); and the mitosis phase (M). Mammalian tissues are usually more complex, and may contain a population of potentially proliferative G_0 cells, which may divide at a very low rate or only on stimulation (Fig. 6).

The non-proliferative, G_0 phase was first defined with reference to the stem-cell compartment (Lajtha et al., 1962). They are indistinguishable

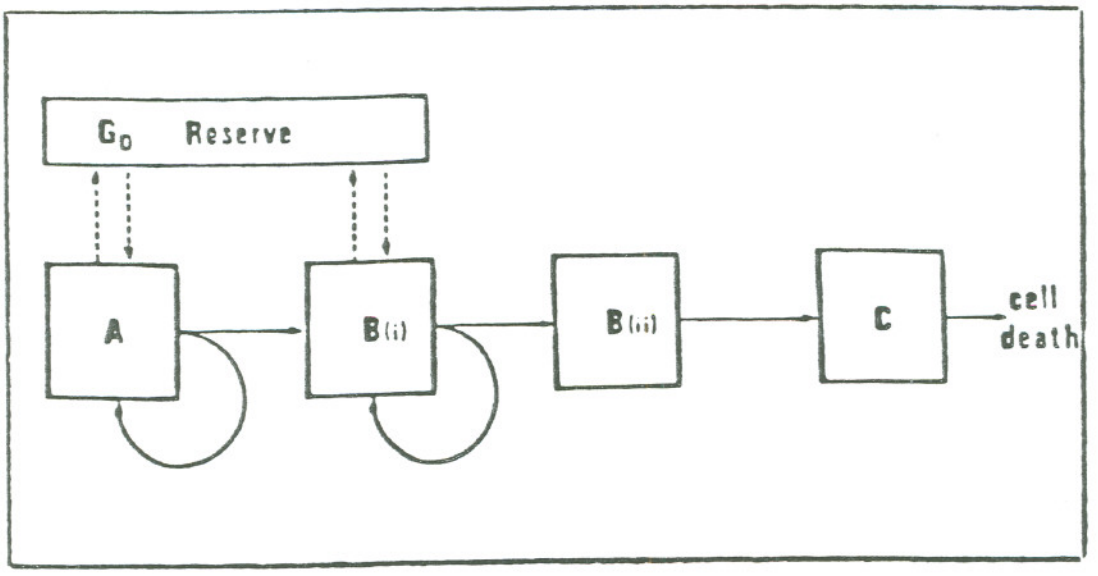

Figure.6 Four-compartment cell reneval system. A is a self-maintaining stem cell compartment; B(i) a maturation compartment which contains dividing cells; B(ii) a maturation compartment which does not contain dividing cells; C a mature functional compartment. The Go reserve consists of cells that are indistinguishable morphologically from the cells of either compartments A or B(i) but are not involved in proliferation and cell division. Compartments A and B(i) are difficult to distinguish in practice and Go has been drawn common to both. If A and B(i) are clearly distinguishable there may be a seperate Go reserve for each (Cleaver J. E., 1967). This model applies to rapidly dividing cell reneval systems, such as erythropoiesis, slowly dividing cell reneval systems, such as spermatogenesis, and conditional reneval systems, such as the regenerating liver.

morphologically from the rest of the cell population. Each proliferative compartment may contain some cells in a G_0 phase, and this arrangement has been illustrated in Fig. 6. The cells in the G_0 phase constitute a reserve of viable cells which can be induced to enter the cell cycle in the event of injury or abnormal cell loss in the renewal system. These G_0 cells may not all be permanently quiescent until required for regeneration; cells may enter and leave the cell cycle continuously and remain in G_0 for an extended but limited period of time. The G_0 cells may consequently be regarded as a fraction of the population in which one of the phases of the cell cycle (G_1 or G_2) is much longer than the rest of the cell population.

Once injury has occured to a cell renewal system, these G_0 cells can respond by commencing rapid proliferation; two types of G_0 cells have been detected on the basis of their initial response. One type corresponds to cells that enter G_0 after mitosis (resemble cells in G_1) and the initial response of these is the onset of DNA synthesis; the other type corresponds to cells which enter G_0 after DNA synthesis (resemble cells in G_2) and their initial response is to enter mitosis without prior DNA synthesis. In the mouse ear epithelium (Gelfant, 1962; Gelfant, 1963) and the gastrointestinal epithelium of the chicken (Cameron and Cleffman, 1964) both types of G_0 cells have been identified in the same tissue, although the G_0 cells resembling G_1 cells appears to be predominant in both cases. In the mouse ear epithelium the ability of cells to rest in a G_0 phase either after mitosis or after DNA synthesis appears to be genetically determined,

and if the cells rest in one phase in one cycle they rest in that phase in the succeeding cycles (Gelfant, 1963).

The formulation of a cell kinetic model helps in describing the various cell populations and their kinetic parameters. Most of the cell cycle and cell population parameters measured are statistical parameters -- averages for a large group of cells. Every cell from a kinetic point of view is an individual, with its own particular intermitotic time, durations spent in the various phases, etc., but it is seldom that such times can be measured as the average of a distribution of unknown shape, together perhaps with less precise information about its variance. When calculations are performed, either the variances are ignored and results discussed in terms of averages, or assumptions are made about the form of the parameter distributions within the population; in either case a model is being used. Steel (1977) describes exponentially growing cell populations in terms of different mathematical models and Fig. 7 summarizes the various types.

2.1 Age Structure of a Simple Exponential Population.

The simplest of models of cell populations is one in which proliferating cells all follow the same intermitotic "cycle," at the end of which they divide to produce two daughter cells. Each division thus contributes to growth, the simplest situation is where all cells are conserved and remain in the proliferative state. This cell population doubles in size every "cell cycle time" (T_c). The assumption of a uniform cell cycle time implies that the progeny of any individual cell will continue to divide synchronously at times that are multiples of the cell cycle

Model	Characteristics	Age distribution
Type A	Uniform population of proliferating cells producing two proliferating cells per division, with no cell loss	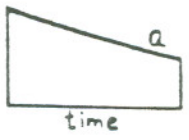
Type B	No-loss population in which at each division there is a fixed probability for the production of non-proliferating cells	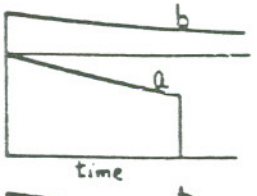
Type C	A Type B Population from which non-proliferating cells are lost at a fixed age T_L	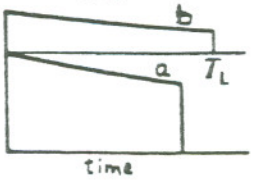
Type D	A Type B population from which cells are lost at mitosis	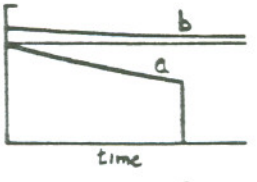
Type E	A Type B population with random cell loss from both the proliferating and non-proliferating categories.	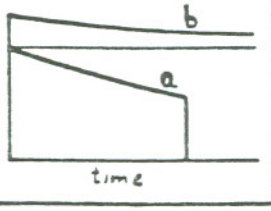

Figure.7 Five types of exponentially growing cell populations as described by Steel (1977). The age distribution for the proliferating cells is described by 'a' and the age distribution for the nonproliferating cells is described by 'b'. In the Type C population the nonproliferating cells are lost from the cell population at a fixed age T_L, this loss maybe through migration or death.

time. In Fig. 7 Type A population follows a smooth exponential growth curve with no superimposed periodicity associated with the cell cycle is said to exhibit asynchronous growth (Steel, 1977). The equation of growth of this exponential population as given by Steel (1977) is:

$$N_t = N_0 \exp(bt) \tag{2-1}$$

where N_0 is the population size at some arbitrary time zero and b is the growth constant. The growth constant in this simplified model is related only to the cell cycle time, T_c, as follows

$$b = \frac{\log_e 2}{T_c} \tag{2-2}$$

This simple form of cell population exhibits an exponential growth pattern without any cell loss; it is not found in vivo, but is used here as the simplest model for mathematical purposes. In most real cell populations a proportion of cells fail to divide. Some may be lost by death or emigration from the proliferating pool, while others may stay in a nonproliferating state. Any such loss will reduce the average number of proliferating cells produced at each cell division.

2.2 Age Structure of an Exponential Population with Growth Fraction but no Cell Loss

Using the parameters from Steel's descriptions, parameter "a" will be used for the average number of proliferating daughter cells produced at each division. The Type B cell population (Fig. 7) describes a cell population growing

exponentially without cell loss; here proliferating cells have a uniform cycle time, T_c, but in which "a" is a constant with value between 1 and 2.

Consider first the proliferating cells only. In the time span of one cell cycle (T_c) every cell will divide once only:

$$aN_0 = N_0 \exp(bT_c) \tag{2-3}$$

$$b = \frac{\log_e a}{T_c} \tag{2-4}$$

and the potential cell population doubling time (T_d) will be:

$$2N_0 = N_0 \exp(bT_d) \tag{2-5}$$

and

$$T_d = \frac{\log 2}{\log a} T_c \tag{2-6}$$

As 'a' is reduced from 2 to 1 the age distribution of the population becomes rectangular since only one proliferating cell is produced at each division and there is no growth. In this type of cell population (Type B), the assumption is that the cells which are not proliferating cells do not leave the population, but accumulate as a subpopulation of nonproliferating cells.

If there are N_0 proliferating cells present at any particular time, each dividing only once during the next cycle, then there will be

N_0 (a - 1) new proliferating cells, and

N_0 (2 - a) new nonproliferating cells after each cell division.

With time as the cell population grows, the proportion of proliferating cells will tend to the ratio:

$$\text{growth fraction} = \frac{\text{new proliferating cells}}{\text{all new cells}} = a - 1 \quad \text{(Steel,1977)} \quad (2\text{-}7)$$

This situation will arise when the growth of a Type B model population has proceeded over many generations. Throughout this time nonproliferating cells will be produced at an exponentially increasing rate and they will have a full range of cell ages -- from zero to the lifetime of the population.

The term "growth fraction" (GF) (Mendelsohn, 1960a) is used to describe the fraction of cells in a population that are regarded as proliferating. It is a useful term because many cell systems behave as though they consist of proliferating, as well as nonproliferating cells, and the proliferating cells usually have a range of ages.

2.3 Age Structure of Cell Populations that are Subject to Loss

Cell loss from biological tissues may occur by various mechanisms such as emigration, maturation, and cell death and these may differ in their dependence upon cell age. In some populations, such as the epithelium, the loss of cells is usually the end result of normal maturation. The cells leaving this cell population are the nonproliferating cells that have embarked on an irreversible process of differentiation and the cells that are lost are predominantly the oldest

nonproliferating cells in the tissue. The death of cells in mitosis, even if it may occur in tumors as a result of mitotic abnormalities, is very unlikely to be the predominant mode of natural cell loss under normal physiological conditions. More commonly, the cells may be lost at various stages of the cell cycle. If they are lost early in G_1, then they are the youngest ones in the cell population; and if they are lost in G_2 or S they may be the proliferating cells.

The different modes of cell loss will affect the age structure of the the cell population. Three simple models with cell loss described by Steel (1977) are Types C, D and E (Fig. 7).

The Type C cell population is a modification of the exponential Type B with cell loss; the cells that are lost are the oldest nonproliferating cells in the population. They are lost at a well-defined age, T_L. In this model, the cell loss does not affect the proliferating cells and they still retain the same age distribution. Hence, the growth rate remains unchanged even with cell loss from the cell population. When nonproliferating cells are suddenly removed, the population size is reduced, and if the same absolute cell production rate is maintained, then a higher growth fraction is the result. In the limiting case where T_L is very short, the growth fraction would be almost 100 percent.

This situation of a sudden removal of aging, nonproliferating cells is however not one that usually occurs in vivo. The age distributions for proliferating and nonproliferating cells are both bounded by a decaying exponential, whose exponent is b. In this Type C model, 'a' is given by:

$$a = \exp(bT_c) \qquad (2\text{-}8)$$

where $b = \log 2 / T_d$, T_c = cell cycle time and T_d = population doubling time.

The other extreme situation, where the nonproliferating cells are lost immediately after mitosis, is described in the model Type D. The age structure of this cell population is also shown in Fig. 7.

The Type E exponentially growing cell population is the model for a cell population with a random cell loss with respect to age or proliferative status. In this model the cell population is subject to random cell renewal at a constant rate, for example in a continuous suspension culture in equilibrium. This type of cell loss does not affect the age distribution of the cell population and the exponential boundaries of this type are determined by the potential doubling time (T_{pot}). Defining the growth fraction (GF) in those cell populations subject to cell loss involves determining the magnitude of the cell loss.

Potential doubling time and cell loss

Cell loss is a common feature of growing cell populations. Loss can occur in various ways under the broad headings of maturation, death and emigration. The processes of loss are often difficult to measure directly. Where loss occurs it is usually suspected either on morphological grounds or through the observation of a discrepancy between the cell production rate and the growth rate of a cell population. The term loss can be applied to the loss of cell number or to the loss of tissue volume. Here, the discussion of the dynamics of cell populations

will be considered in terms of cell numbers, and, loss consists in a cell changing or moving out of the category or compartment of cells that constitute the population.

If a cell population is known not to be acquiring cells by immigration then the rate of addition of new cells is equal to the cell birth rate. If cell loss in mitosis is assumed to be insignificant then the birth rate is equal to the mitotic rate, i.e., the rate at which cells are entering mitosis.

The relation between the mitotic rate and cell production rate is given by

$$\text{mitotic rate} = \frac{MI}{T_m} = \text{cell production rate } (K_p). \qquad (2\text{-}9)$$

The cell production rate is the rate at which a population would be expected to grow if no cell loss occurred. It is useful to derive an estimate of the time within which the cell population would be expected to double in size if there were no cell loss. Assuming that the absolute cell production rate is constant, which implies that the growth of the population occurs by the progressive accumulation of nonproliferating cells, and that the population growth curve is linear. The time required for the cell population to double is the turnover time (T_t). This is given by:

$$\text{turnover time } (T_{t)} = \frac{1}{K_p} = \frac{T_m}{MI} \qquad (2\text{-}10)$$

The turnover time depends only on the rate of cell production within a tissue.

If nonproliferating cells are not accumulated but are lost at the same rate as they are produced, then the population may be held at constant size, but with the same turnover time. Turnover time may be described as the time within which the population would produce a number of cells equal to the number originally present if the absolute cell production rate remained constant.

The alternative to the assumption of constant absolute cell production rate is, to assume that the mitotic rate keeps in constant relation to the population size, and therefore that the growth is exponential. This assumes that the new cells that are produced have the same growth fraction as the population as a whole. The potential doubling time that is characteristic of the assumed exponential growth is given by:

$$\text{Potential doubling time } (T_{pot)} = \frac{\log_e 2}{K_p} = 0.693 \frac{T_m}{MI} \qquad (2\text{-}11)$$

The term potential emphasizes the assumption of no cell loss.

The rate of cell loss from a population can be expressed in terms of cells lost per unit of time (K_L), or in terms of the cell loss factor ϕ (Steel, 1968):

$$\text{Cell loss factor } (\phi) = \frac{K_L}{K_p} \qquad (2\text{-}12)$$

where K_p is the rate constant for cell production. The cell loss factor may be calculated as:

$$\text{Cell production} - \text{Cell loss} = \text{Growth} \tag{2-13}$$

Using the above relationship for growth:

$$NK_p - N(\phi)\,K_p = \frac{dN}{dt} = bN \tag{2-14}$$

Assuming an exponential growth with a population doubling time T_d, then the growth constant b is given by:

$$b = \frac{\log_e 2}{T_d} K_p\,(1-(\phi)) \tag{2-15}$$

Since potential doubling time is defined by

$$T_{pot} = \frac{\log_e 2}{K_p} \tag{2-16}$$

the cell loss factor (ϕ) is given by

$$\phi = 1 - \frac{T_{pot}}{T_d} \tag{2-17}$$

2.3 A Steady-State Population

A proliferating population exhibiting exponential growth can be in a steady state if it does not exhibit any overall growth or regression. The process operating to remove just one cell for every mitosis could be migration, transformation, differentiation or death. The age distribution of cells that are removed can be varied depending on the process of removal. A steady state can be maintained by either an asymmetrical division, where only one proliferating daughter is

added to the population at each mitosis, or by symmetrical division that yields two proliferating daughter cells every other mitotic division. Often there is a mixture of the two processes with a large stochastic element in the selection of cells that leave the population, and the balance between the two types of divisions is maintained well enough to produce a steady state of cell renewal.

2.4 A Proliferating Population with Subpopulations

Intestinal epithelium

A proliferating cell population may be a mixed cell population where the cells are in different phases of differentiation. A good example is the intestinal epithelium. This rapidly renewing population contains a progenitor compartment and a compartment of nonproliferating mature cells with a limited life span. The kinetics of this cell population has been studied extensively and a model for the rat intestinal epithelium has been described by Cairnie, Lamerton and Steel (1965a; 1965b) (Fig. 8).

The location of cells within the tissue is described in terms of the number of cell positions, counting from the base of the crypt, the total height of the crypt being 35 cell positions. The model for this proliferating cell population assumes that at some point, D, the cells stop dividing. The decision to stop proliferating is however taken before the cells reach D; in fact, it is taken at a point D/2. Cells dividing just below D/2 will divide once more just below D, but the cells that divide just above D/2 will not start a new cycle and hence will not divide a cycle later when it reaches a point just above D. This type of model is

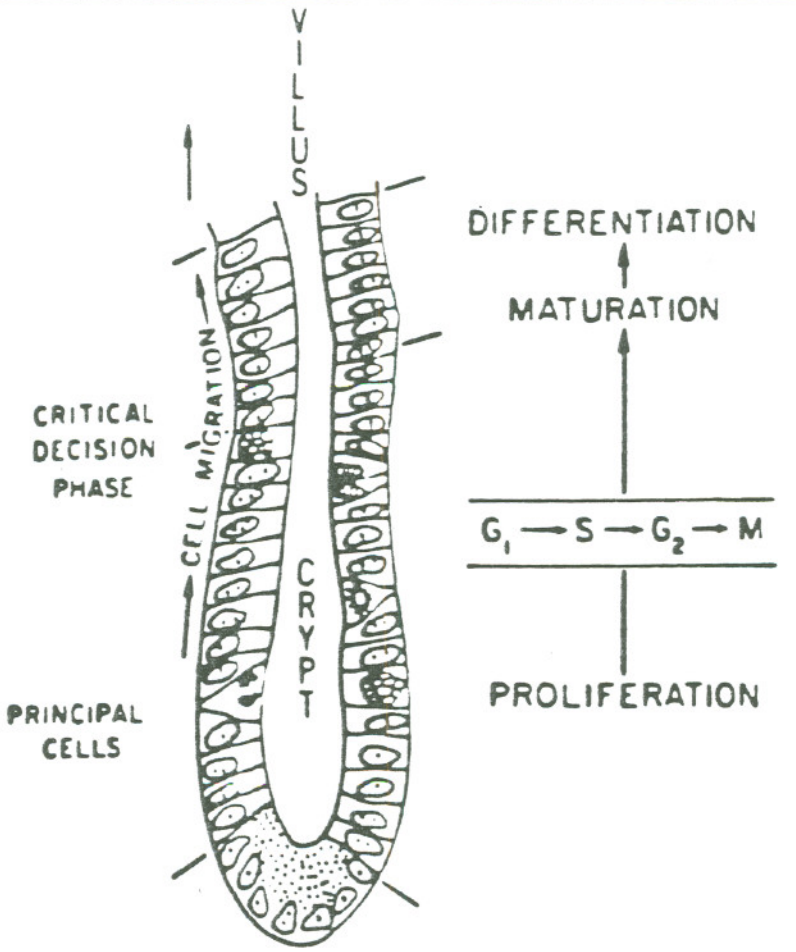

Fig.8 Intestinal epithelium. Crypt of Lieberkühn and villus represented as a cell renewal system (With permission, *Radiobiology*. Fabrikant J. I., Year Book Medical Publishers Inc., Chicago, IL,.1972.)

consistent with an abrupt fall of mitotic index at position D, but with a constant mitotic index up to this point. The thymidine labeling index (LI) falls earlier than D because above D/2 no cells are embarking on new cell cycles and hence are no longer entering the S phase.

The state of this type of cell population is best described by the age structure of cells in various parts of the model. Cells below D/2 make up an asynchronously proliferating group all destined to divide. They are lost across the boundary at D/2 with a random distribution of cell ages. The cells found between D/2 and D are of two types: proliferating cells that are not yet affected by the signal to differentiate, and nonproliferating cells that have responded to the signal. The age structure of all the proliferating cells is found by averaging the distributions for those below D/2 and for those between D/2 and D. The result is a rectangular age distribution Fig. 9(b). Thus, the proliferating cells as a whole, in a steady state cell population, have a rectangular age distribution. In reality, one cannot normally distinguish between proliferating and nonproliferating cells, and if all cells below D are taken together, they will have an exponential age structure, as shown in figure 9(a).

Subependymal cell population

Other cell populations can be examined in this manner and a similar kinetic model can be applied to study the subependymal cell population in the mouse brain. The subependymal cell population in the brain can be divided into three distinct cell types histologically: cells with a small dark nucleus (SD); cells

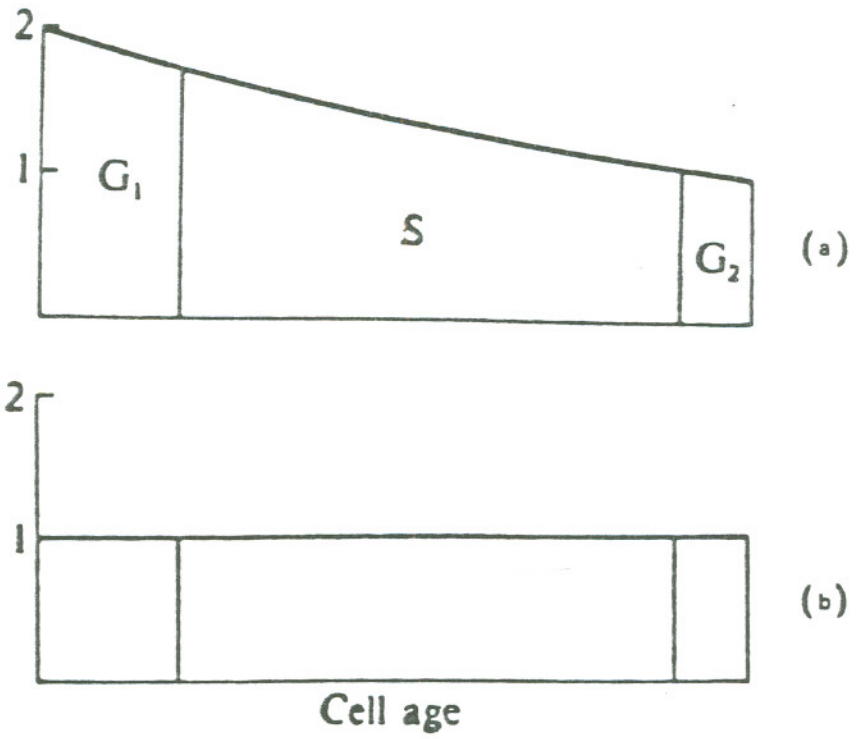

FIG.9 Age distributions for cells in different parts of a model of the intestinal epithelium (see text).

with a small light nucleus (SL); and cells with a large light nucleus (LL) (Smart, 1961; Hubbard and Hopewell, 1980). All three types of cells are proliferating cells. The SL and LL cells will differentiate into glial cells at some point in their lives, whereas the SD cells are believed to be the stem cells for this cell population. The SL and LL cell are also capable of migrating out of the subependymal layer and in doing so, will leave the growth fraction of the subependymal cell population. This cell population shows evidence of cell loss through labeled and unlabeled pyknotic cells. Labeled pyknotic nuclei do not appear immediately after administration of H^3TdR, but only after a delay of 3-4 hrs (Lewis, 1975; Korr, 1978a). This indicates that the cell loss is of two kinds: following mitosis and after a finite lifespan.

The subependymal cells continue to proliferate throughout life; yet, the number of cells in the layer does not increase (Hopewell, 1971). This indicates that the subependymal cell population must be in a steady-state cell renewal. Additional evidence derived from cell kinetic analysis indicates further that the subependymal cell population is a steady-state cell population with an exponentially proliferating compartment, cell loss, cell growth, and various subpopulations of cells.

2.5 The Kinetic Indices Used to Study the Subependymal Layer

The H^3-TdR labeling index (LI).

Tritiated thymidine (H^3-TdR) is a DNA precursor and has been used extensively in the study of cell kinetics of proliferating cell systems. It is incorporated

selectively into DNA and the label is lost only through cell death or by dilution through successive cell divisions. The thymidine labeling index (LI) is the ratio of labeled cells to all the cells in the population . In the steady state cell renewal system, the labeling index is equal, in general, to the fraction of cells that were synthesizing DNA at the time of injection. The duration of the DNA-synthesis phase (S phase) is up to ten times that of the mitotic phase, and hence the labeling index is correspondingly larger than the mitotic index and therefore more readily determined.

Tritium-labeled thymidine was first introduced into biological research by Taylor et al. (1957). The metabolism of thymidine has been very well described by Cleaver (1967). Thymidine is not a normal component of the metabolic pathway producing DNA. The formation of thymine bases takes place at the nucleotide level by the methylation of uridylic acid to thymidylic acid. This is followed by further phosphorylations to the triphosphate level before polymerization, at which time two phosphate groups are lost for each incorporated base. Most cell systems possess the enzyme thymidine kinase, which is a part of the salvage mechanism for nuclei acids. This enzyme phosphorylates exogenous thymidine to thymidylic acid, thus facilitating its entrance into the normal metabolic pathway. This pathway is well-demonstrated in Fig. 10 (Cleaver, 1967).

Detection of the labeled thymidine in the proliferating cell is usually carried out by high resolution autoradiography, where a photographic film is the detector. The longer the exposure time, the greater is the sensitivity; if exposure is

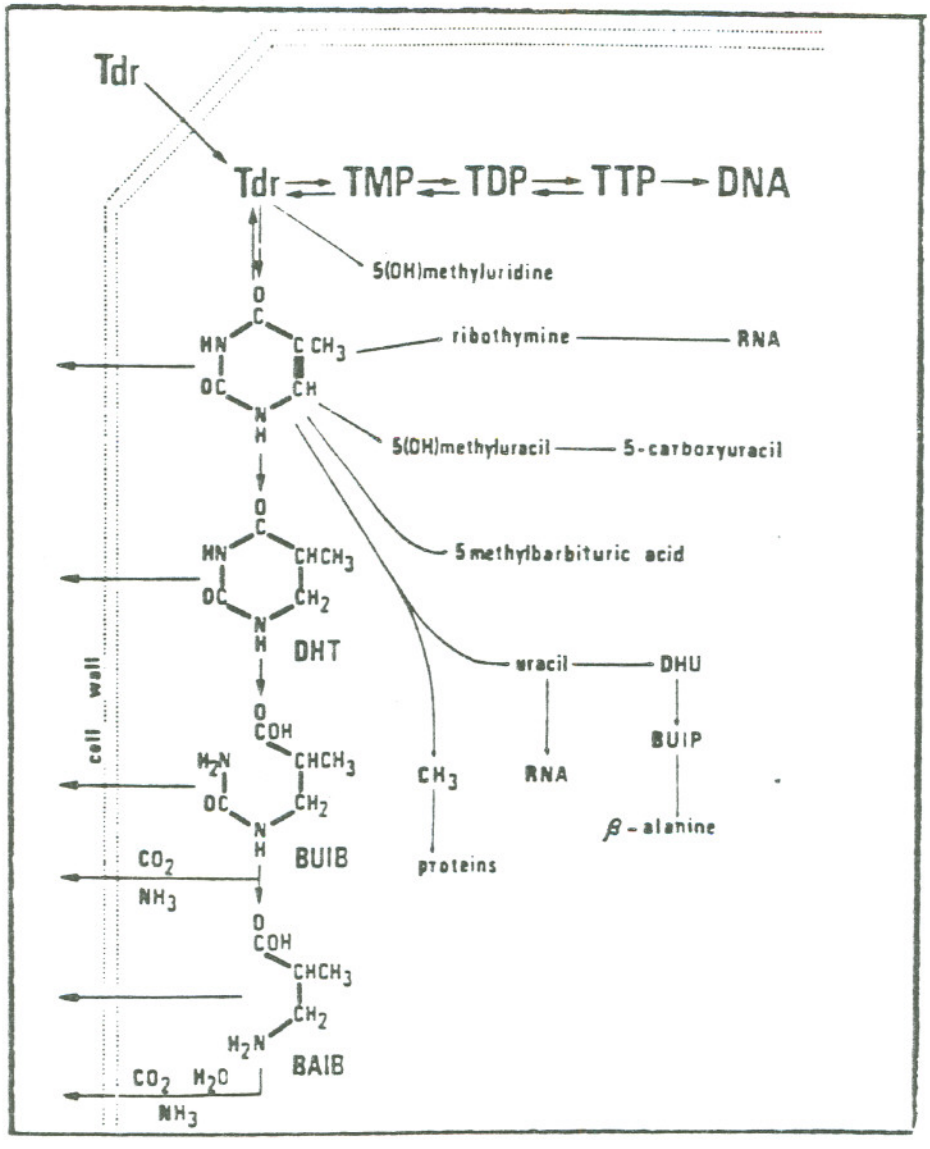

Figure.10 Pathways of incorporation and degradation of thymidine. Major degradation pathway is via reduction to dihydrothymine (DHT), B-ureidoisobutyric acid (BUIB), B-aminoisobutyric acid (BAIB), and CO , NH and H O. Minor pathways are included on the basis of at least one publication but may not be equally prevalent in all organisms (Cleaver J.E., 1967). TdR--Thymidine, TMP--Thymidine Monophosphate, TDP-- Thymidine Diphosphate, TTP-- Thymidine Triphosphate.

continued for many months, even very small amounts of radioactivity can be detected by this method (Pelc, 1964). Long exposures introduce uncertainties in the procedure, and produce such intense blackening over the cells with average to high radioactive content, that their cellular morphology is lost. Most investigators use exposure times that allow the most radioactive cells to accumulate no more than 200 grains, with an average of 30-50 grains per cell.

The effective availability of exogenous labeled thymidine after intravenous or intraperitoneal administration is limited. The rapid metabolism of thymidine in vivo is one of the contributing factors. For intravenous or intraperitoneal routes, the effective availability is 30 min or less. 60 min after systemic administration of thymidine, the radioactivity is largely divided between newly-formed DNA and labeled breakdown products. The principal labeled breakdown product in the case of tritiated thymidine is water (tritiated H_2O), which is then lost from the body with the half-life of body water (i.e., approximately one day in the mouse (Richmond et al., 1962).

The phenomenon of reutilization of the labeled DNA represents a considerable problem for the analysis of long-term experiments with labeled thymidine. Reutilization of the labeled DNA expelled into the population once the initially labeled cells begin to die, will cause a false decrease in numbers within the pool of nonproliferating cells of the cell population. This can be misleading in experiments designed to study cell loss (Steel, 1966). Another drawback to the use of labeled thymidine is the possibility that its administration disturbs the kinetic

state of the cell population being studied because of the radiation or the chemical effects.

Labeling indices can be applied to entire cell populations, or to variously defined subpopulations. The labeling index of the same cell population can vary with location within the tissue (Fabrikant, 1971). This is characteristic of the subependymal cell population in the rodent brain (Gracheva, 1969).

When the proliferating system is in a steady-state of cell renewal, and the distribution of T_c is invariant, then the number of cells in DNA synthesis in the proliferating population is proportional to the time spent in the S period. Hence:

$$\text{Labeling index (L.I)} = \frac{N_s}{N} = \frac{T_s}{T_c} \qquad (2\text{-}18)$$

where

N_s = number of labeled cells in the population (cells in DNA synthesis)

N = total number of cells in the population

T_s = time spent in DNA synthesis (S period)

T_c = cell cycle time

If T_s is known then information of T_c can be determined from the labeling index (N_s/N) and vice versa. The TdR labeling index, therefore, is a valuable parameter providing information on the growth characteristics of the tissue, viz., the sites of cell proliferation, the size of the proliferating population, and the

rates of cell proliferation.

Mean grain count decrements (MGC)

The cell cycle time (T_c) may be estimated from the decline in the mean number of grains per nucleus, as a function of time following a single injection of H^3-TdR (Alpen and Cranmore, 1959; Killmann et al., 1962; Baserga et al., 1963; Fried, 1968, 1970). Since the labeled DNA of the mother cell is distributed more or less uniformly between the two daughter cells, the grain count per nucleus is reduced roughly to half its value after each complete cell division. Initially, the first decrease is only equal to the maximum duration of G_2 +M+S. Thereafter, however, the grain count decreases by half for every complete division (T_c). Korr and his colleages have successfully used this method for determining the mean cell cycle for neuroglial cells, endothelial cells and the subependymal cells (Korr et al., 1975; Korr, 1978a). "Mean grain count" generally refers to the arithmetic mean, although other values such as the median grain count or geometric mean can also be used (Fried, 1970). To determine the cell cycle time (T_c) requires an assumption regarding the patterns of proliferation of the cells; i.e., whether the growth of these cells is exponential, steady-state or declining growth.

Grain count decrements in an exponentially growing cell population

In the case of exponential growth of the labeled cells, each labeled mother cell gives rise to two labeled daughter cells, each of which proliferates further. The mean grain count is initially reduced by a factor of 2 only after an interval

when all the labeled cells have divided ($T_{G2} + T_M + T_s$). The subsequent mitosis will reduce the mean grain count by a factor of 2 following an interval equal to the cell cycle time (T_c).

The overall decline in the mean grain count per nucleus when the growth of the labeled cells is exponential, is explained mathematically in the following equation (Korr, 1980).

$$A_n = A_o \cdot \frac{1}{2^n} \qquad (2\text{-}19)$$

where A_n is the mean grain count per nucleus after n=1, 2, 3,--- mitotic divisions, and A_o is the mean grain count per nucleus shortly after H^3-TdR injection. When the data points are plotted on a semilog arithmetic scale as a function of time after the H^3-TdR injection, a straight line drawn through the data points can be used to determine the grain-count halving time. This period can be considered only a rough estimate of T_c. A straight line assumes that the labeled cells are distributed uniformly over the cell cycle shortly after the H^3-TdR injection. Owing to the variations that exist in the length of the cell cycle phases, the above assumption will be approximately true as soon as the labeled cells have undergone several cycles, but not in the first cycle after labeling.

Grain count decrements in a cell population exibiting steady-state growth

In the model of steady-state growth, where cell birth equals cell loss, only one of the two daughter cells produced by mitosis proliferates further, while the other daughter cell is nonproliferating, but still a part of the cell population. The result is that the mean grain count per nucleus of the proliferating cells decreases with time in the manner described above. However, when the mean grain count of all labeled cells is determined, the labeling of those cells which do not proliferate further must also be taken into account. On the whole, the mean grain count (MGC) per nucleus of all labeled cells (A^*_n) will decrease after further mitoses according to the following equation (Korr, 1980).

$$A^*_n = A_o \cdot \frac{1}{n+1} \qquad (2\text{-}20)$$

where A_o is the mean grain count per nucleus immediately after labeling, and n is the number of divisions.

Here the mean grain count per nucleus of all labeled cells is reduced to half its value after the first mitosis following labeling, but is only reduced to one third of the original value after the second mitosis, instead of one quarter -- as in the case of exponential growth -- and so on. Hence a straight line through the data points plotted on a semilog arithmetic scale would give a value for T_c which overestimates the true value.

Korr (1980) has used the method of grain count halving for glial cells, which exhibit a pattern of steady-state growth. The following assumptions are made: (a) When labeled cells undergo one mitosis, their mean grain count per nucleus is reduced to half its value following cell division. (b) On the average, only one of the two daughter cells resulting from a mitosis proliferates further. The daughter cell which does not proliferate further remains a part of the cell population, and does not migrate from the proliferating population. (c) The cells proliferate with certain cell cycle parameters (T_s and $T_{G2} + M$) which have been determined independently and an assumption is made for the cell cycle time (T_c). (d) No variations occur in the durations of the cell cycle phases. This assumption is made to simplify the construction of the grain count decrement curve. The presence of cycle variations, which are quantitatively unknown has the effect of changing the step-by-step decline of the mean grain count into a continuous function. The theoretical curve obtained by using the above assumptions and that best fits matches the data points will give the approximate value for T_c.

The mitotic index (MI)

The most direct evidence of population growth is the observation of mitosis in the cells. In cell cultures, it is possible to observe and time the mitoses individually, but with in vivo cell populations, it is very often difficult to identify mitoses and indirect means are often used to study the kinetics of cell division. In a single tissue specimen, cells are often seen to be in different stages of

mitosis. It is usually assumed that these stages faithfully represent the cells that were undergoing division at the time of sampling. This is true if the cell fixation is prompt and efficient. If fixation is delayed, the proportion of observed mitotic figures frequently decreases, owing to existing mitoses going to completion, combined with the failure of premitotic cells to enter division (Fabrikant, 1965; Rajewsky, 1965; Denekamp and Kallman, 1973). If however, the fixation is prompt, then a reliable count may be made of the number of cells in mitosis. When this is expressed as a proportion of the total number of cells in the population it is called the mitotic index (MI):

$$\text{mitotic index (MI)} = \frac{\text{number of cells in mitosis}}{\text{total cells in population}} \qquad (2\text{-}21)$$

This was the earliest cell kinetic technique, and in many cell populations, the magnitude of the mitotic index is a reliable index of the rate of cell production. The limitation of the mitotic index lies in the fact that its magnitude depends not only on the rate of entry of cells into mitosis, but also on the duration of mitosis:

$$\text{mitotic index} = \text{mitotic rate} \times \text{duration of mitosis}$$

The central phases of mitosis -- metaphase and anaphase -- are the most easily recognizable. If these are all that are being counted, then a narrower "window" is being used, and the duration of the process is shorter than the full duration of mitosis. Providing the cell preparation is of high quality, cells may be recognized in early prophase and through to late telophase in many tissues

and these counts could then be a better indication of the true mitotic index; however, few tissues, such as the bone marrow, the intestinal epithelium, and the regenerating liver, can be examined with precision.

Labeled mitoses

Tritiated thymidine labeling of cells will produce labeled mitoses in cells previously synthesising DNA, and this is a very effective tool in studying the kinetics of a proliferating cell population. Counting the number of labeled mitoses following a pulse of tritiated thymidine, and then plotting them as a percentage of labeled mitoses against time will result in a oscillating curve related to the phases of the proliferating cell cycle; this is known as a Percent Labeled Mitosis Curve (PLM curve). This is a valuable technique for the study of the proliferating cell cycle of cell populations in vivo. It has been extensively used in the study of normal tissues and tumors (Quastler, 1960).

A considerable amount of theoretical work has been done on the analysis of the results so produced. The development of the method was introduced by Howard and Pelc (1953). In their work with bean-root meristems labeled with P^{32} they found bound radioactivity mainly in DNA, only in a proportion of cells within the rapidly proliferating cell population of the meristem. They also noted that initially, the mitotic figures were unlabeled and started to become labeled afted 5-10 hr of incubation in the presence of the P^{32} radioisotope (Howard and Pelc, 1953). This was evidence to them that there was a metabolic gap between the end of DNA synthesis and beginning of mitosis, and this gap

was termed the G_2 period. Their data also led them to believe that there was a metabolic gap (the G_1 period) between the end of mitosis and the beginning of DNA synthesis.

The introduction of H^3-labeled thymidine (Taylor et al., 1957) greatly simplified the recognition of cells in DNA synthesis. A number of investigators explored the timing of DNA synthesis in relation to mitosis. The technique of labeled mitosis was applied to tumors first by Mendelsohn et al. (1960). The principle of the method is explicitly illustrated Figure 11 (Steel, 1977).

If all the proliferating cells have the same duration of the mitotic cycle with the same durations of the constituent phases, then the form of the labeled mitosis curve should be a regular saw-tooth wave with the period of the wave equal to the intermitotic time or the "cell cycle". As the leading edge of the cohort passes through mitosis, the fraction of labeled mitoses rises from zero to 1.0. As the trailing edge passes through mitosis, it returns to zero. The rise and fall occur within the duration of mitosis. The duration of the G_2 phase is from time zero to the first appearance of the labeled mitosis. The duration of the S phase is the width of each peak at half-height -- the time taken for the cell cohort to pass a fixed point in time.

There is, however, a considerable difference between the theoretical PLM curve, and the curves obtained from experimental data. These differences were attributed by Quastler and Sherman (1959) largely to the variability in durations of the phases of the mitotic cycle within the cell population, and to

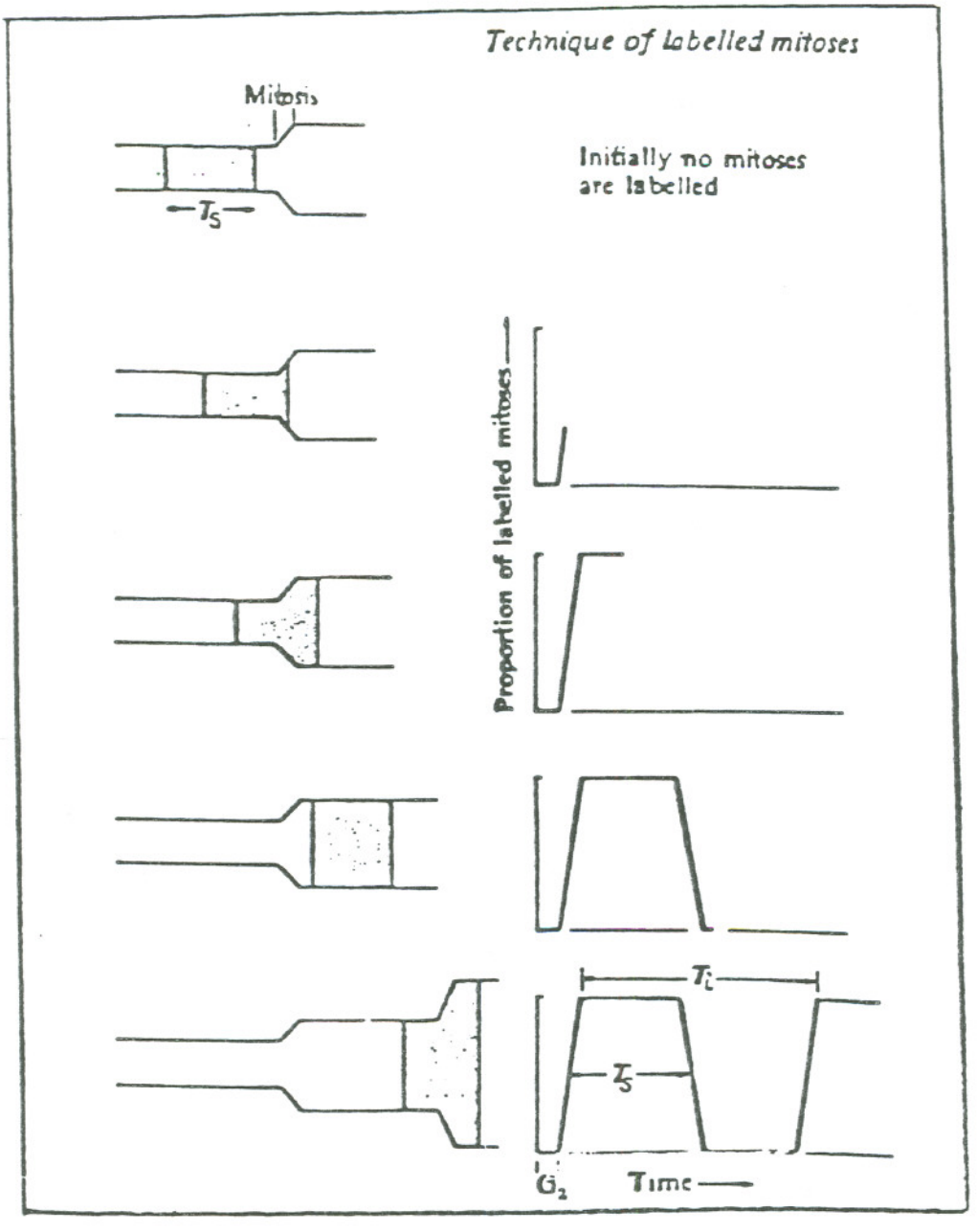

Figure.11 After a single administration of H-thymidine the labeled cohort (the stippled area) moves through mitosis. As it does so, the proportion of labeled mitoses describes a peak whose width is equal to the duration of the DNA-synthetic period. Subsequently, the proportion of labeled mitoses peaks again; the peak-to-peak interval is equal to the intermitotic time (T_i). Taken from Steel (1977).

artifacts due to autoradiographic false negatives. The complete disappearance of the second peak in their data implied the loss of the initial synchrony of the cohort of labeled cells following one cell cycle. Quastler and Sherman (1959) were able to make some estimates of the range of phase durations. Later work on the intestinal epithelium has shown that well-defined PLM curves with a good second peak have been observed in the mouse intestine, by Lesher, Fry and Kohn (1961) and in rat intestine, by Cairnie et al. (1965a).

Analyzing the labeled mitoses curve presents certain problems. The experimental data usually define a curve that shows damped oscillations. The majority of the published labeled mitoses curves have been analyzed by empirical methods. Quastler and Sherman (1959) used the width of the first peak at the 50% level as an approximate value for the average duration of the DNA synthesis. Later Quastler (1963) suggested that the 50% level method must underestimate the mean S- duration, and so suggested the use of the width of the first peak at the 37% level as a better approximation of the S-phase. Mendelsohn (1965) suggested that a reasonably reliable estimate of the mean duration of DNA synthesis would be the measurement of the area under the first peak of a labeled mitoses curve. This becomes a difficult measurement when the first trough lies well above the abscissa. With the development of theoretical methods for simulation of labeled mitoses curves, statistical methods of analysis were introduced. Barrett (1966) developed a method based on the three cell cycle phases, G_1, S, and G_2. He made the assumptions that the residence times

in these phases were described by independent log normal distributions. Steel and Hanes (1971), using Barrett's method of simulation, made a limited study of the empirical rules and came to the conclusion that, if the peak rises above 60%, the 50% level is a reasonably satisfactory estimate of the median intermitotic time. Takahaski, Hogg and Mendelsohn (1971) made a detailed study of the PLM curves using Takahashi's method of simulation (1968); they found that errors in the use of empirical rules were large in heavily damped curves. The general conclusion is that in cases where the labeled-mitoses curves show two high and well-defined peaks separated by a low trough, the empirical method (50% level) worked reasonably well.

The alternative to the empirical methods has to be resorted to very often, because the PLM data do not normally describe two well-defined peaks to characterize the cell cycle durations. A theoretical model that can simulate all of the data, and enable one to measure the cell kinetic parameters has been proposed by many investigators. The earliest method of calculating labeled-mitoses curves was derived by Barrett (1966), as described above. The mathematical representation was by Laplace transforms and the calculations were performed by a Monte Carlo procedure. These equations given by Barrett applied strictly to only nongrowing cell systems, but the error in their application to exponential growth was small (Trucco and Brockwell, 1968).

Steel and Hanes (1971) described an optimal version of Barrett's method (Barrett-Steel Model). This curve is divided into three sections. The shape of

the first rising limb depends largely on the mean and the standard deviation of G_2. The slope of the first fall depends on the four parameters: The mean and the standard deviation for the durations of G_1 and S. The rest of the curve depends on all six parameters. A polynomial fitting procedure was applied to each section in turn. This procedure has worked well on a wide range of types of data and it has been modified for use on the labeled-mitoses data in this experimental study (Modified Barrett-Steel Model). This modification assumes that there are 2 subpopulations with different cell cycle phase durations, that are proliferating at different rates. The same polynomial fitting procedures as in the Barrett-Steel Model were used on each sub-population, the second wave in the PLM curve was assumed to be due to the preponderance of one of the subpopulations. Thus the 2 waves in the PLM curve had different parameters. The 2 waves were then added mathematically to give a composite curve that gave the best fit to the data points. This modification was used on the data from the irradiated animals as it gave a better fit to these data points than the unmodified Barrett-Steel Model. However, the unmodified Barrett-Steel Model worked well for the control data, and was used to obtain the cell cycle phase durations for the control population.

There are other mathematical models which have been used by investigators. Among them: 1) the Takahashi-Mendelsohn method, described by Takahashi (1968), and the optimizing version developed by Takahashi, Hogg and Mendelsohn (1971); 2) the Bronk-Dienes-Paskin (1968) model of a proli-

ferating cell system, which may be used to examine transient responses to perturbation, and has been used to study cell synchrony and radiation response; 3) the Macdonald (1970) model, which provides a very comprehensive mathematical discussion on the labeled mitosis technique, information on the means and variances of the phase durations, along with a measure of the standard error of these parameters, as well as a maximum-likelihood solution. The list of mathematical models is long, and serves to indicate the considerable interest mathematicians have shown in the technique of labeled mitosis in biological systems. A comparison of the computing methods indicates that in most cases, the methods agree reasonably closely (Hartmann et al., 1975).

Chapter 3

Materials and Methods

3.0 Animals.

The mouse strain used for all the studies was CB6F1 from Jackson Laboratories in Maine. Four-week-old male mice were considered to be the most suitable sex age-group animals for the experiments. They were fed Purina Mouse Chow and given acidic water to drink ad libitum. This reduced the likelihood of pseudomonas contamination while they were housed at the animal house at the Lawrence Berkeley Laboratory.

3.1 Irradiation Procedures.

Mice were irradiated at the 184-inch Synchrocyclotron at the Lawrence Berkeley Laboratory, with the 230 MeV/amu helium beam, using the Irradiation Stereotactic Apparatus for Humans (Fig. 12). The neon irradiations were carried out at the Lawrence Berkeley Laboratory Bevalac, with the 425 MeV/amu beam. A specially-designed mouse holder was used to irradiate 6 mice at a time. A small collimator with a rectangular aperture of 2.5 mm x 15 mm was used to irradiate one-half of the head. This permitted comparison of the responses occurring in the irradiated cortex with those seen in the unirradiated cortex. This method served as an internal control. In addition sham-irradiated animals were used as additional controls for each experiment. The unirradiated animals were handled in the same manner as the irradiated animals.

The plateau region of the unmodified Bragg ionization curve (Appendix A) was used for the irradiations with the helium and the neon ions. The dosimetry was carried out with a tissue-equivalent (TE) ionization chamber (Far West Technology, Goleta, CA), located at the isocenter of the patient positioner. Depth dose curves were obtained by scanning the TE ionization chamber along the beam path in an acrylic box filled with water (Lyman et al., 1986).

The animals were prepared for the charged particle irradiation procedure using a careful, well-established procedure. The animals were anesthetized with an intraperitoneal injection of nembutal (50 mg/ml) diluted with saline (1:10) before irradiation. They were immobilized in the body holder by suspending them by their incisor teeth and taping their bodies to the metal spatulas. The deep anaesthesia guaranteed complete immobilization during irradiation. Figure 12 illustrates the animal holder and the positioning of the mice and the irradiation beam at the 184-inch Synchocyclotron. The experiments carried out involved a number of acute irradiations with helium-ion and neon-ion beams, limited to a selected brain hemisphere, and delivered at different doses. Time-dependent cell and tissue studies following irradiation were conducted at various intervals after the irradiations. For purposes of clarity, the design of the experiments are described in sequence, where appropriate, in Chapter 4, Experiments and Results, so as to provide a framework for the scientific questions to be examined.

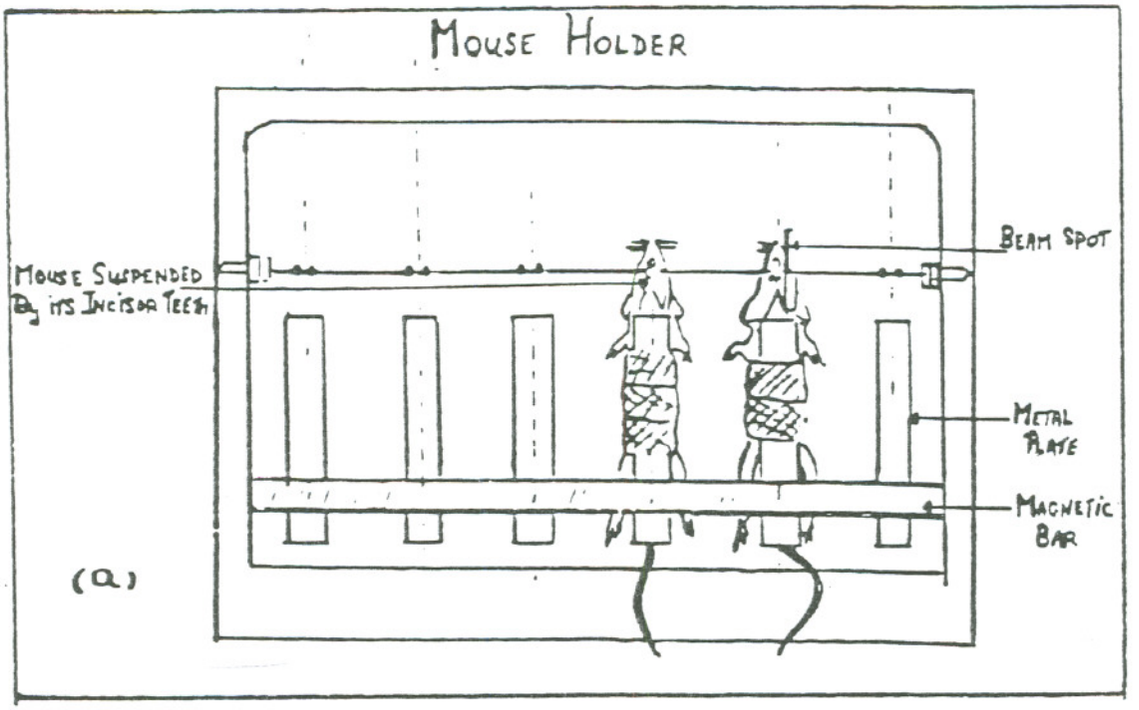

Figure.12a Orientation of animal holder and restrainer for immobilizing during helium-ion and neon-ion irradiation.

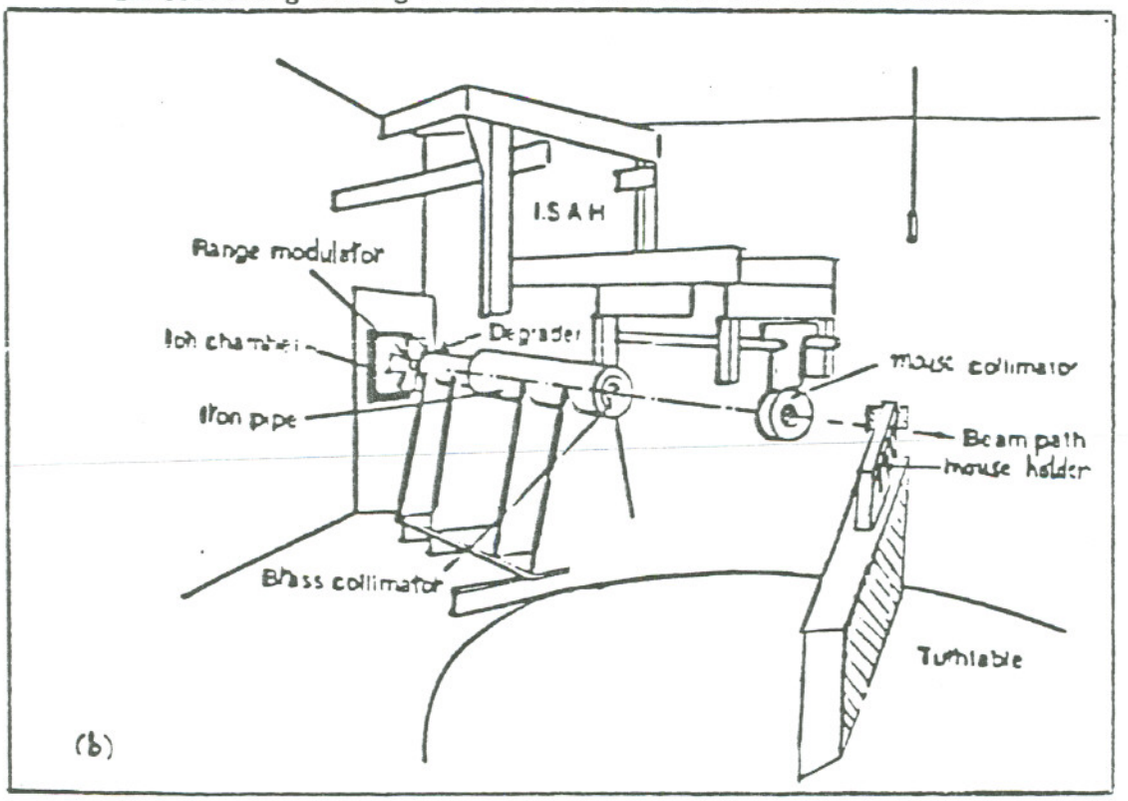

Figure.12b Illustrating the helium ion beam delivery procedure in relation to the mouse holder in the medical cave at the Lawrence Berkeley Laboratory's 184-inch Synchrocyclotron.
I.S.A.H.--Irradiation Stereotactic Apparatus for Humans.

3.2 Euthanasia Procedures

In the experiments measuring the H^3-TdR labeling indices and requiring high resolution autoradiography, the animals were anesthetized with an intraperitoneal injection of Nembutal diluted with saline (1:1) before cervical dislocation which killed the animal. The brain was dissected and immersed in 10% neutral formalin for fixation. This entire procedure from the cervical dislocation to the final immersion of the brain in formalin was completed in less than 5 min. In the experiments measuring the mitotic indices for quantitative histological analysis, cervical dislocation followed rapid cardiac perfusion of 1% glacial acetic acid in 10% formalin, the procedures were carried out under deep Nembutal anaesthesia.

3.3 Fixation Procedures

The brain was dissected out and rapidly immersed in 10% formalin immediately after dissection. This was done using enough formalin to equal at least 10 times the volume of the brain. This perfusion-fixation with formalin was very effective in those studies using the H^3-TdR labeling indices as the end points for cell kinetic analysis. In the studies measuring the mitotic indices, prompt fixation was essential for detection of the mitoses in the brain. The simple perfusion-fixation was not rapid enough and no mitoses were seen in the brain; the mitoses apparently progressed to completion before the brain was fixed when the fixation process was not rapid. In order to fix the brain rapidly to preserve the cells in the process of mitotic division, cardiac perfusion under

Nembutal anaesthesia with 10% glacial acetic acid in 10% formalin was used to fix the brain. Following a slow 5 ml cardiac perfusion with this solution, the mice underwent cervical dislocation, and the brains were dissected as usual. The brain was immediately immersed in 10% formalin and tissue fixation was continued for an additional week. This process allows the identification of mitotic figures in the histological sections. The criteria for identifying mitoses were a combination of cytological events: a loss of nuclear membrane; chromosomal configurations resembling metaphase or anaphase (Fig. 15), or; any mitotic figures.

In the experiments for evaluation of the effects of charged particle irradiation on the cell cycle kinetics of the subependymal layer, the animals were injected with tritiated thymidine 1 week after irradiation. This allowed a sufficient time for recovery following the initial phase of mitotic inhibition immediately following high-dose acute exposure. The examination of cell cycle kinetics and the response to heavy charged particle irradiation involved the technique of analyses of pulse labeled mitoses curves. This was carried out following irradiations of the brain with 10 Gy He, 10 Gy Ne, and 25 Gy He.

3.4 Histological Preparations

Following fixation, the brain was cut coronally into 4 blocks. These blocks were marked levels 1 through 4 (Fig. 13).

The tissue-section blocks were processed through a Fisher Tissuematon for embedding the brain in paraffin. The paraffin blocks were marked level 1

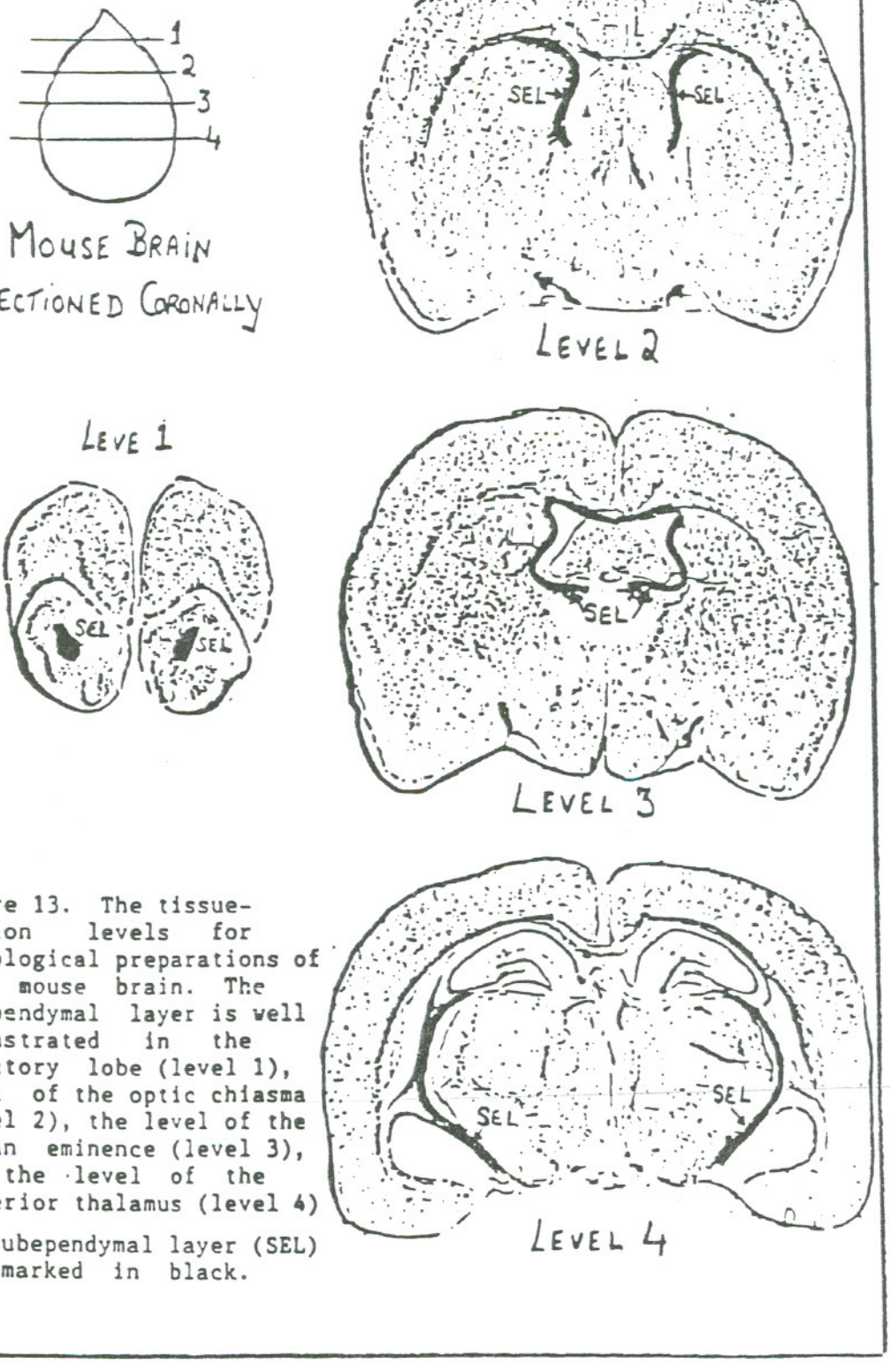

Figure 13. The tissue-section levels for histological preparations of the mouse brain. The subependymal layer is well demonstrated in the olfactory lobe (level 1), level of the optic chiasma (level 2), the level of the median eminence (level 3), and the level of the posterior thalamus (level 4)

The subependymal layer (SEL) is marked in black.

through level 4 for each brain. The paraffin blocks were sectioned using an American Optical tissue microtome. 0.5 μ sections were cut off the paraffin blocks and long strips of tissue sections were thus produced. Every fourth section was mounted on an acid-cleaned glass microscope slide after it was carefully stretched flat in a water bath (60 C°). Mounting every fourth section was necessary to avoid the possibility of counting the same cells more than once in the same tissue preparation.

The sections were deparaffinized and stacked in black light-proof plastic boxes for high resolution autoradiography. Hematoxylin and eosin tissue staining was carried out after the liquid-emulsion autoradiography.

3.5 Labeling with Tritiated Thymidine

The use of H^3-TdR combined with high resolution autoradiography has been one of the most useful techniques for studying DNA metabolism. Chemically TdR is a relatively stable compound and can be heated in neutral or alkaline solution for an hour at 120 C° without significant decomposition or loss of the H^3 atoms from the molecule. Solutions of labeled TdR can be sterilized by autoclaving without any decomposition (Crowter et al., 1960). In aqueous solution at room temperature hydrolytic cleavage of the N-glycosidic bond occurs at a very slow rate of about 1% to 2% of the original TdR/y (Evans and Stanford, 1963). For the experiments to follow, an aqueous solution of H^3-TdR was used; it had a specific activity of 6.7 Ci/mmol and a concentration of 5 mCi/5 ml, and was prepared by New England Nuclear Company (Boston, MA).

Mice were injected intraperitoneally with the labeled thymidine. The dose used was 20 μCi/gm body wt. This high dose was required to insure adequate availability to the subependymal cells in the brain, since only about 10% of the intraperitoneally injected thymidine crosses the blood-brain barrier (Korr, 1980). Maximum available time for H^3-TdR incorporation into the subependymal cells is about 1 hour. The beta-particles emitted by the tritium atom have a very low energy (a few KeV) and high resolution autoradiography is a valuable method for the detection of their relatively short (about 1 μm) tracks.

3.6 High Resolution Autoradiography

High resolution autoradiography is a very useful method for studying biochemical reactions "in situ" at the level of the individual cell (Leblond, 1961). The tissue specimen containing the radioactive precursor is covered with a layer of photographic emulsion designed specially for autoradiography. The specimen and the emulsion are in contact for a defined exposure period during which the radioactive atoms decay. The emitted beta-particle radiation from H^3-TdR strikes the photographic emulsion and reduces the silver halide grains, forming a latent image; on photographic development of the emulsion, the image faithfully represents the distribution of the radioactive material within the tissue architecture. Thymidine is a DNA precursor and is selectively incorporated into the DNA molecule during synthesis. The autoradiographs thus show the labeled DNA molecules in the cell nucleus, and because of the very short range of the beta tracks, the grains are confined only to the nuclear region in the cell. This

has proven to be a method for studying cell and tissue kinetics, e.g., the sites of cell proliferation, the size of the proliferating populations and the proliferating cell cycle and its component phases.

The nuclear track emulsion (NTB2) used on these experiments was manufactured by Eastman Kodak Co. This emulsion will record electron tracks with energies less than 0.2 MeV and is suitable for light microscopic techniques. The nuclear track emulsion was stored in the refrigerator at 4 C°. The emulsion is in a solid state when received and must be liquified before use. Under recommended safelight conditions (Kodak Safelight Filter No.2), a measured amount of the emulsion is placed in a measuring flask, and an equal amount of distilled water, warmed to 41 C°, is added; this results in an emulsion with a 1:1 dilution. The measuring flask with the diluted emulsion is then placed in a water bath heated to 41 C°. Gentle stirring is used to melt and mix the emulsion.

Clean blank slides were repeatedly dipped in the liquid emulsion, and then closely examined for bubbles under the safelight. A layer of emulsion without bubbles meant it was time to coat the slides with the tissue specimens on it. The slides coated with an even layer of emulsion are placed vertically to drain any extra emulsion and then allowed to dry in the same position.

Once dry (approximately 20 min) the slides are placed in the light proof black plastic boxes along with some Drierite (a dessicant). These boxes were also packed in aluminum foil to prevent any light leakage exposure. They were placed in the refrigerator for the exposure period, maintained at 4 C° for 2

weeks.

Before starting the photographic processing, the cold slides were allowed to return to room temperature in the dark or under 'safelight conditions'. Kodak developer-19 (D-19) and the Kodak fixer were used for processing the slides. Both the solutions were prepared according to the manufacturers instructions. The temperature of both the solutions is maintained at 16 C° in each tank; a stop bath of distilled water was used. The slides were developed for 6 min and fixed for 6 min, and then rinsed in running water for 30 min after fixing. They are then ready for staining with hematoxylin and eosin, using standard histologic techniques.

3.7 Quantitative Histology

Tritiated thymidine labeled subependymal cells

The subependymal cells line the lateral ventricles and are easily identified. The H^3-TdR labeled cells have a cluster of fine black grains over their nuclei. The grains in the background are very few and scattered. A grain count of 5 or more over the nucleus identifies a labeled cell, excluding the artifacts. A 40 x objective was used to count the labeled cells. Figure 14 illustrates the characteristic labeled subependymal layer lining the lateral ventricle in the unirradiated mouse brain.

Figure.14 Photograph of a Hematoxylin Eosin stained histological preparation following high resolution autoradiography showing the labeled subependymal layer lining the lateral ventricle. As can be seen the layer in this region of the lateral ventricle (level of the median eminence--level 3) is several cells thick. The black spots over the nuclei are the reduced silver halide grains (40 x magnification).

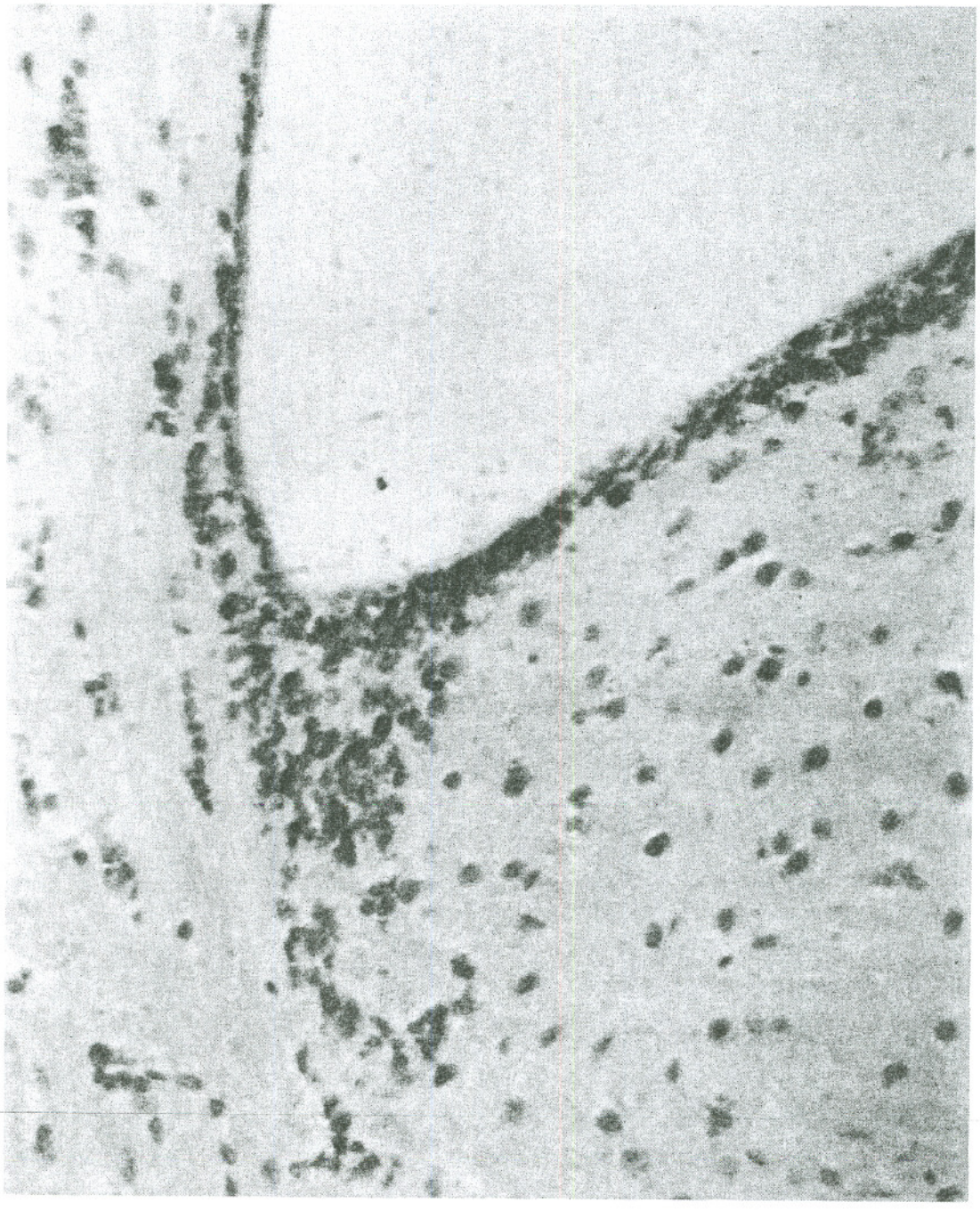

XBB 884-2776

Grain counting

Using a 100 x oil-immersion objective, the grains over the nucleus are clearly visible and can be counted. A grain count of 25-30 grains over each subependymal cell nucleus is the limit for an accurate count. A higher concentration of grains will cause them to be confluent with overlapping which results in an inaccurate count. Grain count decrements following a pulse label of H^3-TdR were used to measure population doubling times.

Counting mitoses

Using a 100 x oil-immersion objective, it is possible to identify individual cytological stages of mitosis in dividing subependymal cells. Metaphase and anaphase stages of mitosis are often the ones most readily identified, but with experience it is possible to identify with accuracy both prophase and telophase using a 100 x oil-immersion objective. Identifying the discrete mitotic phases in dividing subependymal cells was difficult at times, and loss of a nuclear membrane along with a mitotic figure was sufficient to characterize a cell undergoing mitosis. A labeled mitotic figure can be much more difficult to identify, as the overlying grains tend to distort the nuclear morphology. False positives are more common with labeled cells in interphase as the the dark grains tend to obscure the underlying clumped chromosomes. Fig. 15 illustrates a cell in anaphase and a labeled mitotic cell.

The percentage of labeled mitoses in the subependymal cell population, occurring over a period of time following a pulse of tritiated thymidine was used

Figure.15 Photographs of Hematoxylin Eosin stained histological preparations of the subependymal cells in the mouse brain, showing labeled and unlabeled mitosis following incorporation of tritiated thymidine and, high resolution autoradiography. They show cells in anaphase, one of the stages of mitosis that is clearly distinguishable under the light microscope (100 x oil-immersion objective).

Cell in Mitosis

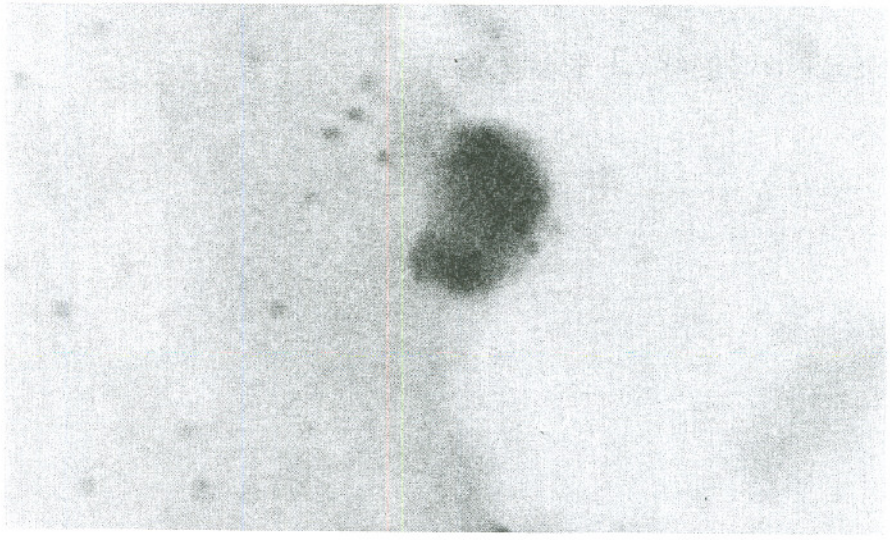

Labeled Mitosis

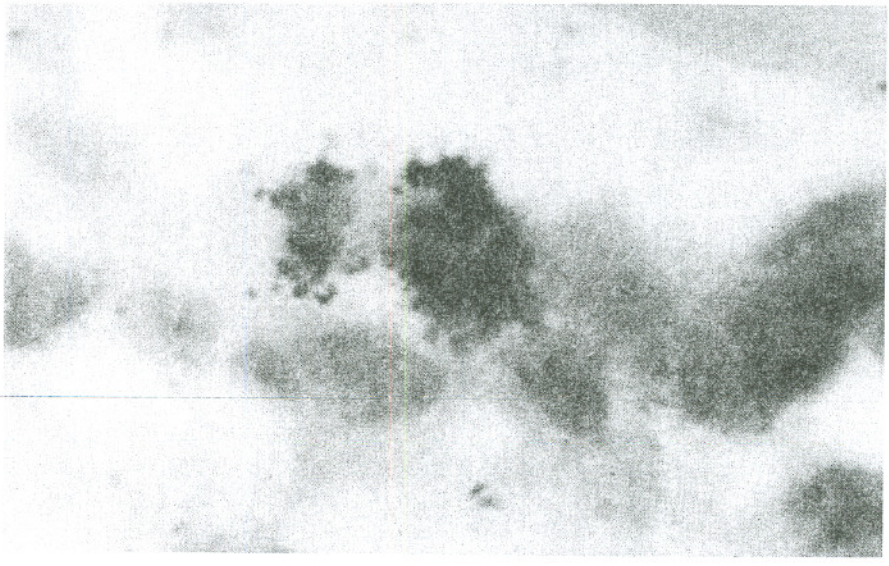

XBB 884-3284

to generate the PLM curve for cell cycle kinetic analysis. These curves were analyzed to estimate the durations of the various cell cycle phases of the subependymal cells according to the method of Quastler (1959) and modified by Barrett (1966) and Steel (1977).

Chapter 4

Experiments and Results

4.0 Scientific Objectives

The objective of the experiments on the subependymal layer in the mouse brain was to characterize the cell population kinetics of this layer and to evaluate the early effects of charged particle radiation on these cell and tissue kinetic parameters. These experiments have been designed to study the early effects of these irradiations on the brain, as early as 24 hr, 48 hr and 1 wk. The subependymal cell population is an actively proliferating cell population, and as such, one of the only cells in the brain to show the early cellular effects of irradiation of the brain. The early effects of charged-particle irradiation on the histology of the subependymal layer have been noted by Kraft et. al., (1980), but quantitative evaluations have yet to be made. These experiments use quantitative histological techniques, to study the cell population kinetic parameters, and the cell cycle phase durations of the proliferating subependymal cell population in the mouse brain.

4.1 Labeling Indices following Pulse Labeling with Tritiated Thymidine

The H^3-TdR labeling indices in the various regions of the subependymal layer following a pulse of tritiated thymidine (H^3-TdR) identifies the sites of cell proliferation, the number of proliferating cells and the pattern of changes in the

cell population kinetics with time. Mice were injected intraperitoneally and H^3-TdR labeling indices were determined at 1 hr, 12 hr, 24 hr, 36 hr, 48 hr, and 168 hr following the single injection. Each of the four levels in the mouse brain (Fig. 13) was examined. Two slides with three histological sections per slide were examined for each level. Approximately 5,000-6,000 cells were counted for each level where possible. At Level 1, the subependymal layer in the olfactory lobe has the smallest subependymal cell population, and a total of approximately 2,500-3,500 cells were counted. Four animals were killed for each time interval following H^3-TdR. In some instances, the sections on the levels were damaged by the processing technique limiting complete examination.

Labeling indices at different sites in the subependymal layer

There is a wide variation in the percentage labeling indices (LI) of the 4 levels (Fig. 16 and Table 1b). This is in agreement with the findings in other studies in the literature (Korr, 1980). The LI values observed in the olfactory lobe (1.3%-9.8%) are consistently lower than those seen in the optic chiasma (21.4%-33.3%), the level of the median eminence (13%-33.7%) and the level of the posterior thalamus (19.3%-29%) as seen in Table 1b. The LI values seen in Levels 2 and 3 are consistently higher than those seen in the other levels.

There are differences in labeling indices observed in each mouse, even when they are killed at the same time interval following the pulse of H^3-TdR. Each data point in Fig. 16 is an average of the values obtained for the 4 animals; 5,000 - 6,000 cells are counted in each animal. As can be seen from Table 1b

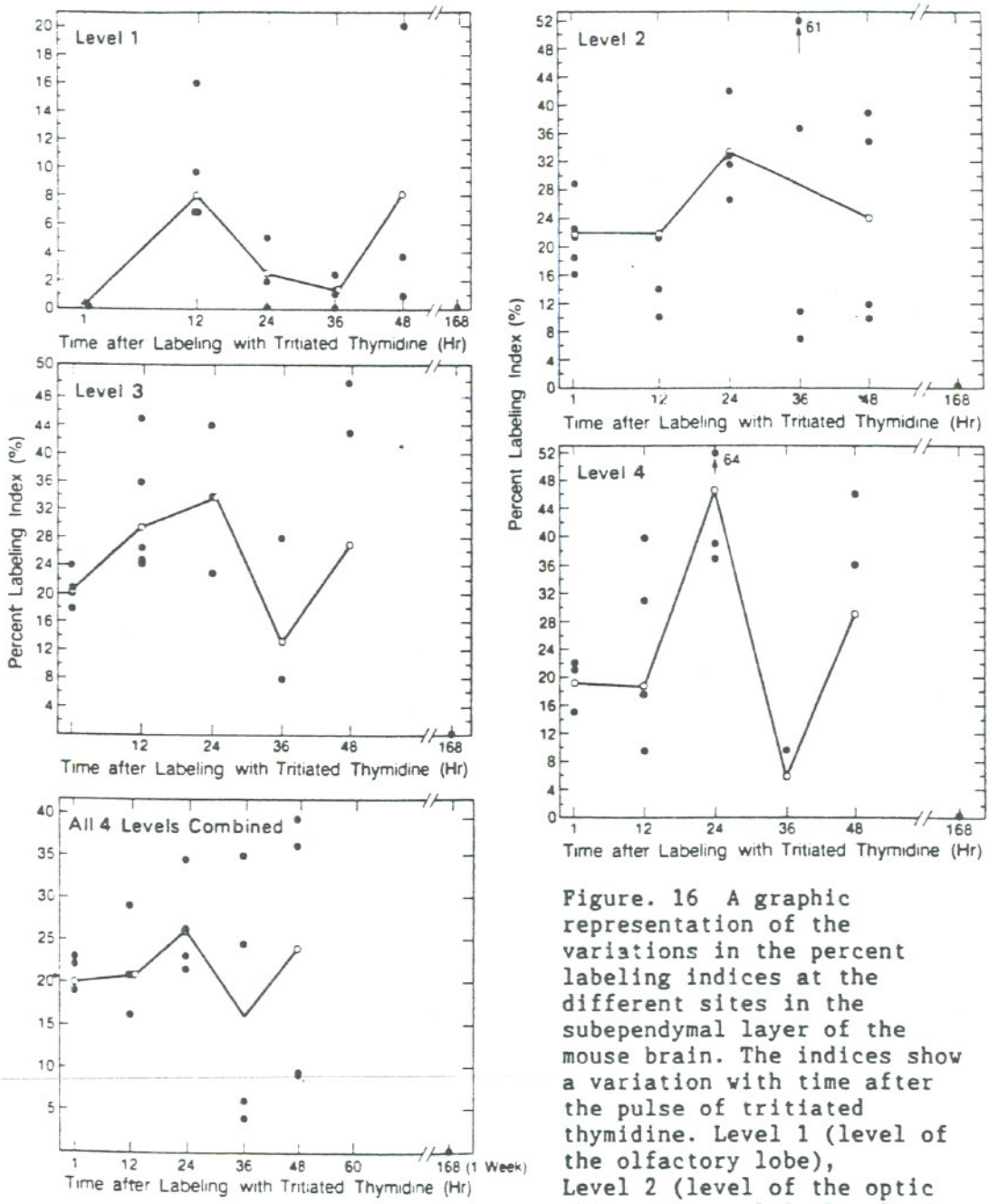

Figure. 16 A graphic representation of the variations in the percent labeling indices at the different sites in the subependymal layer of the mouse brain. The indices show a variation with time after the pulse of tritiated thymidine. Level 1 (level of the olfactory lobe), Level 2 (level of the optic chiasma), Level 3 (level of the median eminence), Level 4 (level of the posterior thalamus). The open circles represent the mean values.

Table 1a: Pulse Labeling with H^3TdR

Number of Animals	Hours after H^3TdR pulse	% Labeling Indices				
		level 1	level 2	level 3	level 4	S.E. layer
4	1	0.1	16.0	17.8	15.0	17.0
		0.2	18.4	20.0	19.0	21.0
		0.15	22.4	21.0	21.0	22.0
		0.2	28.8	24.0	22.0	23.0
4	12	6.8	10.0	24.6	9.4	16.0
		6.8	14.2	26.6	17.6	21.0
		9.7	21.2	36.0	31.0	21.0
		16.0	52.0	45.0	39.8	29.0
4	24	0.1	26.6	23.0	36.8	21.5
		2.0	31.6	33.6	39.0	23.0
		5.0	33.0	34.0	64.0	26.5
		-	42.0	44.0	-	34.4
4	36	0.1	7.0	3.0	1.6	4.0
		1.0	11.0	8.0	6.6	6.0
		1.4	36.8	28.0	9.6	24.4
		2.4	61.0	-	-	35.0
4	48	1.0	10.0	6.0	5.0	9.2
		3.6	12.0	7.2	36.0	9.4
		20.0	35.0	43.0	46.0	36.0
		-	39.0	50.0	-	38.0
2	168	0	0	0	0	0
		0	0	0	0	0

Table 1b: A table of means and their standard deviations plotted in Figure 16.

Number of Animals	Hours after H^3TdR	% Labeling Indices									
		level 1		level 2		level 3		level 4		S.E. layer	
		Mean	S.D.	Mean	S.D.	Mean	S.D.	Mean	S.D.	Mean	S.D.
4	1	0.163	0.05	21.40	5.60	20.70	2.57	19.25	3.10	21.25	1.71
4	12	9.83	4.34	24.35	19.0	33.05	9.39	24.45	13.56	21.75	5.38
4	24	2.37	2.47	33.30	6.42	33.65	8.58	46.6	15.11	26.35	5.76
4	36	1.23	0.954	28.95	25.12	13.00	13.23	5.93	4.04	17.35	14.93
4	48	8.20	10.30	24.00	15.12	26.55	23.22	29.0	21.38	23.15	16.01
2	168	-	-	-	-	-	-	-	-	-	-

there is a wide standard deviation for the average value, indicating considerable biological variation among animals.

As seen in the graph in Fig. 16 the labeling index rises after 1hr (about 21.3%) in all the levels to a maximum LI (about 26.4%) at 24 hr, and then falls to a low level at 36 hr (about 17.4%). This would indicate that (1) the cells continue to divide within the first 36 hr, and (2) the cells appear to leave the proliferating pool of cells as well as the non-proliferating pool of cells. The cells of the subependymal layer apparently migrate out of this layer (Patterson et al., 1973; Hubbard and Hopewell, 1980) and leave the proliferative zone, ultimately differentiating into mature neuroglial end-cells distant from the subependymal layer.

4.2 Histopathological changes seen in the subependymal layer following irradiation with helium ions (230 MeV/amu) and neon ions (425 MeV/amu).

Figure 17 illustrates the histologic and autoradiographic appearances of the subependymal layers in the unirradiated and irradiated cortices of irradiated animals, one week after 10 and 25 Gy He and 10 Gy irradiations. The subependymal layer is thinner in the irradiated cortices due to the decreased cellularity as compared to the unirradiated ones, but the difference is much more evident following the neon irradiation. There are fewer labeled cells in the irradiated subependymal populations, as compared to the unirradiated ones; this effect is dose-dependent for the helium ions, and much more apparent following neon

Figure.17 Photographs of the Hematoxylin Eosin stained histological preparations of the unirradiated and the irradiated subependymal layers in the mouse brain (25 x magnification) 1 week following partial irradiation of one cortex with 10, 25 Gy He (230 MeV/amu) and 10 Gy Ne (425 MeV/amu).

Following irradiation with 10 Gy He, the subependymal layer in the irradiated cortex is thinner and shows fewer labeled cells than the layer in the unirradiated cortex. There are no vacuoles or hemorrhages seen after irradiation with 10 Gy He.

Following irradiation with 25 Gy He the subependymal layer in the irradiated cortex is just 1 cell thick and has fewer labeled cells. Whereas the subependymal layer in the unirradiated cortex is 6-7 cells thick and shows many labeled cells. Vacuoles and hemorrhages were seen frequently in the irradiated cortex.

Following irradiation with 10 Gy Ne the subependymal layer in the unirradiated cortex shows very few labeled cells. The subependymal layer in the irradiated cortex showed even fewer labeled cells (Table 10a). Vacuoles and hemorrhages were seen frequently in the irradiated cortex.

Table 2 is a quantitative representation of the histopathological findings that were seen following these radiations.

He 10 Gy (un-ir)

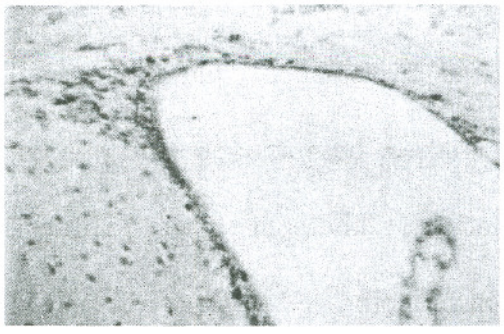

He 10 Gy (ir)

He 25 Gy (un-ir)

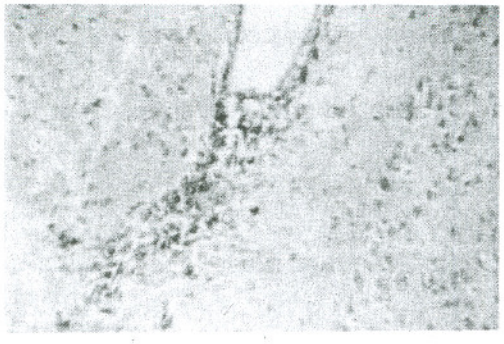

He 25 Gy (ir)

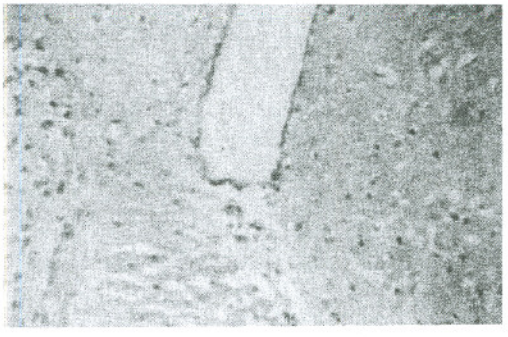

Ne 10 GyE (un-ir)

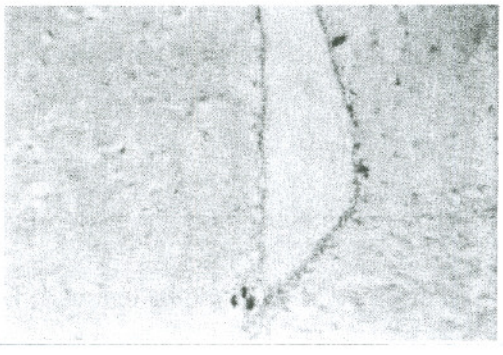

Ne 10 GyE (ir)

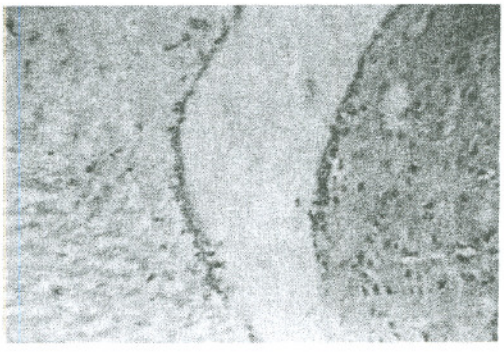

XBB 884-3285

irradiation than helium irradiation. The irradiated subependymal populations show numerous pyknotic neurons, pyknotic neuroglial cells, small hemorrhages within the tissue and a generally vacuolated appearance. The neon-irradiated population shows a greater number of pyknoses, hemorrhages and vacuoles as compared to the helium irradiated populations. These histologic findings indicate that the neon ions are more effective in inducing cell damage and cell killing of the nervous tissue than the helium ions.

Comparing the histological appearances in the subependymal layers of the unirradiated and the irradiated cortices in the irradiated mice after exposure to 10 Gy He (Fig 17); the layer in the unirradiated cortex is 6-7 cells thick whereas the layer in the irradiated cortex is 1-2 cells thick; there are more labeled cells in the unirradiated side even though this difference was not very marked following irradiation with 10 Gy He; there are fewer vacuoles in the unirradiated side as compared to the irradiated side; there were similar numbers of mitoses seen in both the subependymal layers (Table 8a)

Comparing the histological appearances in the subependymal layers following irradiation with 25 Gy He (Fig 17); there is a marked difference in the cellularity of the subependymal layers, the unirradiated side shows a layer that is 6-7 cells thick while the irradiated side shows a denuded layer with very few cells; there are labeled cells clearly visible in the unirradiated while the irradiated side shows no labeled cells in this section; the vacuolated appearance of the layer in the irradiated side is much more pronounced than the unirradiated side; there

were more mitoses seen in the unirradiated side than the irradiated side even though there is a marked decrease in the total number of mitoses seen after 25 Gy He irradiation (Table 9a); there were many more pyknoses and hemorrhages seen following this irradiation than seen in the unirradiated control mice.

Comparing the histological appearances in the subependymal layers following irradiation with 10 Gy Ne (Fig 17); there was a dramatic decrease in the number of labeled cells seen in both the layers in the irradiated mice as compared to the unirradiated mice (compare Tables 7a and 10a); however there were more labeled cells in the unirradiated side than the irradiated side (Table 10a); there is a decrease in the cellularity of both the layers in the irradiated mice, but it is slightly more so in the irradiated side (Table 10a); there were more hemorrhages seen in the irradiated side as compared to the unirradiated side; pknotic neurons were more frequent following the neon-ion irradiation than any of the other helium-ion irradiations.

A table (Table 2) has been made to quantitate the histological findings.

4.3 Response of the subependymal layer following irradiation with helium ions (230 MeV/amu).

Partial irradiation of one cortex of the mouse brain.

Experiment

The labeling indices in the subependymal cell population following irradiation with 10, 20, and 30 Gy of helium ions were examined. Mice were irradiated

Table 2.

Histopathologic changes in the unirradiated and the irradiated cortices, 1 week following irradiation with 10, 25 Gy He (230 MeV/amu) and 10 Gy Ne (425 MeV/amu).

	Unirradiated Control	Unirradiated Cortex Internal Control			Irradiated Cortex		
		10 Gy He	25 Gy He	10 Gy Ne	10 Gy He	25 Gy He	10 Gy Ne
reduction in subependymal cell number	0	0	+	+++	+	+++	++++
reduction in labeled subependymal cells	0	+	++	+++	+	+++	++++
microscopic hemorrhage	0	0	+	+	+	+++	+++
vacuoles	0	0	+	+	+	++++	+++
pyknotic subependymal cells	+	+	+	+	+	+++	+++
pyknotic neurons	0	0	0	0	0	+	+

Legend:

0 - none

+ - mild

++ - moderate

+++ - marked

++++ - very marked

at the 184-inch Synchrocyclotron at the Lawrence Berkeley Laboratory, using the Isocentric Stereotactic Apparatus for Humans (Fig 12, I.S.A.H.). The irradiation procedure and set up are described in detail in Chapter 3, and doses of 10, 20, and 30 Gy were used. A low-dose helium beam spot was taken before irradiation to mark the irradiated region (Fig 18). Animals were killed 48 hr after irradiation; two animals were used per experimental point. The results are illustrated in Figure 19.

Results

There was a linear dose-dependance in reduction of LI with increasing dose in the irradiated cortex. There is a declining labeling index with increasing dose falling from 16% to approximately one-half this value after 30 Gy. The dose-response relationship is: about 3% decrease in the LI at 10 Gy, about a 5% decrease at 20 Gy and about a 9% decrease at 30 Gy, that is, a 3% decrease per 10 Gy.

The unirradiated contralateral subependymal layer also showed decreasing H^3-TdR labeling indices with increasing dose. The labeling indices were consistently higher in the unirradiated side (i.e., 13.1% vs. 11.8%) but only slightly, than those seen in the irradiated subependymal layer (Table 3). As can be seen from Table 3, there is a decrease of 0.31% per Gy in the LI (%) in the irradiated cortex, and a decrease of 0.23% per Gy in the LI (%) in the unirradiated cortex. This response in the unirradiated cortex appears to be an indirect effect of the irradiation, possibly mediated through altered regional cerebral blood flow

Figure.18 Immobilisation technique for heavy charged particle irradiation of the brain in mice. The port film (dark area) demonstrates the portion of the charged particle beam through which the plateau region of the Bragg ionisation curve traverses. As can be seen from this photograph the contralateral cortex in the irradiated mice did not receive any irradiation.

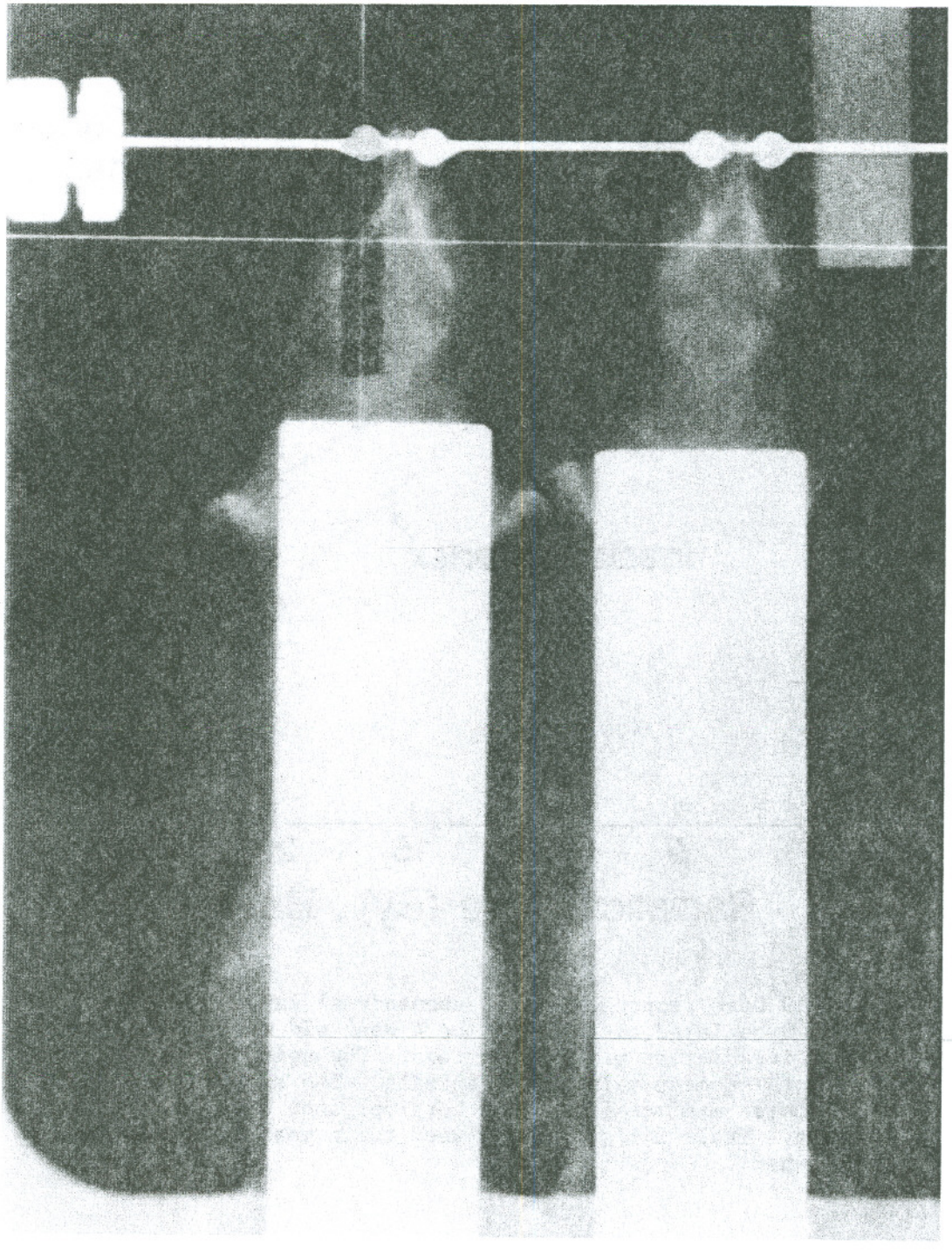

XBB 884-3287

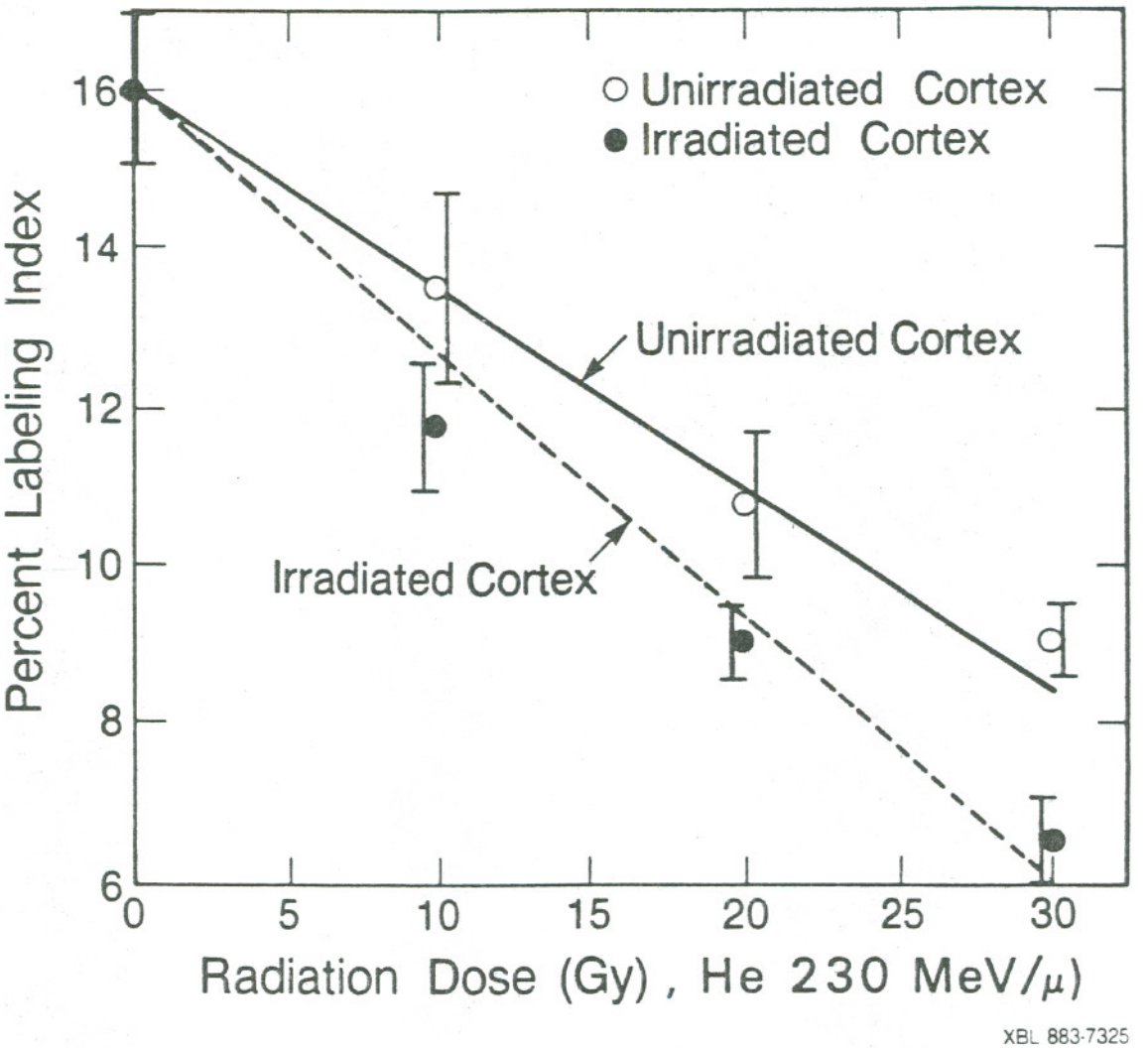

XBL 883-7325

Figure.19 Dose response in the subependymal layer of the unirradiated and the irradiated cortices of the 4 week old mose brain 48 hr after partial irradiation with helium ions. The points on the graphs represent the mean value for 2 animals. The subependymal layer in the unirradiated and the irradiated cortices show a similar pattern of response. Table 3 lists the values, their means and the standard deviations.

Table 3: Dose response in the Supependymal cells of 4 week old mice brains, 48 hours after irradiation with Helium ions (230 MeV/amu)

Number of Animals	Dose (Gy)	H^3TdR Labeling Index (%)		Mean		Standard Deviation	
		Irradiated Cortex	Unirradiated Cortex	Irradiated Cortex	Unirradiated Cortex	Irradiated Cortex	Unirradiated Cortex
2	0	18.1 13.9	18.4 13.6	16.0	16.0	2.97	3.39
2	10	11.3 12.3	14.1 12.1	11.8	13.1	0.71	1.41
2	20	9.1 8.9	11.4 10.2	9.0	10.8	0.14	0.849
2	30	7.1 6.1	9.1 8.9	6.6	9.0	0.71	0.141

involving altered metabolic mechanisms, and may be a response that is essential for maintaining homeostatic control.

4.4 Size of proliferating populations and response to irradiation of the subependymal layer cells after exposure to 45 Gy He (230 MeV/amu)

Experiment

In order to determine the size of the proliferating population and its response to irradiation an estimate of the growth fraction of the subependymal cell population was determined using repeated labeling with H^3-TdR. In this experiment the cell population is exposed to the DNA label repeatedly and so care is taken to avoid any radiation effects due to incorporation of tritium. 18 mice were irradiated with 45 Gy He (230 MeV/amu and the other 18 were used as unirradiated controls. The beam was focused on the left cortex using a rectangular apperture (25.5 mm by 3.5 mm). The right subependymal layer served as internal control. The control animals were sham-irradiated in a manner similar to irradiated mice. Three animals were used per experimental point, for the control and the irradiated dose responses (Fig. 20). The animals were injected with 150 μCi of H^3-TdR every 6 hr for 6 injections. The injections were started 23 hr following the irradiation. 6 mice (3 controls and 3 irradiated) were killed 1 hr following each H^3-TdR injection. At 23 hr 36 animals had been injected with 150 μCi of H^3-TdR each. At 29 hr 30 animals were injected with another 150 μCi and so on. The injection time intervals are 6 hr apart, a period less than the known duration of DNA synthesis for subependymal cells (8 hr-12 hr).

Repeated injections up to 54 hr insures that all the cells passing through the cell cycle will be labeled. Since all the proliferating cells in the population should be labeled, the maximum LI would give an estimate of the growth fraction.

Results

Labeling indices in the control animals

The labeling index rises from 8% to 22% in the first 20 hr following the first injection of H^3-TdR, and then falls to 10% where it appears to plateau. A similar decrease in the labeling index following an initial rise was observed in the first experiment. The decline in the labeling index may be due to migration of the labeled cells out of the subependymal layer by 48 hr.

Labeling indices in the 2 subependymal layers of the irradiated animals

The subependymal layer in the irradiated cortex has a maximum percent LI of 8%, as compared to 9% for the subependymal layer in the unirradiated cortex (Table 4). Since the injections of H^3-TdR were started 23 hr after the irradiation, the decrease in the LI in the irradiated mice as compared to the LI in the control mice (Fig. 20), could be probably due to arrest of the proliferating cells that are cycling, i.e., a G_2 -block, a spreading out of the T_{G2}, or a decrease in the number of proliferating cells. The two curves in the irradiated mice are otherwise similar (Fig 20).

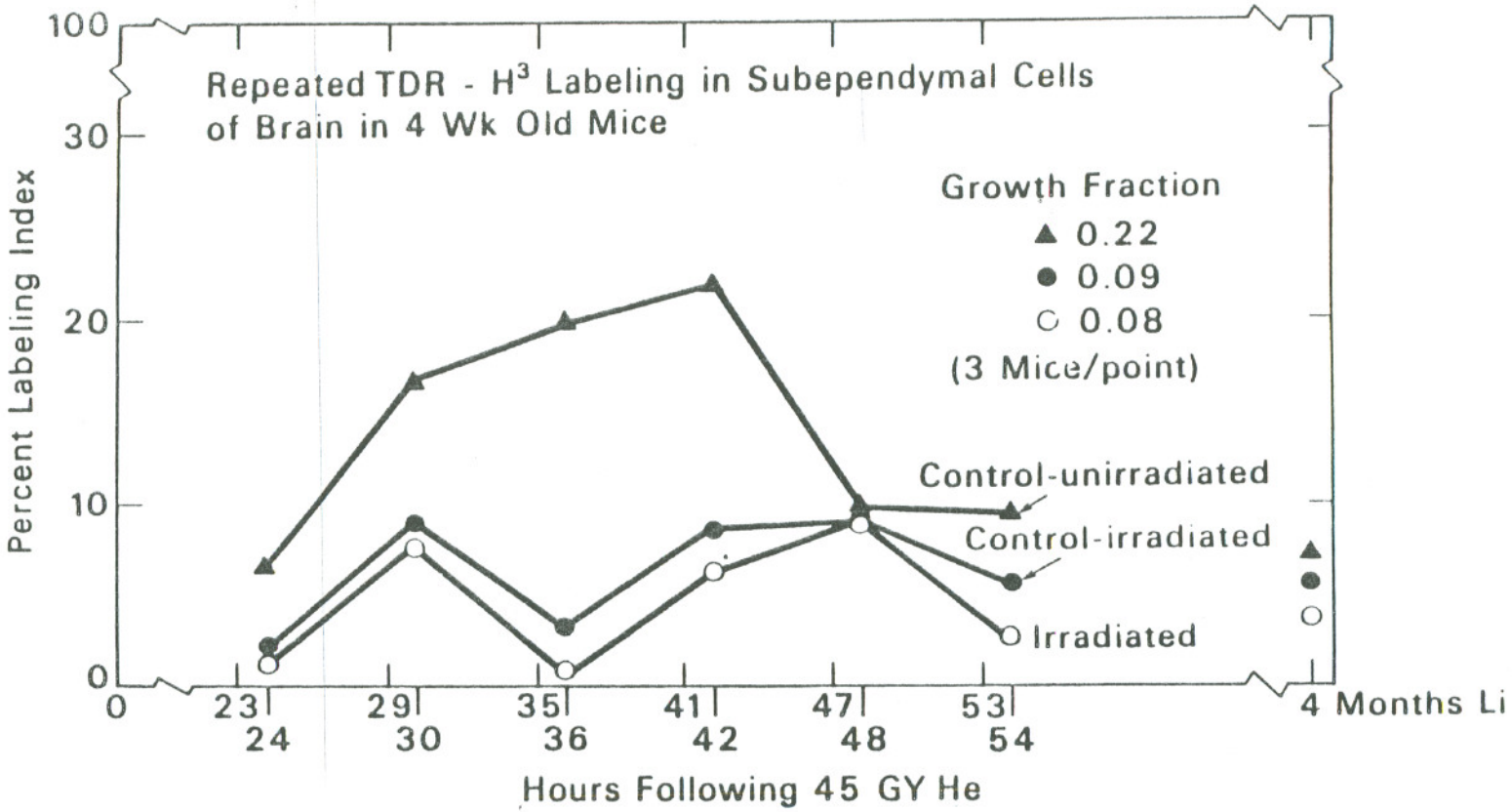

Figure.20 The size of the subependymal cell populations in the unirradiated and the irradiated mice was estimated by repeated labeling with tritiated thymidine. The points on the curves are the mean values for 3 mice. The standard deviations are wide and have been omitted here for clarity. Table 4 lists all the values along with the means and their standard deviations. The growth fraction in the control population is estimated to be 0.22. There is a decrease in the growth fraction of the cell populations in the unirradiated and the irradiated cortices 24-52 hr following the irradiation with 45 Gy He (230 MeV/amu). However, 4 months after the experiment the labeling indices were similar in the control and the irradiated mice.

XBL 8411-80668

Table 4: Repeated H^3TdR Labeling in Supependymal Cells, 24 hours after irradiation with 45 Gy He

Number of Animals	Hours after Irradiation	Dose (μCi)	Control			Irradiated Cortex			Unirradiated Cortex		
			%H^3TdR LI	Mean	S.D.	%H^3TdR LI	Mean	S.D.	%H^3TdR LI	Mean	S.D.
3	24	150	7.88 0.46 11.0	6.45	5.41	0.50 2.07 0.14	0.90	1.03	2.70 1.99 0.86	1.85	0.93
3	30	300	19.0 12.50 19.30	16.93	3.84	10.30 0.72 12.51	7.84	6.27	14.0 0.62 12.26	8.98	7.27
3	36	450	15.4 18.90 26.0	20.10	5.40	0.30 0.97 0.28	0.52	0.39	4.61 3.83 6.97	3.2	1.85
3	42	600	16.10 23.90 26.70	22.23	5.49	1.22 17.0 0.48	6.23	9.33	4.66 14.30 6.97	8.64	5.03
3	48	750	4.09 22.20 3.51	9.93	10.63	17.10 6.80 3.10	9.0	7.25	14.50 2.15 10.40	9.02	6.29
3	54	900	12.33 3.90 11.96	9.40	4.76	2.06 2.82 2.91	2.50	-	2.80 6.97 7.61	5.79	-
2	4 months	-	6.80 7.65	7.23	0.60	5.0 1.86	3.43	-	7.13 3.80	5.4	-

Growth fraction in the unirradiated and the irradiated animals

The growth fraction (Mendelsohn, 1960) is defined as the proportion of proliferating cells to the total cells in the cell population. The repeated injections of H^3-TdR will label all the cells entering the S phase and these labeled cells represent the proliferating cell population. The labeling index will increase with the repeated injections of H^3-TdR until all the cells that are proliferating pass through the S phase. Following this, the labeling index should level off if there is no movement of the proliferating or the nonproliferating cells in or out of the zone of proliferation. If the proliferating cells leave the population, the H^3-TdR labeling index should decrease with time, whereas if the nonproliferating mature cells emigrate or die, the labeling index should rise.

In Fig. 20, the higher LI for the control cell population is 22% (GF = 0.22) and this is a measure of the growth fraction for this cell population. Similarly, the maximum LI for the unirradiated subependymal layer in the irradiated mouse is 9% (GF = 0.09), and that for the irradiated one in the same animals is 8% (GF = 0.08).

4.5 Grain counts in the unirradiated and the irradiated animals

Experiment

The mean grain count of labeled cells could serve, in principle, as a method for determining the duration of DNA synthesis (Koburg, 1963), especially in those tissues where it is difficult to identify mitoses. Assuming that diploid cells have the same DNA content at the end of their cell cycle and providing that the

rate of DNA synthesis is approximately constant, it should be possible to calculate the duration of DNA synthesis in a given cell type by comparing the mean grain count of the cells in question with that of a cell type for which the duration of DNA synthesis has been determined by an independent method (for example, by comparison with intestinal crypt cells). If the rate of DNA synthesis is constant throughout the replication phase, the activity of the incorporated tritium in the nuclei in the DNA synthesis stage should be equal whatever stage of the DNA replication period is involved. The variation of grain counts seen in the autoradiographs should be the result of a random disintegration process, i.e., the frequency distribution of grain counts should be a Poisson distribution (Koburg, 1963).

The control animals for this experiment were three mice (7, 8 and 9) from the previous experiment. The irradiated mice (10 and 12 from the previous experiment) were used for the irradiation study. These animals had received 300 μC of H^3-TdR, and this minimized the possibility of intranuclear isotope toxicity or unavailability of the radionuclide for all proliferating cells. The autoradiographs were exposed for 10 days at which time approximately 50% of the cells had nuclear grain counts roughly between 25-30; this density proved satisfactory for studying the nuclear grain count distribution.

Results

Grain count distributions in the irradiated and the unirradiated animals

Figs. 21 and 22 and Table 5 demonstrate the nuclear grain count distribution following a pulse of H^3-TdR. There is no evidence of a Poisson distribution in the control or the irradiated animals. There is a shift to the right as well as a broadening of the grain count frequency. The reasons that lead to the broadening of a grain count distribution could be technical, eg. exposure time, availability time of H^3-TdR, the influence of nuclear geometry and nuclear structure in relation to the plane of section, and self-absorption (Koburg, 1963). They may also be biological, i.e., variation in the DNA synthesis rate per unit nuclear mass, and differences in nuclear DNA content i.e., aneuploidy and polyploidy. There are arguments in favor of an asynchronous replication of chromosomes given by Lajtha and Wimber (Koberg, 1963).

The grain count frequency distribution suggested that the DNA replication may very well be asynchronous. Thus, the frequency distribution the mean grain counts could not provide a reliable estimate of the duration of DNA synthesis in the control and irradiated subependymal cells.

4.6 Mean grain count decrements in unirradiated and irradiated animals; duration of T_c

Experiment

In this experiment 18 male mice were irradiated with 45 Gy of helium ions. The left cortex was irradiated using an aperture of 4 mm x 25.5 mm. The left subependymal layer was irradiated and the right one served as an internal control. The rest of the irradiation procedure is described in Chapter 3. Forty-

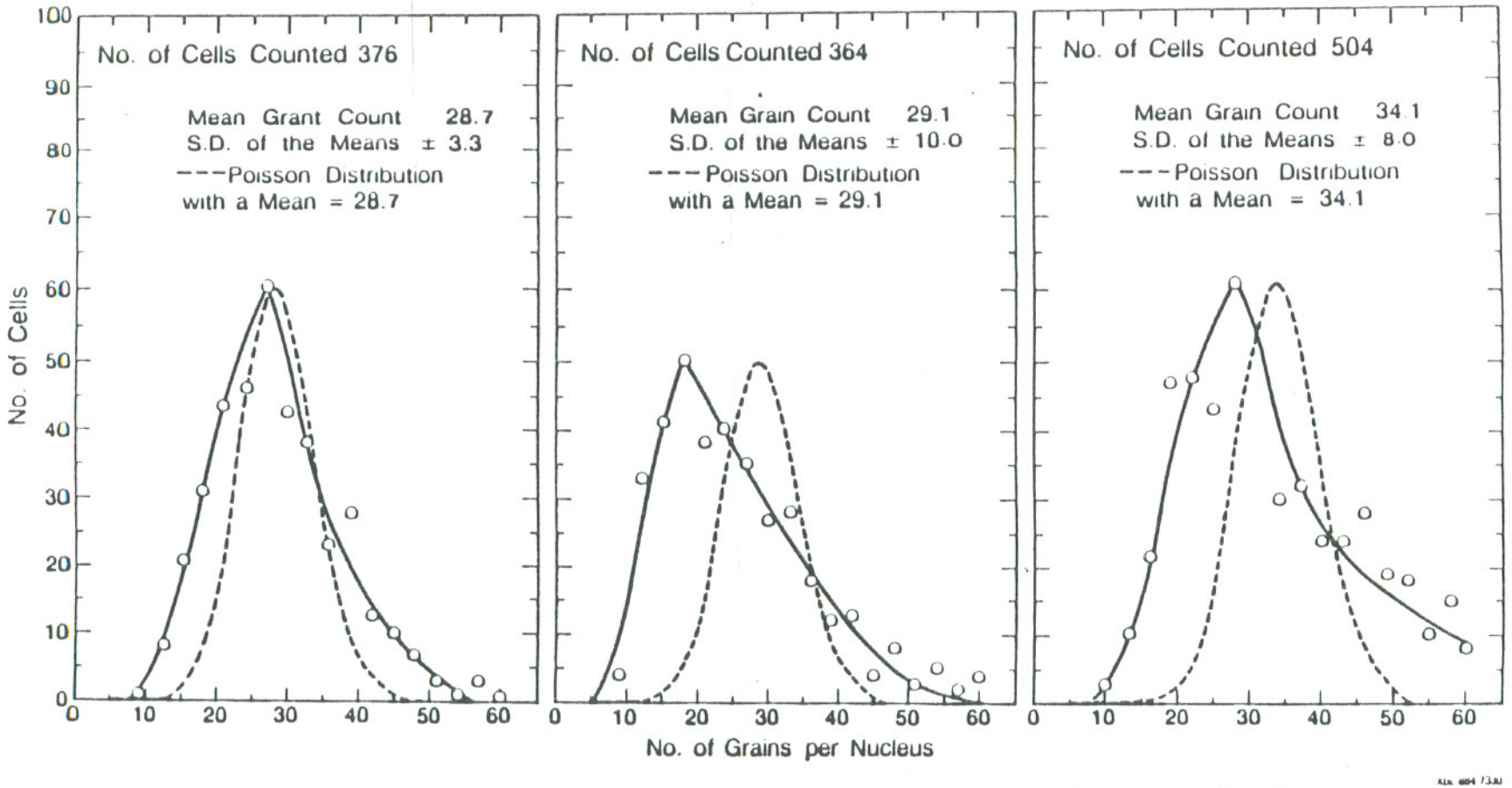

Figure 21. Frequency distribution of the nuclear grain counts in the subependymal cells of the unirradiated mice. The dashed curve represents a Poisson distribution with the same mean as the mean for the frequency distributions of the data points.

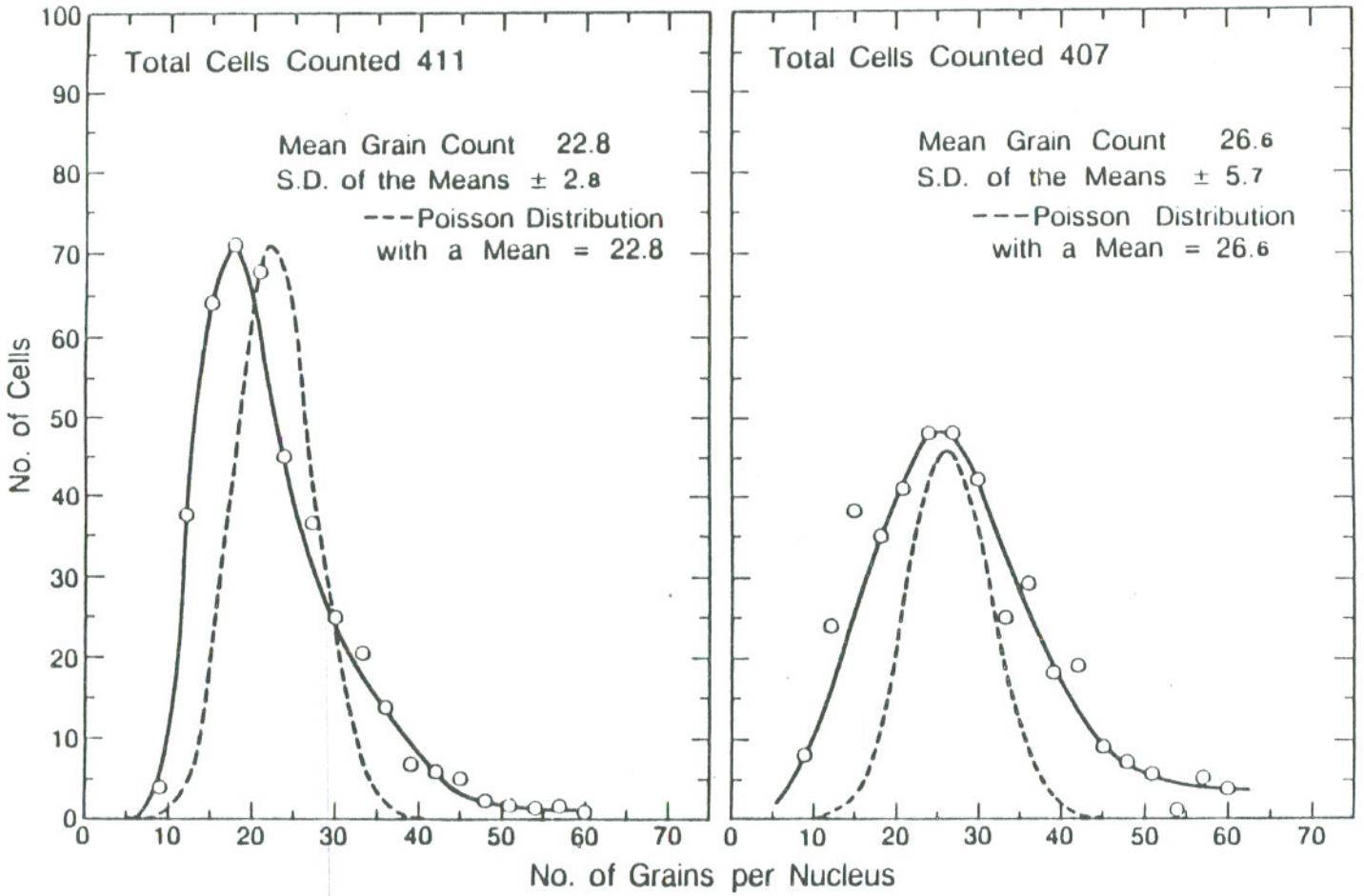

Figure.22 Frequency distribution of the nuclear grain counts in the subependymal cells of the irradiated mice (45 Gy He) 30 hr following the irradiation. The dashed curve represents a Poisson distribution with the same mean as the mean for the frequency distribution of the data points.

Table 5: Frequancy Distribution of Mean Grain Counts per Nucleus in the Supependymal Cells

Part a: Controls

Animal Number	Mean Grain Count / Nucleus–Section	Total No. of Cells Counted	Mean Grain Count / Nucleus	S.D. of the Mean
10	26.0 25.0 22.0 20.0 19.0 20.5 25.0 25.0	411	22.8	2.75
12	31.8 28.9 31.3 21.0 20.0	407	26.6	5.68
Part b: 30 hours after Irradiation with 45 Gy He (230 MeV/amu)				
7	22.8 26.8 31.9 27.0 32.3 28.8 31.9 28.0	376	28.7	3.31
8	24.0 17.0 31.0 24.0 35.0 50.0 25.0	364	29.1	10.0
9	45.0 33.9 33.8 26.4 37.0 24.9 45.0 26.5	504	34.1	7.99

eight hr after irradiation, 36 animals were injected intraperitoneally with 150 μCi of H^3-TdR each. The same pulse label was repeated every 6 hr for 4 injections. The total dose of isotope each animal received was 600 μCi. The 18 control animals all received the same treatment as the irradiated ones, the 6-hourly injections of H^3-TdR assures labeling of the whole proliferating cell population, assuming T_s is $>$ 6 hr.

Three irradiated and 3 control animals were killed 1 hr after the last injection. 6 animals (3 irradiated and 3 control) were killed every 10 hr after the first killing for the next 50 hr. The brain was processed and the histological sections prepared (see Chapter 3). The histological sections were exposed for 10 days during autoradiography. Grain count decrements were counted (Table 6 a,b). Some cells in the population show a faster decrement than others (Appendix B). This is an indication of a mixed cell population, i.e., the cells are proliferating with different cell-cycle times. This may be an indication of cells in different phases of their cell cycles. The Hubbard-Hopewell model (Hubbard and Hopewell, 1980) for cell population kinetics of the subependymal cells (see Chapter 1) would give the distribution of grain-count decrements observed.

Results

Comparing the grain-count decrements

The irradiated subependymal cells demonstrate a rapid grain-count decrement; this is a more rapid decline than that seen in any of the other subependymal layers (Fig. 23 and Table 6). The unirradiated subependymal cells in the

irradiated animals (internal controls) show a grain-count decrement similar to the irradiated ones, but their rate of decrement is not as rapid. This would indicate a longer cell cycle time in the unirradiated (internal control) subependymal cells. The subependymal layer in the unirradiated control animals shows a very slow grain-count decrement (Fig. 23). This would indicate that this cell population has a longer cell cycle time. The subependymal cells in the irradiated animals show a higher initial grain count than that seen in the control animals. This may indicate an initial increased rate of DNA synthesis in the irradiated cells; and has been seen in a number of proliferating cell systems, e.g., the regenerating liver (Fabrikant, 1964, 1966).

Analysis of the mean grain count decrements

The grain count decrements in the control subependymal layer indicate that a 'mixed cell population' (SD, SL, LL) is present. The cells show different patterns of grain count decrements. The cells are proliferating with different durations of their cell cycle phases, and thus different cell cycle tissues. Some of the cells are either differentiating or maturing, others are synthesizing DNA, in the proliferating compartment. A measure of the time required for halving the nuclear grain count as a whole, would not therefore give a true measure of the cell cycle time for any of the subpopulations in the subependymal layer. The mean grain count (MGC) values averaged for 3 mice show a fairly wide standard deviation (Table 6), and an estimate of the mean cell cycle time using the grain count-halving method in this case does not provide an accurate measure. Linear

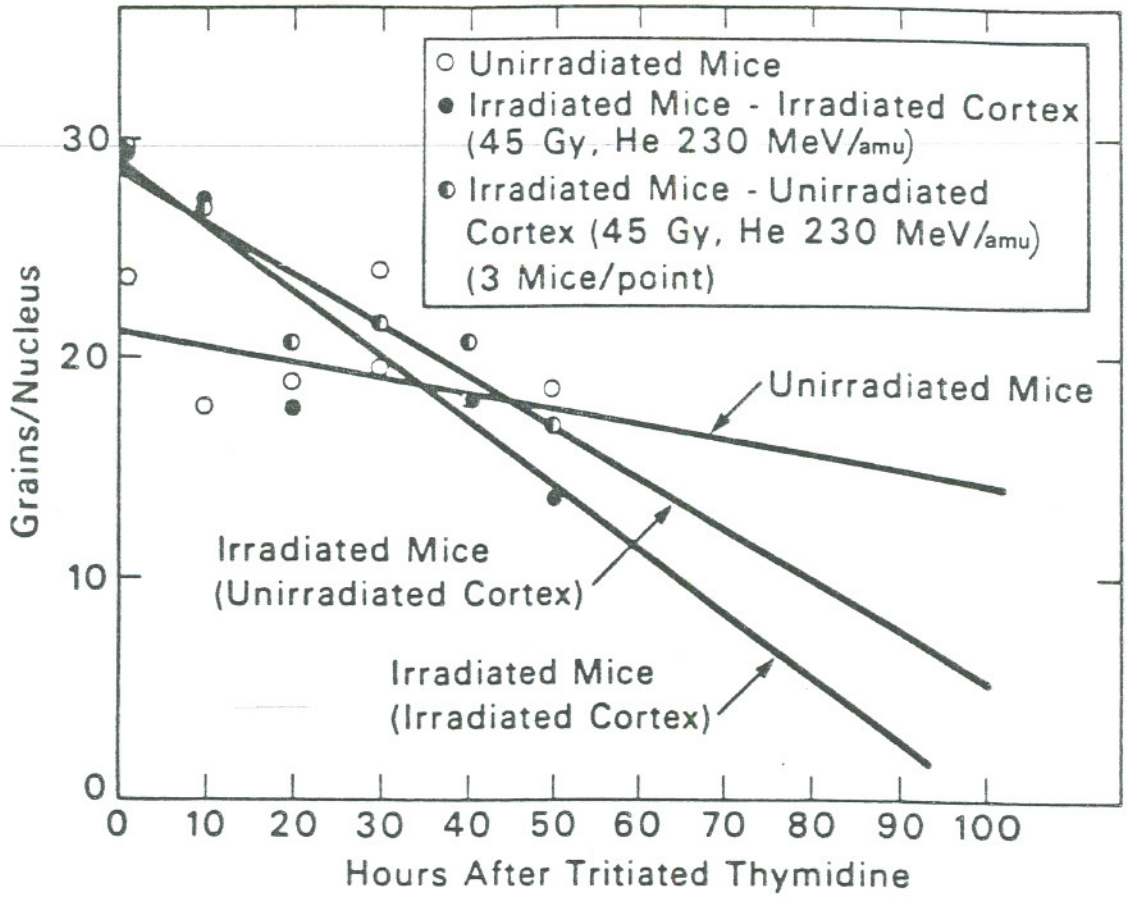

XBL 8511-8597B

Figure.23 These graphs represent the mean grain count decrements in the subependymal cells of the unirradiated and the irradiated mice, 48 hr after exposure to 45 Gy He (230 MeV/amu). The points on the graphs are the mean values for 3 mice. The standard deviations of the mean values are wide and have been omitted here for clarity. Table 6 lists the values along with the means and their standard deviations.

Table 6: Mean Grain Count Decrements in Subependymal Cells of Brains in 4-week Old Mice

Part a: Control Animals

Number of Animals	Hours after H^3TdR pulse	M.G.C. Nucleus–Animal		Mean		S.D.	
		Left Cortex	Right Cortex	Left Cortex	Right Cortex	Left Cortex	Right Cortex
3	1	23.89 23.89 21.30	24.60 23.57 22.62	23.03	23.60	1.50	0.990
1	10	17.77	17.96	17.77	17.96	-	-
3	20	22.18 17.82 15.85	20.53 20.85 15.36	18.62	18.91	3.24	3.08
3	30	19.67 18.98 20.16	18.52 19.25 20.81	19.60	19.53	0.593	1.17
3	40	19.26 17.46 20.43	17.37 16.94 20.10	19.05	18.14	1.50	1.71
3	50	18.6 17.66 20.05	18.34 17.43 19.27	18.75	18.35	1.20	0.92

Part b: 48 Hours after Irradiation with 45 Gy He (230 MeV/amu)

Number of Animals	Hours after H^3TdR pulse	M.G.C. Nucleus–Animal		Mean		S.D.	
		Irradiated Cortex	Unirrad. Cortex	Irradiated Cortex	Unirrad. Cortex	Irradiated Cortex	Unirrad. Cortex
3	1	29.51 29.26 29.18	34.17 26.81 27.91	29.32	29.63	0.172	3.97
2	10	26.90 27.17	29.75 23.90	27.04	26.83	0.191	4.14
2	20	15.46 20	19.25 21.86	17.73	20.56	3.21	1.85
3	30	21.80 27.76 22.03	18.53 23.19 22.90	23.86	21 54	3.38	2.61
3	40	20.46 17.36 16.20	22.25 23.30 17.01	18.01	20.85	2.20	3.37
3	50	12.0 6 14.14	16.48 13.69 20.32	13.07	16 83	4.22	3.33

regression was used to define the straight lines through the data points. Grain count-halving times using the 50% level are: (1) Unirradiated controls, 150 hr; (2) Irradiated controls (45 Gy He), 62 hr; and (3) Irradiated (45 Gy He), 50 hr.

4.7 The effect of heavy charged particle irradiation on the cell cycle kinetics of the subependymal cells of the mouse brain

Experiments

Three animals were used for each of the data points on the PLM curve and the animals were killed at 1, 5, 9, 13, 17, 21, 25, 29, and 33 hr after pulse labeling with H^3-TdR. The helium irradiations (doses, 10 Gy and 25 Gy; 230 MeV/amu) were carried out at the 184-inch Synchrocyclotron at LBL, the neon irradiations (dose, 10 Gy; 425 MeV/amu) were carried out at the Bevalac. Rectangular apertures of 3 mm x 15 mm were used for the half-brain irradiations. Labeled and unlabled mitoses were counted in the irradiated and unirradiated subependymal cells in the control and irradiated animals, and tabulated separately (Tables 7a-10a). Labeling indices and mitotic indices were also estimated for the subependymal cell populations in the unirradiated and irradiated animals (Tables 7a-10a).

Because of the wide variation in the distribution of labeled mitoses at each interval, resultant PLM curves fitted by eye were highly uncertain (Figs. 24, 26, 28, 30). PLM curves were also computer generated using the Barrett-Steel modified model (Barrett, 1966) for computer fit of the data points; this modification permitted characterization of the cell cycle duration and its

Table 7a: (Control) Pulse labeling with H^3TdR in the subependymal cells of 5-week-old mice

Number of Animals	Hours after H^3TdR	Left cortex							Right cortex						
		LM	M	UL	L	LI	PLM	MI	LM	M	UL	L	LI	PLM	MI
3	5	3	21	7027	1387	0.17	12.5	0.003	7	30	8379	1803	0.18	18.9	0.004
		29	28	7081	1023	0.13	50.9	0.01	48	31	10535	1574	0.13	60.8	0.01
		2	36	8553	1019	0.11	5.3	0.004	7	36	9017	1746	0.16	16.3	0.004
3	9	83	53	6951	2085	0.23	61.0	0.02	73	52	9552	3133	0.25	58.4	0.01
		38	41	8375	1746	0.17	48.1	0.01	41	49	10312	2399	0.19	46.	0.01
		40	17	6752	610	0.083	70.2	0.008	38	22	7553	836	0.10	63.3	0.01
2	14	59	15	5126	1898	0.270	79.7	0.011	57	14	4979	1729	0.26	80.3	0.01
		54	12	5006	1762	0.260	81.8	0.010	53	11	4871	1699	0.26	82.8	0.01
2	17.30	42	10				81.0		37	6				86.0	
		47	5				90.3		41	3				93.2	
3	25	13	5				72.2		7	1				87.5	
		17	14				54.8		19	9				67.9	
		46	30				60.5		28	18				60.9	
2	29	11	17	6338	668	0.095	39.3	0.004	13	6	8663	1001	0.10	68.4	0.002
		54	30	7133	1563	0.180	64.3	0.010	34	26	8156	1753	0.18	56.7	0.01

LM: labeled mitoses, M: unlabeled mitoses, UL: unlabeled cells, L: labeled cells, LI: labeling index, MI: mitotic index, PLM: percent labeled mitoses

Table 8a: Pulse labeling with H^3TdR in the subependymal cells one week following irradiation with 10 Gy He (230 MeV/amu)

Number of Animals	Hours after H^3TdR	Unirradiated Cortex							Irradiated Cortex						
		LM	M	UL	L	LI	PLM	MI	LM	M	UL	L	LI	PLM	MI
3	1.15'	2	7	8094	860	0.10	22.2	0.001	1	8	9311	785	0.07	11.1	0.00
		-	6	9811	978	0.09	-	0.01	-	7	11379	1016	0.08	-	0.00
		-	-	5185	1124	0.18	-	-	-	-	2779	160	0.05	-	-
4	5.45'	-	-	5760	1330	0.19	55.0	-	-	-	4447	599	0.11	51.8	-
		71	54	5692	798	0.12	56.8	0.02	61	55	8521	1168	0.12	52.6	0.01
		179	46	9085	1389	0.13	76.6	0.02	177	41	11293	1706	0.13	81.2	0.02
		98	94	7326	1516	0.17	51.0	0.02	136	84	4171	264	0.06	61.8	0.05
3	9	76	122	5801	1027	0.15	38.4	0.03	45	107	4967	193	0.04	29.6	0.03
		204	184	7974	2354	0.23	52.6	0.04	197	168	6419	1602	0.20	54.0	0.05
		57	49	6358	1904	0.23	53.8	0.01	120	90	5209	1880	0.27	57.1	0.03
3	13	28	3	4441	2393	0.35	90.3	0.01	37	10	2877	1236	0.30	78.7	0.01
		7	2	1943	610	0.24	77.8	0.003	8	1	1046	215	0.17	88.9	0.01
		101	10	3383	889	0.21	91.0	0.03	45	5	4606	648	0.12	90.0	0.01
4	17	107	14	3900	1423	0.27	88.4	0.02	90	9	3991	938	0.19	90.9	0.02
		87	8	3452	1716	0.33	91.6	0.02	79	17	3459	1499	0.30	82.3	0.02
		71	7	3046	1460	0.32	91.0	0.02	64	7	2958	1332	0.31	90.1	0.02
		16	4	2391	551	0.18	80.0	0.01	35	9	1571	155	0.09	79.6	0.02
2	21	33	18	2568	349	0.12	64.7	0.02	48	21	2758	427	0.13	69.6	0.02
		15	6	3354	738	0.18	71.4	0.01	15	5	3635	774	0.18	75.0	0.01
2	25	23	5	3693	1592	0.30	82.1	0.01	18	4	3427	987	0.22	81.8	0.01
		13	5	4267	961	0.18	72.2	0.003	21	8	4862	752	0.13	72.4	0.01
2	29	19	-	5603	2112	0.27	100	0.003	32	4	4459	1433	0.24	88.9	0.01
		44	10	6175	1881	0.23	81.5	0.01	51	3	7124	2128	0.23	94.4	0.01
2	33	36	14	5350	1471	0.22	72.0	0.01	24	10	3632	489	0.12	70.6	0.01
		45	7	5684	1257	0.18	86.5	0.01	37	6	6182	1589	0.20	86.1	0.01
2	35.30'	37	3	5395	1773	0.25	92.5	0.01	27	3	4672	404	0.08	90.0	0.01
		22	5	5138	1236	0.19	81.5	0.01	37	9	4945	1284	0.21	80.4	0.01

LM: labeled mitoses, M: unlabeled mitoses, UL: unlabeled cells, L: labeled cells, LI: labeling index, MI: mitotic index, PLM: percent labeled mitoses

Table 9a: Pulse labeling with H^3TdR in the subependymal cells one week following irradiation with 25 Gy He (230 MeV/amu)

Number of Animals	Hours after H^3TdR	Unirradiated Cortex							Irradiated Cortex						
		LM	M	UL	L	LI	PLM	MI	LM	M	UL	L	LI	PLM	MI
3	1	12	26	5146	1506	0.23	31.6	0.01	11	35	4279	1172	0.22	23.9	0.01
		10	37	6942	1564	0.18	21.3	0.01	3	39	4417	1159	0.20	7.1	0.01
		5	33	6484	1742	0.21	13.2	0.01	9	16	3953	33	0.01	36.0	0.01
3	5	20	24	3090	460	0.13	45.5	0.01	14	24	4216	812	0.16	36.8	0.01
		23	32	4911	683	0.12	41.8	0.01	6	14	3485	66	0.02	30.0	0.01
		47	41	7823	1769	0.18	53.4	0.01	24	25	3926	218	0.05	49.0	0.01
3	9	58	65	9139	2994	0.25	47.2	0.01	6	13	4420	103	0.02	31.6	0.004
		47	41	8545	1487	0.15	53.4	0.01	41	19	9638	926	0.09	68.3	0.01
		74	48	8369	3188	0.28	60.7	0.01	69	44	7317	2180	0.23	61.1	0.01
3	13	51	23	4285	601	0.12	68.9	0.02	6	10	3143	33	0.01	37.5	0.01
		87	47	11416	987	0.08	64.9	0.01	27	13	7179	216	0.03	67.5	0.01
		91	56	6963	1478	0.18	61.9	0.02	48	22	5008	463	0.09	68.6	0.01
3	17	48	57	7236	915	0.11	45.7	0.01	59	52	6788	636	0.09	53.2	0.01
		41	33	3047	678	0.10	55.4	0.01	2	4	3478	21	0.01	33.3	0.002
		19	12	8082	483	0.06	61.3	0.004	16	17	5899	305	0.05	48.5	0.01
3	21	26	38	9575	2662	0.22	40.6	0.01	16	33	8471	2031	0.19	32.7	0.01
		24	16	7827	998	0.11	60.0	0.01	20	5	6509	625	0.09	80.0	0.003
		33	22	7467	1916	0.20	60.0	0.01	41	26	6806	1360	0.17	61.2	0.01
3	25	18	14	5743	679	0.09	56.3	0.004	22	17	5228	449	0.08	56.4	0.01
		16	2	4525	162	0.03	88.9	0.003	13	2	3029	83	0.03	86.7	0.01
		11	10	8058	404	0.05	52.4	0.003	13	8	7119	128	0.02	61.9	0.003
3	29	53	26	5972	1482	0.20	67.1	0.01	31	19	5688	881	0.13	62.0	0.01
		8	13	6030	451	0.07	38.1	0.003	8	10	4208	204	0.05	44.4	0.004
		8	3	7800	561	0.07	72.7	0.001	11	8	5552	84	0.02	57.9	0.003
3	33	9	10	5028	871	0.15	47.4	0.003	15	22	3981	252	0.06	40.5	0.01
		20	19	6336	1917	0.23	51.3	0.01	21	26	5499	1058	0.16	44.7	0.01
		24	22	9501	848	0.08	52.2	0.004	7	13	6504	327	0.05	35.0	0.003

LM: labeled mitoses, M: unlabeled mitoses, UL: unlabeled cells, L: labeled cells, LI: labeling index, MI: mitotic index, PLM: percent labeled mitoses

Table 10a: Pulse labeling with H^3TdR in the subependymal cells one week following irradiation with 10 Gy Ne (425 MeV/amu)

Number of Animals	Hours after H^3TdR	Unirradiated Cortex							Irradiated Cortex						
		LM	M	UL	L	LI	PLM	MI	LM	M	UL	L	LI	PLM	MI
3	1	-	3	3459	25	0.01	-	0.00	-	1	2916	3	0.00	-	0.00
		14	10	2249	101	0.04	58.3	0.01	5	3	1865	12	0.01	62.5	0.00
		18	10	6492	1063	0.14	64.3	0.004	4	3	4036	187	0.04	57.1	0.002
1	4.10'	57	6	6869	328	0.05	90.5	0.01	12	7	6515	15	0.002	63.2	0.003
3	5	62	9	4969	244	0.05	87.3	0.01	82	23	6649	228	0.03	78.1	0.02
		25	6	5751	18	0.003	80.6	0.01	44	13	5155	27	0.01	77.2	0.01
		26	4	5874	44	0.01	86.7	0.01	34	8	4993	9	0.002	81.0	0.01
3	10	27	4	4000	72	0.02	87.1	0.01	22	3	3712	2	0.001	88.0	0.01
		162	30	5656	432	0.07	84.4	0.03	24	24	5538	23	0.004	50.0	0.01
		48	8	1969	123	0.06	85.7	0.03	37	4	1488	93	0.06	90.2	0.03
3	15.45'	44	18	4217	148	0.03	71.0	0.01	42	21	2774	13	0.01	66.7	0.02
		56	20	3419	220	0.06	73.7	0.02	9	28	3225	6	0.002	24.3	0.01
		43	16	3531	88	0.02	72.9	0.02	30	14	2194	14	0.01	68.2	0.02
3	20.45'	86	14	4613	278	0.06	86.0	0.02	21	7	3209	17	0.01	75.0	0.01
		38	13	5494	88	0.02	74.5	0.01	23	7	5567	16	0.003	76.7	0.01
		136	2	4412	403	0.08	98.6	0.03	23	1	3713	14	0.004	95.8	0.01
4	25.40'	56	27	7268	226	0.03	67.5	0.01	55	14	6617	141	0.02	79.7	0.01
		14	2	2858	26	0.01	87.5	0.01	23	7	1746	23	0.01	76.7	0.02
		25	2	3274	63	0.02	92.6	0.01	14	2	1753	14	0.01	87.5	0.01
		85	18	7485	1056	0.12	82.5	0.01	35	8	5900	34	0.01	81.4	0.01
3	29.40'	39	17	4645	192	0.04	69.7	0.01	25	31	3561	25	0.01	44.6	0.02
		20	20	3845	40	0.01	50.0	0.01	3	13	2853	5	0.002	18.8	0.01
		12	16	3407	12	0.004	42.9	0.01	16	15	4341	21	0.01	51.6	0.007

LM: labeled mitoses, M: unlabeled mitoses UL: unlabeled cells, L: labeled cells, LI: labeling index, MI: mitotic index, PLM: percent labeled mitoses

component phases derived from the experimental data. The modification of the Barrett-Steel model (Barrett, 1966) was made in order to accommodate the assumption of a 'mixed cell population' with at least two cell populations, one proliferating with a shorter cell cycle. This theoretical curve gives a satisfactory fit to the data points. The first wave of the PLM curve is indicative of the 'mixed cell population', while the second part of the curve simulates the cell population with the shorter cell cycle. This assumption is compatible with the model of the stem-cell compartment proposed by Lajtha (1963) and others in which two or more subpopulations are cycling at different rates. In this model, a stem cell population that is cycling at a fast rate maintains the stem cell compartment, while a second (or more) compartment(s) made up of proliferating and differentiating cells serving as precursor cells for the recognizable proliferating cell compartment of the cell renewal system.

The subependymal cell cycle in control mice

The PLM curves for the control subependymal cell populations, using both the best fit method and the Barrett-Steel model for a computer fit are illustrated in Figs. 24 and 25. The data points plotted are a mean for 2-3 mice per data point. These mean values and their standard deviations are given in Table 7b. The durations for the cell cycle phases derived by using the Barrett-Steel model for a computer fit to the data points are given in Table 11. Comparing the values for the DNA synthesis phase (T_S), both the methods give very similar values. For T_S, (1) PLM curve by 'eye', T_S = 21-24.5 hr, and PLM curve using

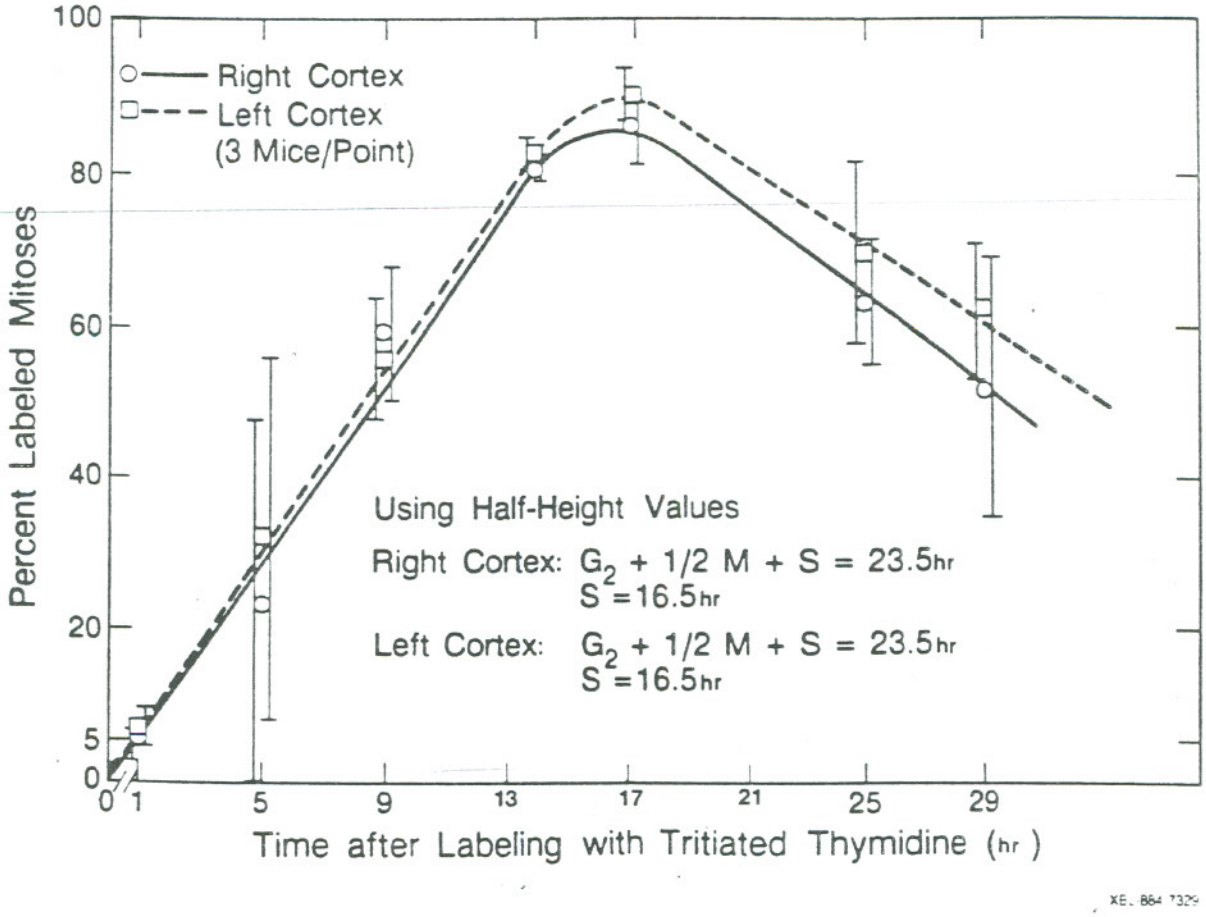

Figure.24 Percent labeled mitoses curves in the subependymal layers of the right and left cortices of the mouse brain. The ascending and the descending limbs of the initial wave were used to estimate the half-height values. The points on the curves represent the mean values for 3 mice per data point. The wide standard deviations are an indication of the individual biological differences among the mice. Table 7b lists the values, their means and the standard deviations.

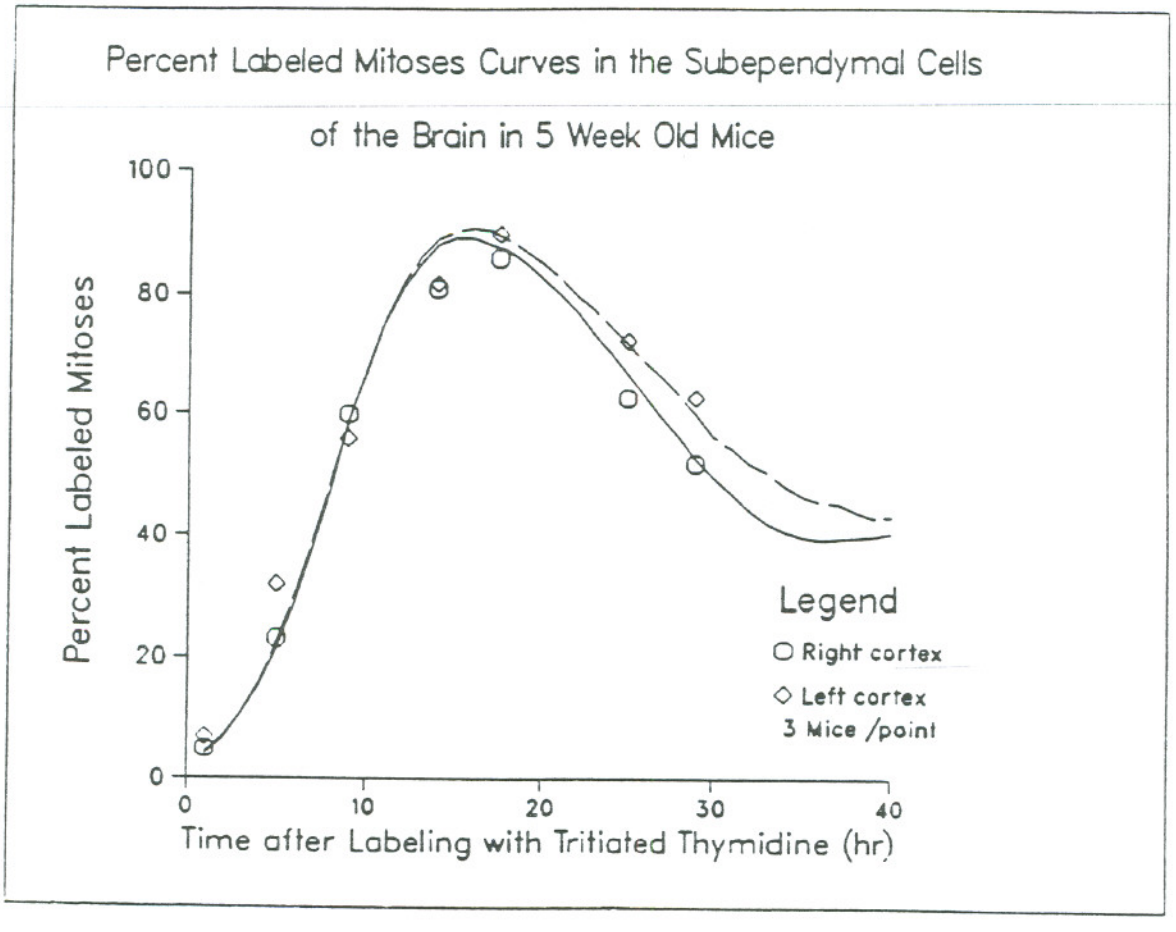

Figure.25 These computer generated PLM curves were drawn by applying the Barrett-Steel Model (Chapter 2). The data points represent the mean values for 3 mice, the standard deviations in the mean values are omitted because the computer model uses these values for generating the curves.

Table 7b: (Control) Percent labeled mitoses after a pulse of H^3TdR in subependymal cells of 5-week-old mice

No. of Animals	Hours after H^3TdR	Left Cortex			Right Cortex		
		Percent Labeled Mitoses	Mean	S.D.	Percent Labeled Mitoses	Mean	S.D.
2	1	6.0 8.0	7.00	1.41	4.0 6.0	5.00	1.41
3	5	18.9 60.8 16.3	32.00	24.98	12.5 50.9 5.3	22.90	24.51
3	9	58.4 46.0 63.3	55.9	8.92	61.0 48.1 70.2	59.76	11.10
2	14	80.3 82.8	81.55	1.77	79.7 81.8	80.75	1.49
2	17.30'	86.0 93.2	89.60	5.09	81.0 90.3	85.65	6.58
3	25	87.5 67.9 60.9	72.10	13.79	72.2 54.8 60.5	62.50	8.87
2	29	68.4 56.6	62.50	8.34	39.3 64.3	51.80	17.68

the Barrett-Steel model, T_S = 20-22 hr.

The Barrett-Steel model gives a value for the variations in the durations of the cell cycle phases (Table 11). Three mice were used per data point, and the error bars on the PLM curve by 'eye' are a measure of the individual biological reponse among the mice. The subependymal cells appear to be proliferating with a cell cycle time, T_C, of approximately 37-39 hr, and the times spent in the individual phases are: T_{G_1} = 8 hr, T_{G_2} = 8 hr, and T_S = 20-22 hr.

The subependymal cell cycle in irradiated mice, one week after exposure to 10 Gy He (230 MeV/amu).

PLM curves fit by 'eye' and those using the Barrett-Steel model are illustrated in Figs. 26 and 27. Here it was necessary to modify the Barrett-Steel model thereby identifying two cell populations with different cell cycle phases (Table 11). This modification results in a better fit to the data points than the original Barrett-Steel model and therefore was used to estimate the durations of the cell cycle phases. The irradiated and the unirradiated subependymal cell populations have similar cell cycle characteristics. The values proved to be so close (Fig. 27) that the same computer-generated curve was generated to fit the data points for both the subependymal cell populations. The data points on the PLM curves are a mean value for 2-4 animals and there is a wide standard deviation for these values as illustrated by the error bars in Fig. 27 and by the values in Table 8b.

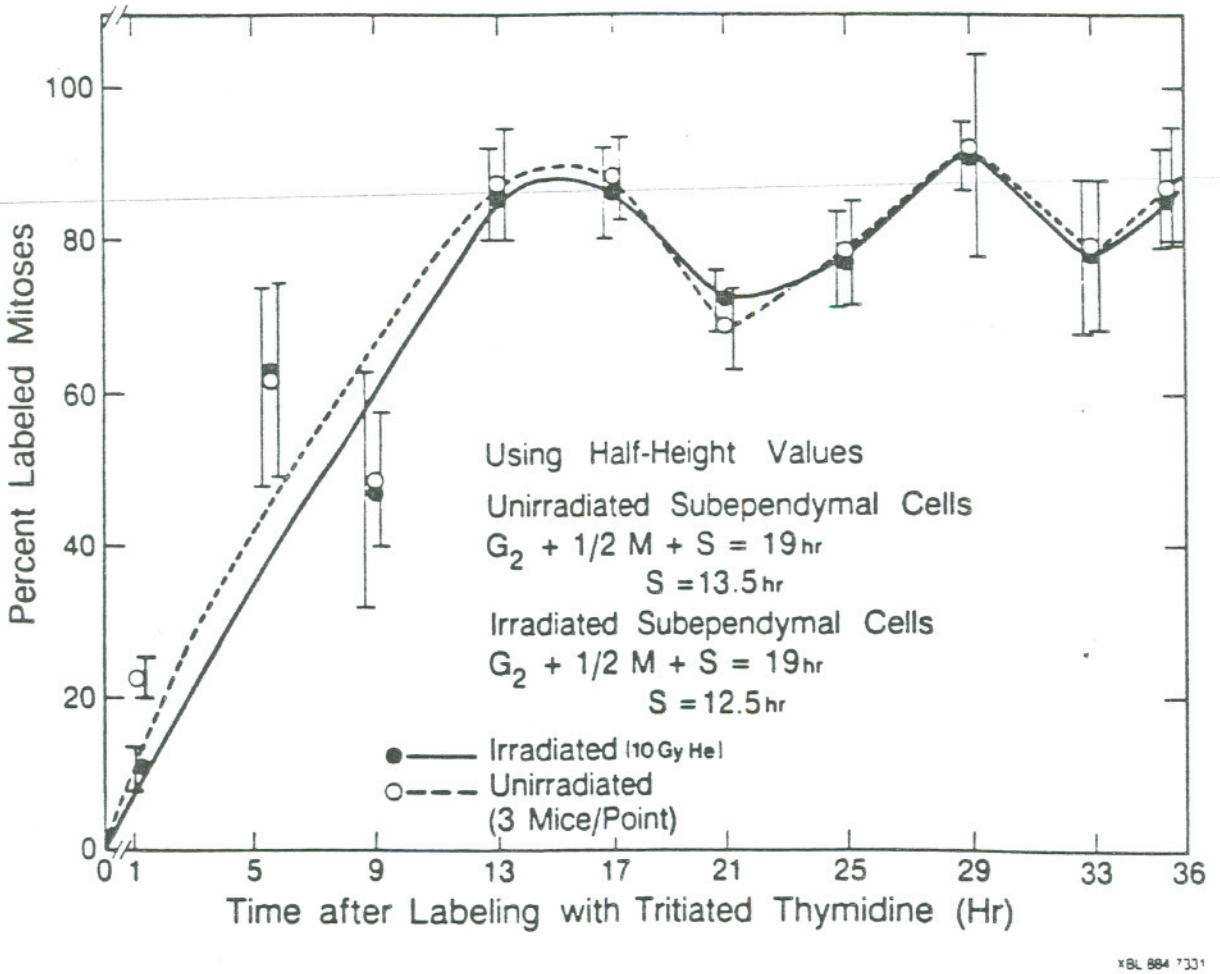

Figure.26 Percent labeled mitoses curves in the subependymal layers, of the unirradiated and the irradiated cortices of the mouse brain, 1 week after partial irradiation of one cortex with 10 Gy He (230 MeV/amu). The ascending and descending limbs of the initial wave were used to estimate the half-height values. Each point on the curves represents the mean values of 3 mice. Table 8b lists the values, their means and the standard deviations.

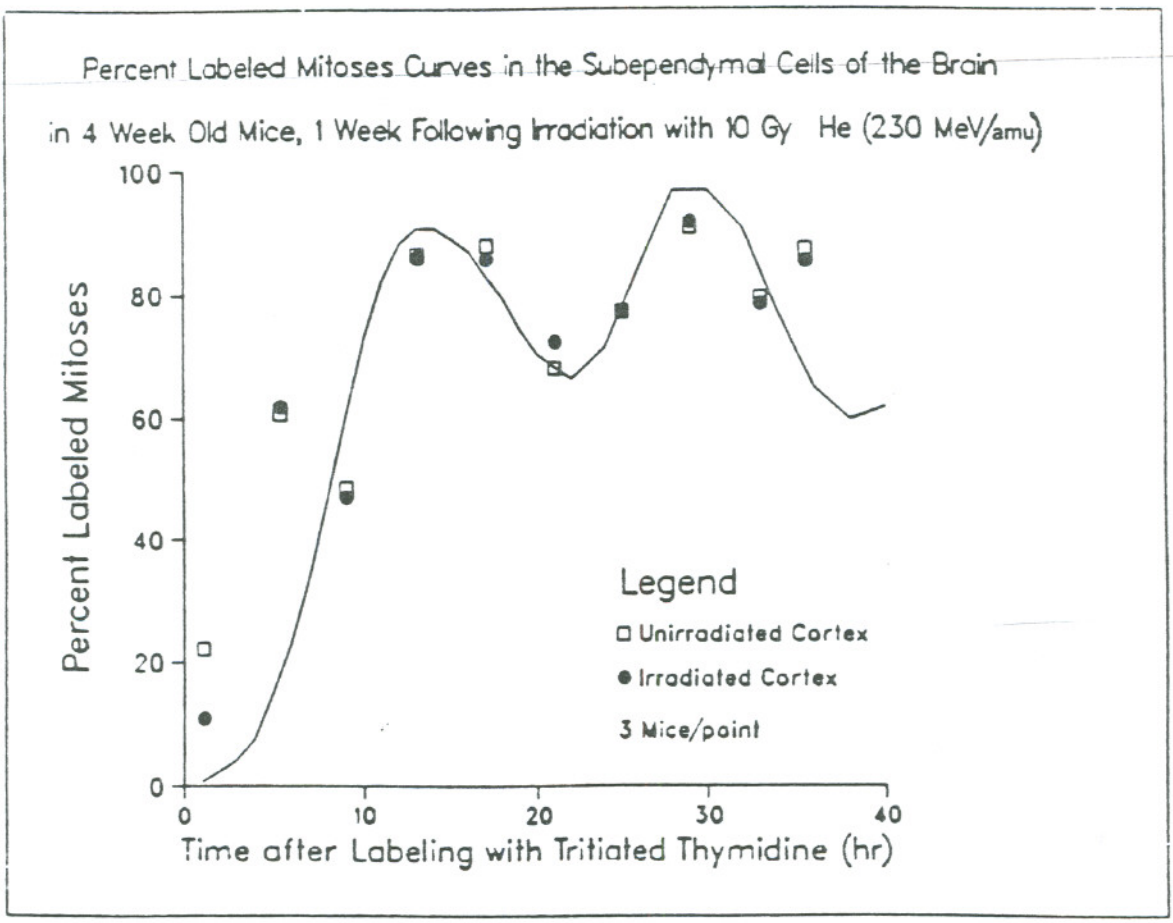

Figure.27 The computer generated PLM curve was drawn by applying the Modified Barrett-Steel Model (Chapter 4). The best computer fit to the sets of data points, in the unirradiated and the irradiated cortices of the irradiated mice generates the same PLM curve. The data points represent the mean values for 3 mice, the standard deviations in the mean values are omitted because the computer model uses these values for generating the curve.

Table 8b Percent labeled mitoses after a pulse of H^3TdR in subependymal cells one week after irradiation with 10 Gy He (230 MeV/amu)

No of Animals	Hours after H^3TdR	Unirradiated Cortex			Irradiated Cortex		
		Percent Labeled Mitoses	Mean	S.D.	Percent Labeled Mitoses	Mean	S.D.
3	1.15	22.20 - -	22.20	-	11.10 - -	11.10	-
4	5.45	56.8 79.6 51.0 55.0	60.60	12.90	51.8 52.6 81.2 61.8	61.85	13.68
3	9	38.4 52.6 53.8	48.27	8.57	29.8 54.0 57.1	46.90	15.06
3	13	90.3 77.7 90.9	86.30	7.45	78.7 88.8 90.0	85.83	6.21
4	17	88.4 91.6 91.0 80.0	87.75	5.35	90.9 82.3 90.1 79.5	85.70	5.67
2	21	64.7 71.4	68.05	4.74	89.3 75.0	72.30	3.82
2	25	82.1 72.2	77.25	7.00	81.8 72.4	77.10	6.65
2	29	100.0 81.5	90.75	13.08	88.8 94.4	91.60	3.96
2	33	72.0 86.5	79.25	10.25	70.6 86.0	78.30	10.89
2	35.30	92.5 81.5	87.00	7.78	90.0 80.4	85.20	6.79

The best fit to the generated curve for a value for the S phase, using the half-height values for the ascending limb and the descending limb of the initial wave, estimates a T_S of 20 hr (unirradiated) and 19 hr (irradiated). This compares well with the value for T_S obtained by using the variation of the Barrett-Steel model, $T_S = 15$ hr. The cell cycle phase durations derived from the computer model identifies two cell populations, one with a cell cycle time, T_C, of 32 hr and, the other with a T_C of 25 hr. The only difference in the phase durations of the two cell populations is the duration of the S phase, the other phase durations are very similar. The mixed cell population has a $T_S = 15$ hr while the second cell population has a $T_S = 8$ hr (Table 11).

Comparing the cell cycle phases for the control subependymal cell population and those in the irradiated mice exposed to 10 Gy He, there is little difference between the phase durations for the mixed cell population and the control cell population. The second cell population, however, has a shorter S phase as compared to the control cell population (20 hr vs. 8 hr), the other cell cycle phases are however the same for both the cell populations.

The subependymal cell cycle one week following irradiation with 25 Gy He (230 MeV/amu)

The PLM curves fit by eye and by the modified Barrett-Steel model in the subependymal cells of the brain in 4 week old mice one week following irradiation with 25 Gy He (230 MeV/amu) are illustrated in Figs. 28 and 29. The data points are a mean value for 3 mice; these are listed along with their standard deviations in Table 9b. The standard deviations are wide, a measure of the individual biological variation in the mice.

The unirradiated and the irradiated subependymal populations in the irradiated mice are similarily affected. The percent labeled mitoses do not rise above 68%. The S phase durations derived by measuring the half-height values of the ascending and descending limbs of the initial wave are: $T_S = 23$ hr (unirradiated population), $T_S = 18.5$ hr (irradiated population). These do not compare well with the value, $T_S = 8$ hr, derived from the computer-generated curve. The computer-generated PLM curve is based on 2 cell populations with the same cell cycle phases, i.e., the T_{G_1} is extended to 40 hr, the T_S is 8 hr and the T_{G_2} is 8 hr (Table 11).

Comparison of the cell cycle phases of the control cell population with that of the cell population following irradiation (25 Gy He) demonstrates an increase in the cell cycle duration, T_C, mainly due to an increase in the G_1 phase (8 hr vs. 40 hr). The S phase durations derived by the eye-fit are similar to the T_S in the control population (12 hr vs. 20 hr), whereas the value for T_S derived from

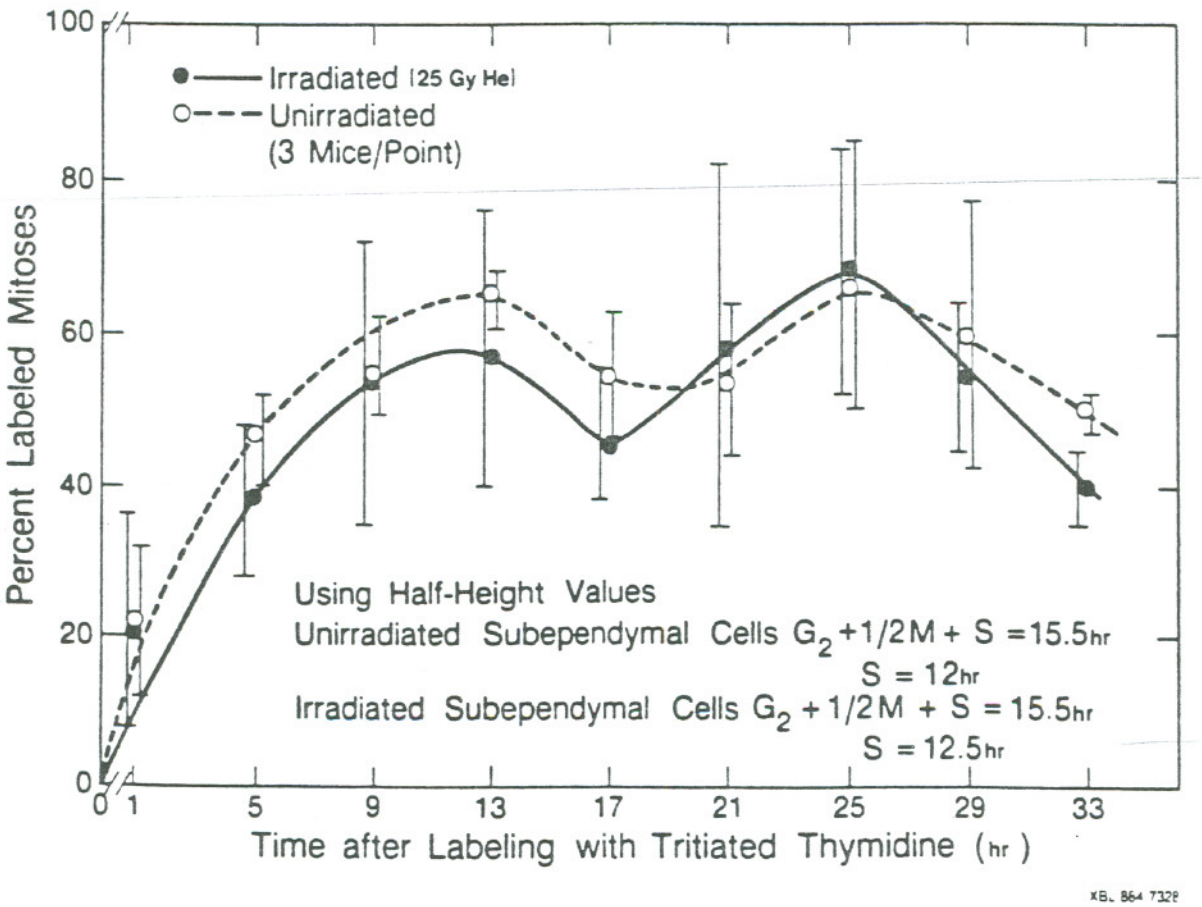

Figure.28 Percent labeled mitoses curves in the subependymal layers, of the unirradiated and the irradiated cortices of the mouse brain 1 week after partial irradiation of one cortex with 25 Gy He (230 MeV/amu). The ascending and descending limbs of the initial wave were used to estimate the half-height values. Each point represents the mean values of 3 mice per data point. Table 9b lists the values, their means and the standard deviations.

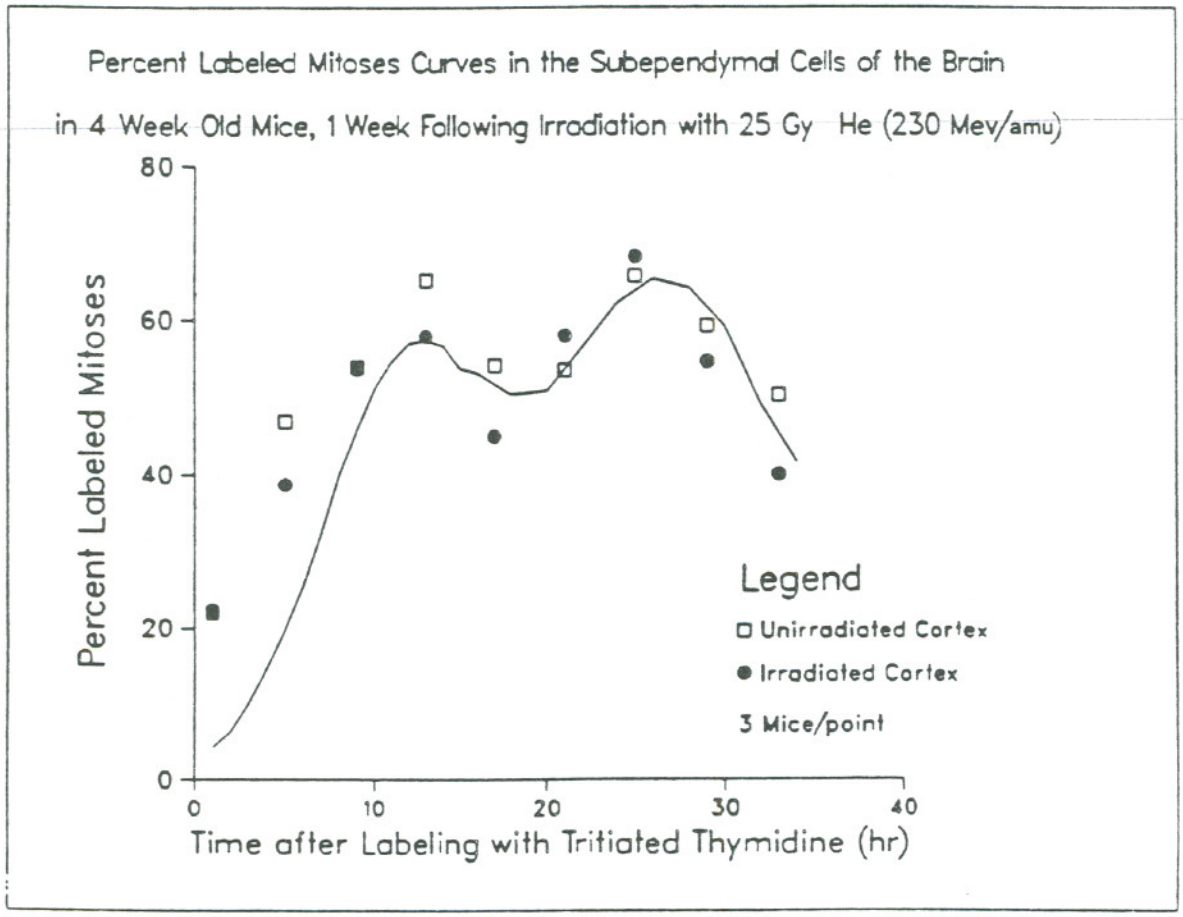

Figure.29 The computer generated PLM curve was drawn by applying the Modified Barrett-Steel Model (Chapter 4). The best computer fit to the sets of data points, in the unirradiated and the irradiated cortices of the irradiated mice generates the same PLM curve. The data points represent the mean values for 3 mice, the standard deviations in the mean values are omitted because the computer model uses these values for generating the curve.

Table 9b: Percent labeled mitoses after a pulse of H^3TdR in subependymal cells one week after irradiation with 25 Gy He (230 MeV/amu)

No. of Animals	Hours after H^3TdR	Unirradiated Cortex			Irradiated Cortex		
		Percent Labeled Mitoses	Mean	S.D.	Percent Labeled Mitoses	Mean	S.D.
3	1	31.6 21.3 13.2	22.03	9.22	23.9 7.1 36.0	22.33	14.51
3	5	45.5 41.8 53.4	46.90	5.43	36.8 30.0 49.0	38.60	9.63
3	9	47.2 53.4 60.7	53.77	6.76	31.6 68.3 61.1	53.67	19.45
3	13	68.9 64.9 61.9	65.23	3.51	37.5 67.5 68.6	57.87	17.65
3	17	45.7 55.4 61.3	54.13	7.88	53.2 33.3 48.5	45.00	10.40
3	21	40.6 60.0 60.0	53.53	11.20	32.7 80.0 61.2	57.97	23.83
3	25	56.3 88.8 52.4	65.83	19.99	56.4 86.6 61.9	68.30	16.09
3	29	67.1 38.1 72.7	59.30	18.57	62.0 44.0 57.9	54.63	9.43
3	33	47.4 51.3 52.2	50.30	2.55	40.5 44.7 35.0	40.07	4.86

the computer model is much shorter (8 hr). A better minimization routine for the computer model would be necessary to derive more accurate cell cycle phase durations. There is no evidence of the second cell population with a shorter cell cycle time. This subpopulation could have been severely damaged resulting from irradiation with the relatively high dose of 25 Gy He.

The subependymal cell cycle one week follwing irradiation with 10 Gy Ne (425 MeV/amu).

The PLM curves fit by eye and by using the modified Barrett-Steel model in the subependymal cells of the brain in 4 week old mice one week following irradiation with 10 Gy Ne (425 MeV/amu) are illustrated in Figs. 30 and 31; the data points are a mean value for 3 mice. There is a wide variation in the values for each mouse (Table 10b). The irradiated and the unirradiated subependymal cell populations both, have similar PLM curves.

The values obtained for the duration of the S phase in both cell populations are 18-23 hr. This is estimated by using the half-heights of the ascending and the descending limbs of the labeled initial mitoses wave. The values compare well with the value for the S phase in the unirradiated control cell population, viz., 20-22 hr. The duration of the cell cycle phases derived by the computer-generated model are given in Table 11. There appears to be a subpopulation of cells that may be cycling with a shorter cell cycle, viz., $T_C = 25$ hr. This cell population has the same cell cycle parameters as the one following irradiation with 10 Gy He (Table 11). The cell cycle phases for the mixed cell populations

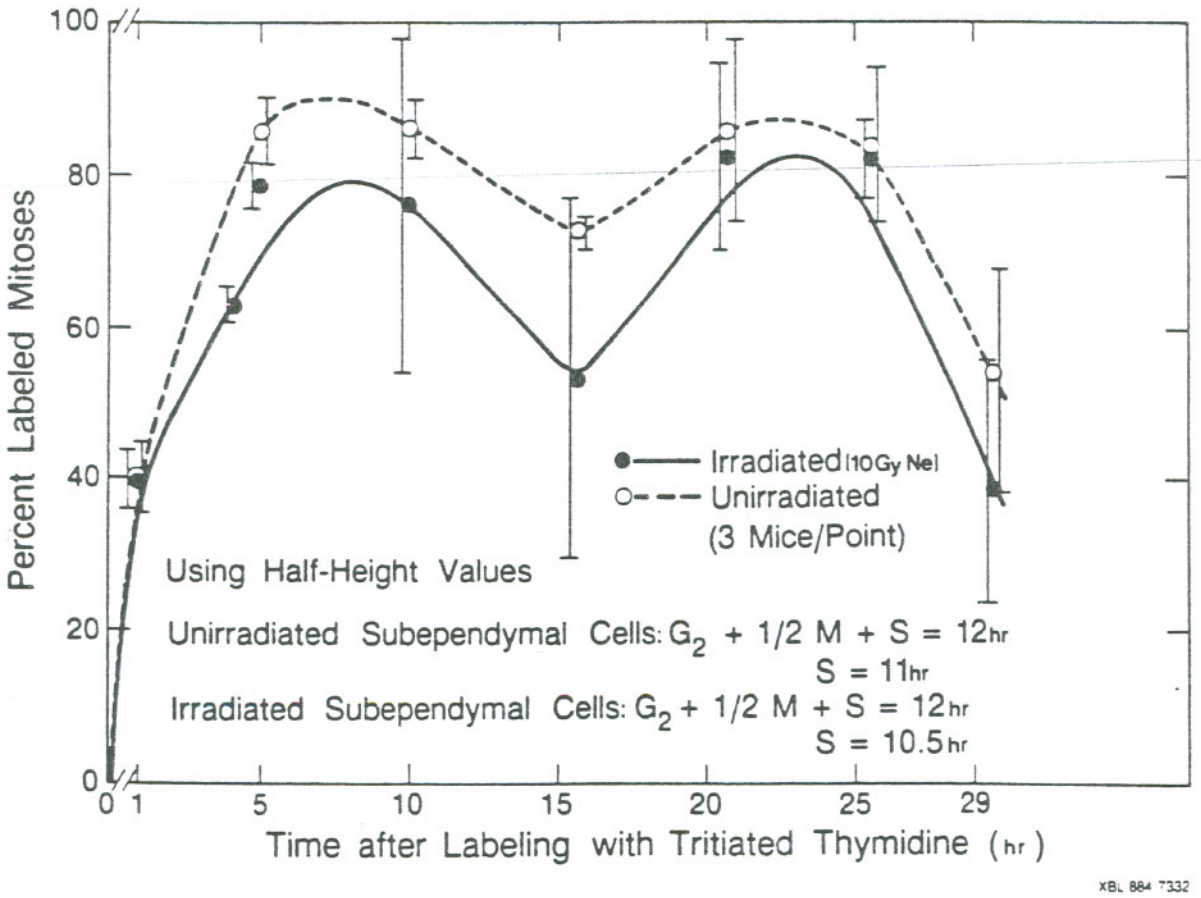

Figure.30 Percent labeled mitoses curves in the subependymal layers of the unirradiated and the irradiated cortices of the mouse brain, 1 week after partial irradiation of one cortex with 10 Gy Ne (425 MeV/amu). The ascending and the descending limbs of the initial wave were used to estimate the half-height values. Each point represents the mean values of 3 mice. Table 10b lists the values, their means and the standard deviations.

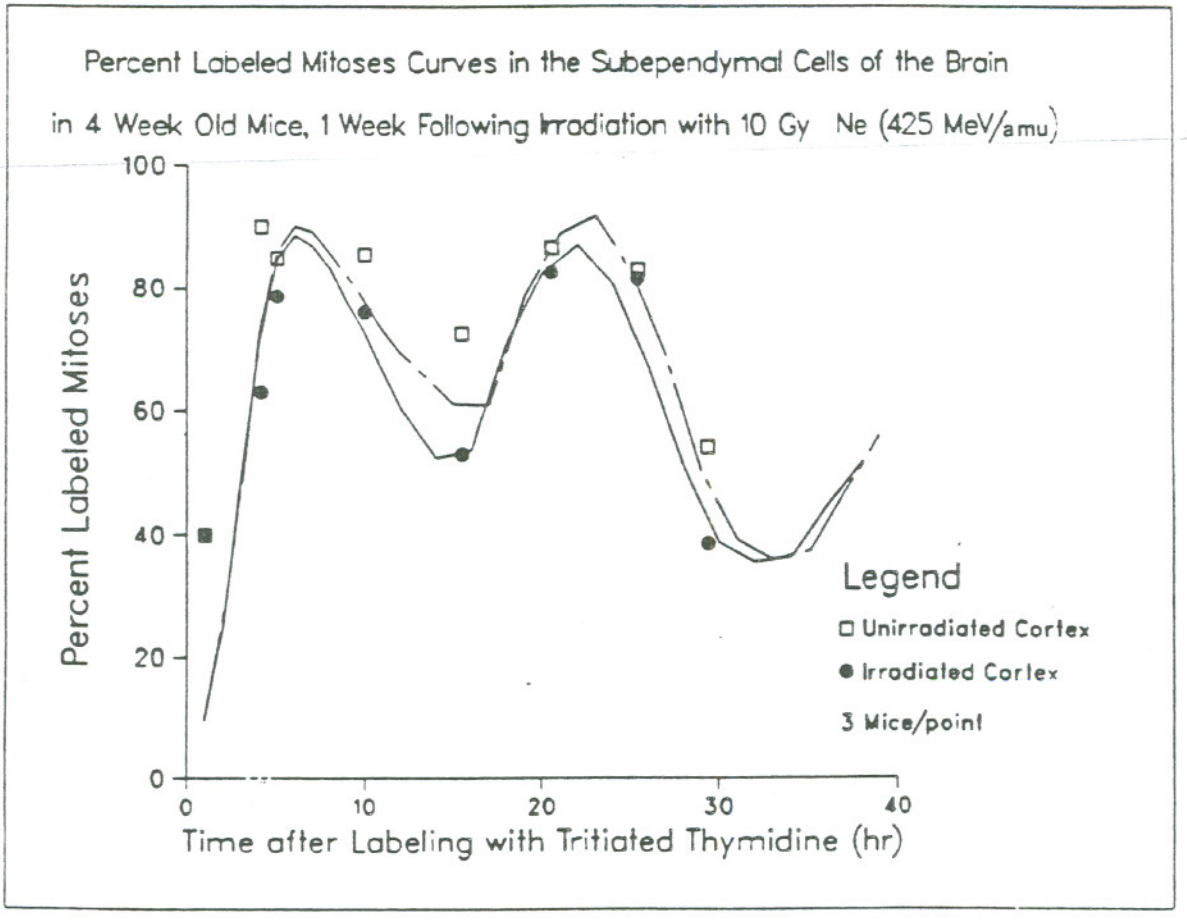

Figure.31 These computer generated PLM curves were drawn by applying the Modified Barrett-Steel Model (Chapter 4). The data points represent the mean values for 3 mice, the standard deviations in the mean values are omitted because the computer model uses these values for generating the curves.

Table 10b: Percent labeled mitoses after a pulse of H^3TdR in subependymal cells one week after irradiation with 10 Gy Ne (425 MeV/amu)

No. of Animals	Hours after H^3TdR	Unirradiated Cortex			Irradiated Cortex		
		Percent Labeled Mitoses	Mean	S.D.	Percent Labeled Mitoses	Mean	S.D.
3	1	- 58.3 64.3	61.30	4.24	- 62.5 57.1	59.80	3.82
1	4.10'	90.5	90.5	-	63.2	63.2	-
3	5	87.3 80.6 86.7	84.87	3.71	78.1 77.2 81.0	78.77	1.99
3	10	87.1 84.4 85.7	84.87	3.71	88.0 50.0 90.2	76.10	22.60
3	15.45'	71.0 73.7 72.9	72.53	1.39	66.7 24.3 68.2	53.01	24.92
3	20.45'	86.0 74.5 98.6	86.37	12.05	75.0 76.7 95.8	82.5	11.55
4	25.40'	67.5 87.5 92.6 82.5	82.53	10.83	79.7 76.7 87.5 81.4	81.33	4.55
3	29.40'	69.6 50.0 42.9	54.17	13.83	44.6 18.8 51.6	38.33	17.28

Table 11: Cell Cycle Durations (hr) for the Control and Irradiated Subependymal Cell Populations

<table>
<tr><td colspan="4">Unirradiated Control Mice‡</td></tr>
<tr><td colspan="2">Left Cortex
$T_{G_1} = 8 \pm 4$ hr
$T_S = 22 \pm 8.8$ hr
$T_{G_2} = 8 \pm 4$ hr
$T_M = 1$ hr
$T_C = 39 \pm 16.8$ hr</td><td colspan="2">Right Cortex
$T_{G_1} = 8 \pm 4$ hr
$T_S = 20 \pm 8$ hr
$T_{G_2} = 8 \pm 4$ hr
$T_M = 1$ hr
$T_C = 37 \pm 16$ hr</td></tr>
<tr><td colspan="4">1 week following 10 Gy He^+ (230 MeV/amu)</td></tr>
<tr><td colspan="2">Mixed cell population
$T_{G_1} = 8 \pm 3$ hr
$T_S = 15 \pm 6$ hr
$T_{G_2} = 8 \pm 3$ hr
$T_M = 1$ hr
$T_C = 32 \pm 12$ hr</td><td colspan="2">Second cell population
$T_{G_1} = 8 \pm 3$ hr
$T_S = 8 \pm 3$ hr
$T_{G_2} = 8 \pm 3$ hr
$T_M = 1$ hr
$T_C = 25 \pm 9$ hr</td></tr>
<tr><td colspan="4">1 week following 10 Gy Ne^+ (425 MeV/amu)</td></tr>
<tr><td colspan="2">Irradiated S.E. Cell Population</td><td colspan="2">Unirradiated S.E. Cell Population</td></tr>
<tr><td>Mixed cell population
$T_{G_1} = 20 \pm 10$ hr
$T_S = 10 \pm 5$ hr
$T_{G_2} = 3 \pm 1.5$ hr
$T_M = 1$ hr
$T_C = 34 \pm 16.5$ hr</td><td>2nd cell population
$T_{G_1} = 8 \pm 3$ hr
$T_S = 8 \pm 3$ hr
$T_{G_2} = 8 \pm 3$ hr
$T_M = 1$ hr
$T_C = 25 \pm 9$ hr</td><td>Mixed cell population
$T_{G_1} = 20 \pm 10$ hr
$T_S = 12 \pm 6$ hr
$T_{G_2} = 3 \pm 1.5$ hr
$T_M = 1$ hr
$T_C = 36 \pm 17.5$ hr</td><td>2nd cell population
$T_{G_1} = 20 \pm 3$ hr
$T_S = 8 \pm 3$ hr
$T_{G_2} = 8 \pm 3$ hr
$T_M = 1$ hr
$T_C = 25 \pm 9$ hr</td></tr>
<tr><td colspan="4">1 week following 25 Gy He^+ (230 MeV/amu)</td></tr>
<tr><td colspan="2">Mixed cell population
$T_{G_1} = 40 \pm 20$ hr
$T_S = 8 \pm 6$ hr
$T_{G_2} = 8 \pm 4$ hr
$T_M = 1$ hr</td><td colspan="2">Second cell population
same parameters, but start cycling 15 hrs later
$T_C = 56 \pm 30$ hr</td></tr>
</table>

† Cell cycle phases obtained by using the Modified Barrett-Steel PLM Model for the "computer fit" to the experimental data points.

‡ Cell cycle phases obtained by using the Barrett-Steel PLM Model for the "computer fit" to the experimental data points.

are: T_{G_1} = 20 hr, T_S = 10-12 hr, T_{G_2} = 3 hr and T_C = 34-36 hr.

Comparison of the parameters for the duration of cell cycle phases of the control cell population and the mixed cell population in the irradiated mice (10 Gy Ne) indicates an apparent increase in the duration of the G_1 phase with a shortening of the S phase following irradiation. However, the cell cycle times in both the populations are similar, viz., T_C = 34-39 hr. The irradiation appears to have triggered a subpopulation of cycling cells with a shorter cell cycle time into the proliferating stem-cell compartment which is proliferating along with the mixed cell population (Table 11). Comparison of the cell cycle kinetic parameters of the subependymal cell population following 10 Gy Ne, and 10 Gy He, shows a population with a shorter cell cycle that has been stimulated to proliferate more rapidly in both cases. There also appears to be a lengthening of the G_1 phase following irradiation with 10 Gy Ne which is not seen after irradiation with 10 Gy He.

Comparison of the cell cycle kinetic parameters in the subependymal population after irradiation with 25 Gy He, and 10 Gy Ne, indicates no evidence of stimulation of a cell population with a shorter cell cycle following irradiation with 25 Gy He. There is a lengthening of the G_1 phase in both groups of irradiated mice, and this appears to be somewhat more after irradiation with 25 Gy He than after 10 Gy Ne.

Cell kinetic analysis of subependymal cells in unirradiated and irradiated mice

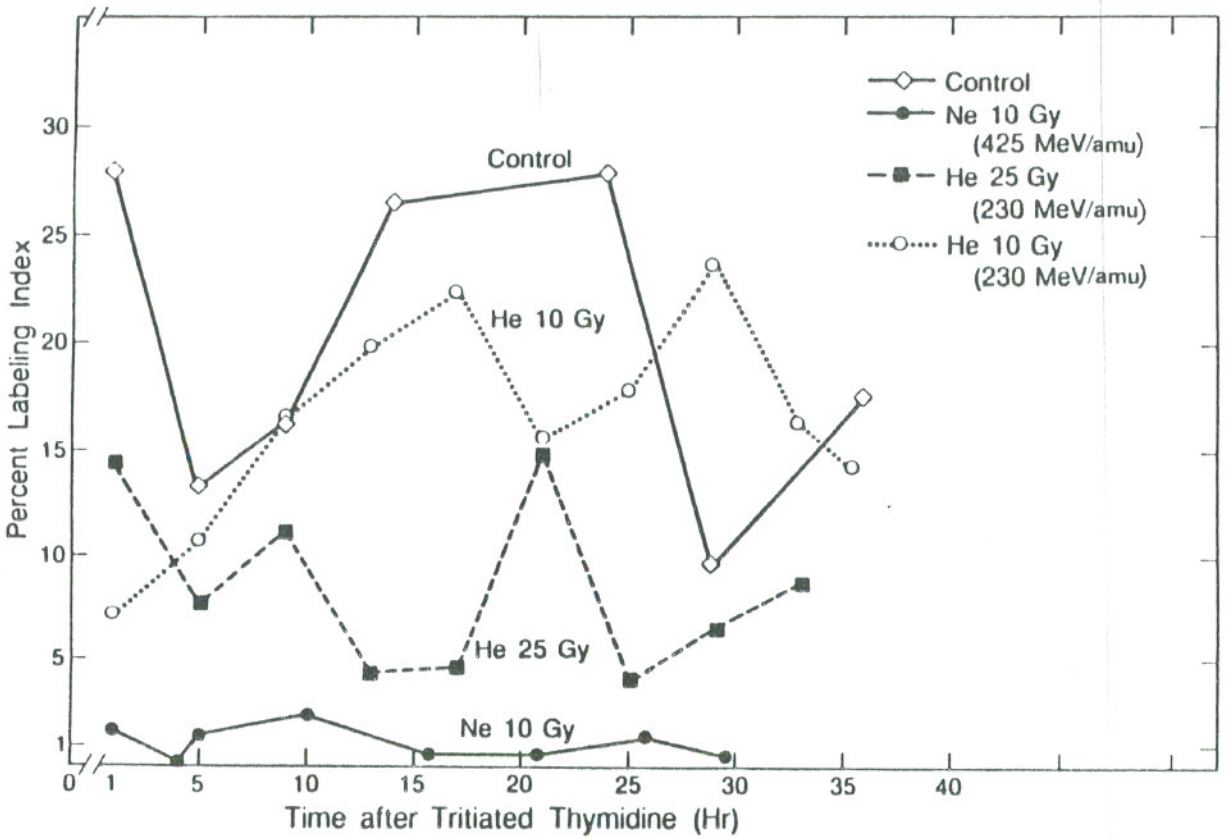

Figure.32 Percent labeling indices in the subependymal layer of the unirradiated mice and the subpendymal layer in the irradiated cortices of the irradiaed mice, 1 week following irradiation with 10 and 25 Gy He (230 MeV/amu) and 10 Gy Ne (425 MeV/amu). The indices vary with time after a pulse of tritiated thymidine. The points on the curves are the mean values for 3 mice. The standard deviations are wide and have been omitted here for clarity. Table 12 lists the values, their means and the standard deviations.

Table 12: Thymidine labeling indices in subependymal cells of control mice and irradiated mice 1 week following exposure to He 10 Gy, Ne 10 Gy, He 25 Gy.

Hours after H^3TdR	% Labeling Indices				Mean				Standard Deviation			
	He 10 Gy	Ne 10 Gy	He 25 Gy	Control	He 10 Gy	Ne 10 Gy	He 25 Gy	Control	He 10 Gy	Ne 10 Gy	He 25 Gy	Control
1	7.78 8.20 5.44	0.10 1.00 4.00	21.50 20.80 0.83	19.0 21.0 22.0	7.14	1.7	14.38	21.35	1.41	2.04	11.74	1.71
4.10'	-	0.20	-	-	-	0.2	-	-	-	-	-	-
5	11.87 12.05 13.12 6.00	3.00 1.00 0.20 -	16.10 1.90 5.30 -	16.5 12.6 10.6 -	10.76	1.4	7.76	13.23	3.22	1.44	7.41	3.0
9	3.70 19.97 26.52	- - -	2.30 8.80 22.90	23.1 17.3 8.3	16.73	-	11.33	16.23	11.75	-	10.53	7.46
10	- - -	0.05 0.40 6.00	- - -	- - -	-	2.15	-	-	-	3.34	-	-
13	30.05 17.05 12.33	- - -	1.04 2.92 8.50	- - -	19.81	-	4.15	-	9.18	-	3.88	-
14	- -	- -	- -	27.0 26.0	-	-	-	26.5	-	-	-	0.71
15.45'	- - -	0.50 0.20 1.00	- - -	- - -	-	0.56	-	-	-	0.40	-	-
17	19.02 30.23 31.05 8.96	- - - -	8.60 0.60 4.90 -	- - - -	22.32	-	4.7	-	10.46	-	4.01	-

Table12 Continued

Hours after H^3TdR	% Labeling Indices				Mean				Standard Deviation			
	He 10 Gy	Ne 10 Gy	He 25 Gy	Control	He 10 Gy	Ne 10 Gy	He 25 Gy	Control	He 10 Gy	Ne 10 Gy	He 25 Gy	Control
20.45'	- - -	1.0 0.3 0.4	- - -	- - -	-	0.56	-	-	-	0.38	-	-
21	13.41 17.56	- -	19.34 8.76	- -	15.49	-	14.92	-	2.93	-	5.50	-
24				34 23 26 28.6	-	-	-	27.9	-	-	-	4.67
25	22.36 13.40 -	- - -	7.9 2.5 1.76	- - -	17.88	-	4.05	-	6.34	-	3.35	-
25.40'	- - - -	2.0 1.0 1 1	- - - -	- - - -	-	1.25	-	-	-	0.50	-	-
29	24.32 23.00 -	- - -	13.4 4.6 1.5	9.53 - -	23.66	-	6.50	9.53	0.93	-	6.17	-
29.40'	- - -	1 0.2 0.5	- - -	- - -	-	0.56	-	-	-	0.40	-	-
33	11.87 20.45 -	- - -	6.0 16.1 4.8	- - -	16.16	-	8.97	-	6.07	-	6.21	-
35.30'	7.96 20.58	- -	- -	- -	14.27	-	-	-	8.92	-	-	-
36	- - - -	- - - -	- - - -	34.9 24.2 4.0 6.7	-	-	-	17.45	-	-	-	14.68

The H^3-TdR percent labeling index in the control animals, 1 hr after the pulse of H^3-TdR is 28%; it falls to 13.2% at 5 hr, and then rises to a maximum of 26.5% at 14 hr. This LI is maintained until 24 hr then falls to 9.53% at 29 hr; this is again followed by a rise to 17.45% at 36 hr. This is illustrated in Fig. 32. One week following exposure to 10 and 25 Gy He (230 MeV/amu), irradiation of the brain with 10 Gy He has very little effect on the percent labeling index, while 25 Gy He decreases the labeling index by as much as 50% as compared to the labeling index in the unirradiated control mice. However the characteristic temporal pattern of the LI curves are the same (Fig. 32).

Comparison of an irradiated percent labeling index curve in the subependymal layer, one week following brain irradiation with a dose of 10 Gy Ne (425 MeV/amu), with the control curve (Fig. 32) demonstrates a marked decrease in the labeling indexes after this irradiation. The maximum percent labeling index after exposure to 10 Gy Ne was 2.15%, whereas the maximum percent labeling index in the control subependymal cell populations was 28%, a decrease by more than a factor of 10 (Table 12). Once again the overall characteristic temporal pattern of the labeling index curves appears the same in both these cases. One week after irradiation with 10, 25 Gy He, and 10 Gy Ne, 10 Gy Ne is the most effective in decreasing the percent labeling index, either by decreasing the number of cells capable of synthesizing DNA or decreasing the duration of the S phase, or both.

Chapter 5

Discussion and Conclusions

5.0 Cell Kinetic parameters in the normal subependymal cell population

H^3-TdR labeling index in the subependymal cell control population

The H^3-TdR labeling index identifies the number of cells in the proliferating pool, the sites of the proliferating cells and the fates of these cells. The percent LI in the subependymal layer varies between 17.35%-26.35% in part, depending on location and types of cells that are in cell cycle (Table 1b) with time after a pulse of H^3-TdR, indicating that a maximum of 26.4% of the cell population is in DNA synthesis at the time of labeling. The LI varies with sites within the mouse brain. The olfactory lobe (level 1, Fig. 13) consistently shows the lowest LI whereas it is the highest in the regions of the optic chiasma (level 2, Fig. 13) and the median eminence (level 3, Fig. 13). The greatest number of cells in the subependymal layer are found at the level of the corpus callosum (seen in level 3) where the layer is 6-7 cells thick and appears to extend out into the corpus callosum. It is at this level in the mouse brain, that subependymal cells were found at any appreciable distance from the lining of the lateral ventricle. The corpus callosum has been identified as the site for migration of these subependymal cells. They migrate to the deeper levels of the cortex. (Leblond, 1961; Patterson et al., 1973).

Histologically, the cell populations of this layer comprise 3 distinct types of cells based on their nuclear appearance, viz., the SD (small dark), SL (small light), and LL (large light) cells (Fig. 4, Chapter 1). It is the SD cells that are labeled most frequently and usually appear as groups of 3 or 4 labeled cells. The SL and LL cells are scattered and more often found on the outer borders of the subependymal layer and in the corpus callosum. The labeling indices in both the subependymal layers of the left and right cortices in the mouse brain were very similar.

Mitotic index in the control population

The percent mitotic index in the control subependymal population varies between 0.2%-1.5%, in part depending on location. The mitotic index is generally a reliable indication of the rate of cell birth and depends on the mitotic rate and the duration of mitosis (Chapter 2). This low mitotic index reflects a low birth rate of cells, due either to a few cells dividing or a very long cell cycle time. Since the labeling index is relatively high, it follows that the cell cycle duration must be relatively long compared to the duration of mitosis, or that there are a number of subpopulations of cells with different cycling times, or both. The mitoses were seen in all 3 types of cells (SD, SL, LL), but were more frequent in the SD cells, indicating that it is the SD cells that are mainly responsible for the birth of new cells in the subependymal cell population. There was no distinct overall pattern of the distribution of the mitotic cells and similar number of mitoses were seen in both the subependymal layers of the left and

right cortices in the mouse brain. Histologic identification of mitoses was very difficult, the low mitotic index may not be a true representation of all the cells entering mitosis, i.e., the value is an underestimate. However, since all the mice show a low MI (Table 7a) and a high labeling index, it is likely that there is a high cell loss rate of cells in the subependymal layer. That this appeared so has been suggested by others (Smart and Leblond, 1961; Korr, 1980) who described numerous pyknotic nuclei in the subependymal layer including labeled pyknotic cells, suggesting a large number of cells enter DNA synthesis but may fail to divide, or die soon after division.

Growth fraction studies in the control subependymal cell population

With repeated H^3-TdR labeling at intervals less than the minimum duration of S and, for a period greater than the maximum cell cycle time, it is possible to label all the cells that are in the proliferative pool and so get an estimate for the growth fraction (GF). For this to be true it is necessary to make specific assumptions about the nature of the nonproliferating cells viz: 1) the static cells will neither divide nor die during the course of the experiment; 2) the end cells will never divide, they have a limited lifespan and may therefore be continuously replaced; 3) the resting cells have the capacity to start proliferation in response to a suitable stimulus but which otherwise may die or leave the population. Hence repeated thymidine labeling will not only progressively label all proliferating cells but will also label the nonproliferating cells that are subject to turnover, if it enters the proliferating cell cycle. Cells identified in (2) and (3) above

will become labeled within approximately one turnover time of the nonproliferating cells, as the latter are replaced by cells (or the descendents of cells) that were proliferated during the administration of the label. In a steady-state population, in a renewing tissue, the proportion of labeled cells during the course of repeated labeling should plateau at a level which includes all but the nonproliferating cells.

Interpretation of a repeated labeling curve should be based on a cell population model that fits the cell population which is being studied. There is usually a short rapid rise in the shape of the curve corresponding to a time equal to the G_2 period which corresponds to the first appearance of labeled cells from mitosis. The change of slope depends on the number of daughter cells produced at each mitosis, and since this is normally two, the link theoretically corresponds to a doubling of the rise of the slope. Only in a cell population in which one cell is lost at the time of each mitosis would the kink be absent. A change of slope is often difficult to demonstrate experimentally due to the effect of variability in the duration of G_2 will be to round off the kink. In such cases it is important to recognize that the early slope of the repeated-labeling curve is not equal to the mitotic rate but is approximately twice the mitotic rate. The rate at which the repeated-labeling curve approaches its asymptote depends in part on the number and distribution of those nonproliferating cells that are being replaced.

The subependymal cell population appears to be an exponentially growing cell population but in a steady-state of growth. There is a wide variation among

the values in individual mice (Table 4) indicating the large biological variations among different animals. In Fig. 20, the slope changes at 7 hr after labeling and the LI approaches a maximum at 19 hr after the first label. This maximum LI is an estimate of the growth fraction (GF = 0.22) for the normal subependymal layer, indicating that more than 20% of cells are in the proliferating population. The rate at which cells are labeled is higher initially (first 7 hr); this could be an indication of the rate at which cells are entering mitoses. The next part of the curve could be an indication of the distributions of the G_1 phase and the age at which the nonproliferating cells are being replaced by newly formed cells. The decrease in LI after the maximum value is reached indicates that the labeled cells are migrating and so leaving the proliferating pool with concomitant decrease in the GF.

Since the LI did not reach 100%, all the cells in the subependymal population are not proliferating. The nonproliferating cells form the non-growth fraction. This pool of nonproliferating cells is believed to consist of differentiating and maturing neural precursor cells, which are migrating into the deeper layers of the cortex (Paterson et al., 1973; Hubbard and Hopewell, 1980). There is probably a constant exchange of cells between the growth fraction and the non-growth fraction within the proliferative zone, as well as a balance between the emigrating and nonmigrating cells, since there is no increase in the total number of cells in the subependymal layer, in spite of the evidence of active proliferation (Smart and Leblond, 1961; Hopewell, 1971).

Mean grain count decrements in the control subependymal cell population

The experimental results (Sec. 4.5, Chapter 4) indicate that all the cells in the subependymal cell population do not show the same rate of decrease of nuclear grain counts over extended intervals (Appendix B). This would suggest the presence of more than one cell population with varying cell cycle durations, and would be in agreement with the concept of a mixed-cell population for the subependymal layer. This is well demonstrated by the presence of the three distinct cell types, the SD, SL, and LL cells, of the subependymal cell layers. The SD cells show a faster grain-count decrease than the SL and LL cells, suggesting that the SD cells are dividing more rapidly with a shorter cell cycle than the SL or LL cells. Since the grain counts (Fig. 19) are average values, variation among different mice could prove important in determining the slope of the decline and thus the decrement in grain counts. The time required for the average grain count to fall to 50% of the original value is a rough estimate of the cell cycle time, and a measure of the population doubling time for the proliferating cells in this population. T_d would be much longer than the cell cycle duration for any of the cells in the population. There is a pool of nonproliferating cells in the subependymal layer as well and some of these cells may be lost through degeneration, death or migration, while some remain a part of the proliferating zone of the subependymal layer. Thus, the population doubling time calculated from the grain-count decrements will not account for these nonproliferating cells which remain unlabeled; the latter cells may be in a G_0 phase, a prolonged G_1

phase, or permanently out of cycle (Fabrikant, 1966).

Cell cycle kinetics in the control subependymal cell population; the PLM curves

The PLM curves derived by best fit to the experimental data and by the computer-generated Barrett-Steel Model give an estimate of the duration of the cell cycle and its phase durations for the cells in the subependymal layer. The computer-generated model includes a value for the means along with their standard deviations in the program and so gives a value for the cell cycle phases and a value for the expected variation (see Table 11). In Fig. 31, for example, the mean of the values for 3 mice per point (Table 7b) are given. The standard deviations indicate the broad biological variation among the individual animals.

The value of $T_s = 16.5$ hr for the duration of the S phase duration obtained by using the half-height values measured directly from the ascending and descending limbs of the initial wave (Fig. 24) is a reliable estimate and falls within the limits of the variation (Table 11). The cell cycle time, $T_c = 37\text{-}39$ hr obtained by the computer-generated model is longer than that obtained by Hubbard and Hopewell (1980) for the subependymal cells in 12 week old rats. They used a similar computer simulation model for their data and derived a value of $T_c = 22.6$ hr. However, they used only one rat per experimental point and did not give values for the possible variations in cell cycle times. The $T_c = 22.6$ hr is however within the limits of the cell cycle time, $T_c = 37 + 16$ hr, and this could be in accord with the mouse dsata. However, species variation would account for major differences in the cell cycle kinetics parameters measured in

this manner.

The values for the durations of the cell cycle phases obtained by Hubbard and Hopewell for the subependymal layer in 12 week old rats are: $T_{G1} = 0.2$ hr; $T_{G2} = 3.1$ hr; $T_s = 18.6$ hr.

Comparing these values with those in table 10 on the 4 week old mouse, the value for $T_s = 22 + 8.8$ hr is the only one that compares well with their values and the value for T_{G2} is close to the minimum value indicated in the control data in the mouse. The value $T_{G1} = 8 + 4$ hr (Table 11) is longer than that obtained by Hubbard and Hopewell (1980). However, they used 1 animal per data point (12 week old rats) whereas we used 3-4 animals per data point (4 week old mice). The control PLM curve generated in the current experiments appear to indicate the presence of of a mixed-cell population, because cells with varying cell-cycle phases would tend to give a greater spread in values for the individual cell cycle phases, if they are all considered as one asynchronous cell population. The shape of the curve will be dominated by the largest fraction of cells that are proliferating which appears to be the SD cell population. Nevertheless, the technique here has certain limitations; it is frequently difficult to identify the precise cell type in mitoses in the three different types of cells (SD, SL, LL) in the subependymal layer with light microscopy techniques. When scoring a labeled mitosis, it is frequently difficult to tell with certainty if the labeled subependymal cell is a SD, SL, or an LL cell. Frequently, only the chromosomal configuration of a cell in metaphase or anaphase with associated silver

halide grains over it is all that is identifiable as a labeled mitosis.

5.0.1 Conclusions on the cell population and cell cycle kinetics of the normal subependymal layer cells in the mouse brain

1) Different histologic sites in the subependymal layer of the young mouse brain show different rates of cell proliferation as indicated by the variations in the LI at the different locations and different levels within the brain. The greatest number of labeled cells appear at the level of the corpus callosum, less at the level of the posterior thalamus, and less in the region of the olfactory lobes.

2) In spite of a moderately high tritiated thymidine LI there is a relatively low MI. This suggests a low birth rate in the proliferating cell population. This may be due to either many cells all proliferating with short T_s , or a few with a large T_s , and a short T_M relative to the mean T_c .

3) This is a mixed cell population of at least 3 types of cells in the subependymal plate (SD, SL, LL). These are in various stages of proliferation, differentiation and migration in the young mouse brain.

4) The SD cells have the highest labeling and mitotic indices, and are mainly responsible for the birth of new cells in the subependymal cell population. All three cell types (SD, SL, and LL) undergo mitosis, however, indicating that all these cells are capable of proliferation and are in the growth fraction of the zone of proliferation.

5) The SD cells show a more rapid grain count decrement than the SL and LL cells. This would indicate that the SD cells have a shorter cell cycle time and could be the more rapidly cycling precursor stem cells for this subependymal cell population.

6) All the cells in the subependymal layer are not proliferating; the growth fraction (GF) does not exceed 0.22 indicating that the size of the proliferating population does not exceed 78% of the cells. Both proliferating and nonproliferating cells appear to migrate out of the zone of proliferation or the subependymal cell population along with a controlled exchange between the growth fraction and the non-growth fraction of the subpopulations of cells.

7) Measurement of cell cycle parameters using analysis of cell population kinetics indicate a cell cycle $T_c = 37 + 16$ hr, $T_s = 20 + 8$ hr, $T_{G1} = 8 + 4$ hr, $T_{G2} = 8 + 4$ hr and $T_M = 1$ hr.

8) There is a wide biological variation among the individual mice as regards tritiated thymidine labeling, sites of cell proliferation, and the sizes of the proliferating populations.

5.1 Effects of 10 Gy He (230 MeV/amu) irradiation on the subependymal layer cell populations

The partial irradiation of one cortex of the mouse brain has similar effects on the cell population and cell cycle kinetics of both subependymal cell layers. The cell population in the irradiated cortex has slightly lower L1 and M1 indices than the one in the unirradiated cortex.

Effects on the labeling and mitotic indices after exposure to 10 Gy He (230 MeV/amu)

The percent labeling index 48 hr after exposure to 10 Gy He was 11.8% in the irradiated cortex as compared to 13.1% in the unirradiated cortex (Table 3). One week later, the H^3-TdR LI varied between 7.14% - 23.66% in the irradiated cortex and between 9.06% - 35.02% in the unirradiated cortex (Table 12). There was no significant difference in the labeling indices, 48 hr or 1 week after the exposure. Comparison of these LI values with those in the unirradiated control population (Table 3) demonstrates there is a decrease of 26.3% in the irradiated cortex and a decrease of 18.1% in the unirradiated cortex. Comparison of the LI curves for the control population and those of the He 10 Gy irradiated population (Fig. 32) the overall temporal pattern of labeled cells in the subependymal layer appears to be roughly the same.

One week after irradiation, the mitotic index in the irradiated cortex varied between 0.59% - 4.5%, whereas in the unirradiated cortex the values vary between 0.56% - 3.7%, once again, no significant differences in the cortices. Comparing these mitotic indices with those in the unirradiated control population (0.4% - 1.1%), the MI values in the control are less variable and somewhat lower. The occasional higher numbers of mitoses seen in the irradiated subependymal population one week following exposure to 10 Gy He appears to be due to an increased birth rate of the SD cells since these are the cells that show mitoses more frequently than the other cells; this could be a compensatory mechanism of

increased cell birth as a result of a loss of cells due to radiation injury.

The cell cycle phase durations and the cell cycle time after exposure to 10 Gy He (230 MeV/amu)

The PLM curves fit to the experimental data and by using the Barrett-Steel Modified model give values for the durations of the cell cycle phases and the cell cycle which compare reasonably well (Table 11 and Fig. 26). The PLM curves for the 2 cortices similar and the computer-generated model indicates that one PLM curve fits for both data sets. The PLM curves demonstrate two waves and a shallow trough of labeled mitoses by 21 hr. A modification of the Barrett-Steel model was necessary to fit the computer-generated curve to the data points. On the assumption of a mixed cell population and of an SD cell response to radiation (see Hubbard and Hopewell, 1980) that is similar to the response of a resting stem-cell population, a modification of the Barrett-Steel model was made. Here, one of the cell populations in the mixed cell population was believed to be stimulated to proliferate with a shorter cell cycle. The cell population stimulated to proliferate is assumed to be a subpopulation within the stem cell population, and with a cell cycle duration T_c of approximately 25 hr (Table 11). The second wave of labeled mitoses (Fig. 34) would represent this cell population which started dividing 10 hr after labeling with H^3-TdR. The first wave is assumed to be derived from a combination of the labeled mitoses seen in SD, SL and LL cells. In the second peak there is probably a preponderance of SD cells which have been stimulated to proliferate due to the irradiation injury (10 Gy

He). Hence, the second wave would be dominated by the cell cycle characteristics of the SD cells.

A similar concept has been discussed by Lajtha and Oliver (1962) in their studies relating to hematopoietic stem cell populations. They describe a proliferating cell population in a steady state where this state is maintained by a continuous removal of cells from a continuously proliferating population (stem type 1). The subependymal cell poulation may have a similar arrangement and a certain dose range of helium ions could damage the cell population sufficiently so that there results stimulation of the stem population to proliferate in order to maintain the irradiated subependymal population levels as near-normal as possible.

The computer-generated Barrett-Steel model analysis demonstrated that there are at least two subpopulations in the subependymal plate layer with different cell cycle parameters (Table 11). The two subpopulations would have similar cell cycle phase durations except for the S phase duration; this would account for the longer cell cycle time for the mixed cell population. The values for the S phase duration measured directly from the experimental data are (Fig. 26) 12.5 - 13.5 hr. These compare well with the values of $T_s = 15 + 6$ hr for the mixed cell population of the computer-generated model.

Comparison of the cell cycle phase durations in this irradiated subependymal cell population with the comparable phase durations in the control population, there appears to be a slight shortening of the S phase duration by about

7 hr (Table 11); this may not be significant. There is evidence of a stimulation of a subpopulation with a shorter cell cycle following irradiation with 10 Gy He.

5.1.1 Conclusions on the effects of irradiation with 10 Gy He on the subependymal cell layer in the mouse brain

10 Gy He (23- MeV/amu) has a moderate effect on DNA synthesis in the subependymal cell layer. 1) There is a 26.3% decrease in the LI of the irradiated cortex at 48 hrs after the exposure and this is still evident 5 days after irradiation.

2) There is a 18.1% decrease in the LI of the unirradiated contralateral cortex of the irradiated mice 48 hr after the exposure and this is still evident 5 days later. The underlying mechanism is not fully understood, but appears to be related to metabolic perturbations affecting homeostatic controls.

3) The rate of accumulation of the labeled cells in the subependymal layer one week after 10 Gy He is the same as that seen in the control population. This suggests that recovery of cell proliferation processes after 10 Gy return to relatively normal levels by about 1 week.

4) Some compensatory cell proliferation occurs after radiation injury within a few days. The mitotic index appears to be slightly higher following irradiation with 10 Gy He as compared to the control subependymal population.

5) There appears to be a subpopulation within the stem cell compartment with a shorter cell cycle that is stimulated into proliferation after exposure to 10

Gy He. This effect is seen in both the subependymal layers in the irradiated and unirradiated cerebral hemispheres of the irradiated mice. This more rapidly proliferating stem cell population which is triggered into proliferation after irradiation, appears to reside within the SD cells of the subependymal layer.

5.2 Effects of 25 Gy He (230 MeV/amu) irradiation on the subependymal cell layer

Effects on the labeling and mitotic indices

Application of the linear dose-response relationship in Fig. 19, the expected LI 48 hr after exposure to 25 Gy He would be expected to be about 7.5% in the irradiated cortex and about 9.5% in the unirradiated cortex. One week after exposure to 25 Gy He the pulse H^3-TdR labeling indices vary between 4.0% - 14.9% in the irradiated cortex and 3.4% and 27.6% in the unirradiated cortex (Table 9a). These values are comparable to those observed 48 hr post-irradiation.

The mitotic indices in both the irradiated and unirradiated subependymal layers of the irradiated animals vary between 0.3% and 1.5%. Again, the radiation response to 25 GyHe is similar in both the cortices.

Comparison of the effects on the LI following this irradiation with the values for LI in the control population (Fig. 32) indicates that the overall pattern of accumulation of the labeled cells in the subependymal layer is the same in the irradiated and contralateral cortex. There is a decrease in the total number of labeled cells following exposure to 25 Gy He (compare Tables 7a and

9a), due to the extent of injury to the proliferating cell populations.

The cell cycle parameters following irradiation with 25 Gy He

PLM curves obtained one week after irradiation with 25 Gy He are much different from those observed following 10 Gy He. The number of mitoses is decreased following 25 Gy He (compare Fig. 28 and 26). The unirradiated subependymal cell layer appears to have more cells in the GF, and they are also less synchronized as compared to the irradiated layer. The computer-generated Barrett-Steel model PLM curve indicates the presence of at least two cell populations with similar cell-cycle parameters, but starting cell division 15 hr apart and with a T_{G1} of 40 hr. (Table 11). This could be due to radiation injury during the G_1 phase, which prolongs its duration, for the necessary time to repair sublethal radiation damage combined with a prolonged G_2 -block and the killing of proliferating cells. These are reasonable assumptions, as G_1 is known to be the phase when the cell repairs its radiation-induced DNA damage, and G_2 -inhibitions would be expected following high-dose radiation. The cell cycle time after exposure to 25 Gy He of $T_c = 56 + 30$ hr, is much longer than the $T_c = 39 + 16.8$ hr observed in the control population (Table 11). Comparing the effects of 25 Gy He and 10 Gy He irradiations, the 'stem cell' compartment appears to be triggered into proliferation only after 10 Gy He while the G_1 phase is prolonged only after 25 Gy He, and not after 10 Gy He.

5.2.1 Conclusions on the effects of irradiation with 25 Gy He

1) There is a maximum decrease of 75% in the L.I. after irradiation with 25 Gy He as compared to the control population.

2) There is a decrease in the GF of 23% after irradiation with 25 Gy He as compared to the control population.

3) There is no evidence of a stimulation of the 'stem cell' compartment following irradiation with 25 Gy He.

4) There is a prolonged G1 phase after irradiation with 25 Gy He.

5) The unirradiated subependymal population in the irradiated animals shows a higher GF and less synchrony than the irradiated population in the same animals.

5.3 Effects of irradiation with 45 Gy He (230 MeV/amu).

The repeated labeling studies were done 24 hr after irradiation with 45 Gy He to determine radiation effects on the growth fraction of proliferating cells, the rate of labeling (the rate of cells entering DNA synthesis), and the rate of the cells entering mitosis in the stem cell and proliferating cell compartments during the acute post-irradiation period, i.e., radiation effects on the first few cell cycles.

Effects on the growth fraction (GF)

There is a decrease of about 64% in the GF of both, the irradiated and unirradiated subependymal cell layers, in the irradiated animals as compared to

that seen in the unirradiated control animals (i.e., 0.09 vs. 0.22, see Fig. 20). Since the experiment was started 24 hr after irradiation and carried through to 54 hr, the effects that are observed may be due to the radiation-induced delay through the cell cycle frequently observed in the first few post-irradiation cell cycles (Lajtha et al., 1958). Immediate post-irradiation delay in all the cell cycle phases following X-irradiation has been demonstrated for some cell populations (Carter et al., 1965; Lajtha et al., 1958; Terasima and Tolmach, 1962). Effects of high LET irradiations in division delay and/or G_2 - block have been studied with neutrons (Schneider and Whitmore, 1963; Ngo et al., 1977b), with α particles (Raju et al., 1980a), and heavy-ion beams, (Lucke-Huhle et al., 1979; Collyn-d'Hooghe et al., 1981). All of these cell- cycle-progression effects have been demonstrated in various cell cultures (see Blakeley et al., 1979)

A general concept for the effects of high-energy monoenergetic heavy-ion beams is that there is a greater delay in the G_2 phase with exposure to these beams than with X-rays and that heavy ions do not affect cell progression through the G_1 and S phase as much as X-rays (Lucke-Huhle et al., 1979). Different results have been seen with α particles (He). Schlag and Lucke-Huhle (1981) have shown that Am^{241} α particles did not prolong the duration of S phase in V-79 cells, as compared to the effect of Co^{60} γ rays in the first 4 hr after irradiation. On the other hand, Raju et al. (1980a) found that exposure to the Pu^{238} α particles did result in a longer retention of Chinese hamster V-79 cells in late S phase than that observed for cells exposed to X-rays, 8-10 hr

post-irradiation. Raju et al. (1980a) concluded that a late- and dose-dependent S- phase delay was seen after higher doses of α particles. These changes in the cell cycle progression may last several cell generations after low-LET radiation injury (Field and Dawson, 1962). However, there are systems in which neither immediate nor delayed cell cycle effects have been reported following irradiation (Alexander, 1961).

In vivo cell populations may show varying degrees of cell cycle progression effects. In the GF studies (Fig. 20), there appears to be a delay in cells entering mitosis (G_2 delay) as evidenced by the decrease in the labeling rate (in LI) by 36 hr, at which time the control curve shows a continuing increase in the LI. The initial increase in the LI by at 30 hr in the irradiated animals may be due to cells entering the S phase after an initial G_1 delay, either speeding up the T_c, an increased rate of cell birth, or the triggering of G_0 cells into cell cycle, or a combination of these effects. After 36 hr, the LI continues to increase to a maximum of 8%-9% by 48 hr. There follows a decrease in the LI (2.6%-5.8%) in the irradiated animals (Table 4) at 54 hr post-irradiation; at this time the control population also shows a fall in the LI to 4.8%. The decrease in the LI in the control population, is probably due to the emigration of the labeled cells from the zone of proliferation in subependymal layer, and this factor along with a cell cycle delay could combine explain the decline in the LI of the irradiated animals. Four months after irradiation, the repeated labeling of the subependymal layer results in LI values that are comparable, LI in all three cell populations, SD, SL

and LL cells.

Effects on the mean grain count decrements

The mean grain count decrements 48 hr after irradiation with 45 Gy He are illustrated in Fig 23. The subependymal cell layers in the irradiated animals, both in the irradiated and in the unirradiated cortex, show a more rapid mean grain-count decrement than those of the control cell population (Fig. 23); this is readily observed by 48 hr after irradiation. This is primarily due to the radiation injury or death in the proliferating cell compartment. The killing of the proliferating cells would decrease the value of the mean number of grains per nucleus in the subependymal. But, this apparently is balanced in part by compensatory cell proliferation in the irradiated animals due to stimulation of the stem cells to proliferate within 48 hr after exposure. The stem cells (SD) show a more rapid grain count decrement (Appendix B) because of their shorter cell cycle duration, and a preponderence of these SD cells in the irradiated subependymal cell population could account for the overall rapid decrement in average grain gount number. The higher grain counts observed initially in the irradiated animals could be due to a stimulation of DNA synthesis in the early post-irradiation phases (Fabrikant 1964, 1966).

5.3.1 Conclusions on the effects following irradiation with 45 Gy He

There are four major conclusions to be drawn from this series of experiments:

1) There is a marked decrease (64%) in the GF 24-48 hr after irradiation; this appears to be a direct effect of cell killing and cell inactivation resulting in profound radiation-induced injury in the proliferating compartments.

2) There is evidence of delays in the progression through the cell-cycle phases (G_1 and G_2) in the acute post-irradiation phase, associated with a decreased rate of entry of cells into DNA synthesis and mitosis, and prolonged G_1 and G_2 phase durations.

3) There is a more rapid MGC decrement in the irradiated animals as compared to the controls, and this is associated primarily with a decreased T_c in the stem cell compartment and a preponderance of proliferating SD cells.

4) There may be a stimulation or trigger of a subpopulation of cells into cell cycle, and with a shorter cell cycle, 48 hr after irradiation. This appears to be primarily within the SD cell population, due either to a triggering into cell cycle from a resting G_0 stage in the stem cell compartment, or a speeding up of the cell cycle, associated with an increased birth rate to compensate for cell injury and death due to radiation.

5.4 Effects of irradiation with 10 Gy Ne on the subependymal cell layer

The subependymal layers in the unirradiated and irradiated cortices, of the irradiated animals show about the same changes in the subependymal cell cycle parameters 1 week after the irradiation, viz., $T_{G1} = 20$ hr, $T_s = 10$ hr, $T_{G2} = 3$ hr, and $T_C = 34$ hr (Table 11).

Effects on the labeling and mitotic indices following irradiation

One week after irradiation, the percent LI varies between 0.56% and 2.15% with time after a pulse of H^3-TdR, as compared with 9.53% and 27.9% in unirradiated controls (Table 12). This may be due either to a decrease in the number of proliferating cells or to a shortening of the duration of the S phase, or both. While there is variation in the values, these are not as wide as seen in the experiments with helium ions. This might be due to the effectiveness of neon in decreasing the LI to profoundly low levels. There is a decrease of about 90% in the LI one week after 10 Gy Ne irradiation as compared to the control population. Comparison of the effect of 10 Gy Ne on the LI with those of 10 Gy He and 25 Gy He, indicates that neon is at least 80% more effective than 10 Gy He and 48% more effective than 25 Gy He in decreasing the LI by 18 hr (Table 12).

The percent mitotic indices one week after the neon irradiation vary between 1% and 3% with time. These values are similar to those found in the control population and after 10 and 25 Gy He (Tables 9a and 10a). Thus, the proportion of mitoses to the number of labeled cells in the neon-irradiated populations is higher than that seen after 10 and 25 Gy He and the control population (Tables 7a and 10a). This could be an indication of a higher birth rate among the surviving proliferating cells after exposure to 10 Gy Ne inorder to maintain the cell population levels of the subependymal cell layer.

Effects on the cell cycle and its phase durations

The percent labeled mitosis curves one week after exposure to 10 Gy Ne irradiation in the two subependymal populations of the irradiated animals (unirradiated and irradiated hemispheres in irradiated mice) are generally similar. The curve by fit to the experimental data (Fig. 30) shows that there are more cells in the GF in the unirradiated cortex, and they are also less synchronized and with wider variation in cell cycle durations and cell cycle phases when compared to the subependymal cell population in the irradiated cortex. The modified Barrett-Steel model suggests a subpopulation of cells with a shorter cell cycle time, similar to that following irradiation with 10 Gy He (Table 11). Thus, there are at least two subpopulations in the subependymal cell layer that are proliferating one week after exposure to 10 Gy Ne; one is a mixed cell population with different cell cycle duration, and the other is a 'stem-cell' population that has been stimulated to proliferate with a shorter cell-cycle time of about 25 hr. The mixed cell population has a mean cell-cycle time of about 36 hr. Comparison of the S phase durations in the neon-irradiated animals to that in the control animals (Table 11), there is a slight decrease in the T_s from 22 hr to 12 hr, but it is within the minimum range of the control population. The decrease in the LI after the neon irradiations can be attributed to the killing of proliferating cells rather than to a decrease in T_s. However, the duration of the G_1 phase of the mixed cell population in the neon-irradiated subependymal cell layer is prolonged as compared to that in the control population (Table 11), i.e., T_s,

increases from 8 hr to 20 hr.

5.4.1 Conclusions on the effects of irradiation with 10 Gy Ne

The following conclusions can be drawn from the results of the experiments with 10 Gy Ne:

1) One week after irradiation, there is 90% decrease in the LI in the subependymal cells as compared to that in the control population, indicating a profound effect of Ne irradiation on the cell proliferation kinetics of the renewal system.

2) The decrease in the LI is mainly due to killing of the proliferating cells, and not due to a decrease in the T_s, although there is considerable perturbation of the cell cycle and cell population kinetics of the subependymal cells.

3) The mitotic indices one week after the irradiation are similar to those seen in the control population, suggesting that recovery of the surviving proliferating cells occurs within 1 week, and that increased cell production rate occurs to compensate for cell death and cell loss from the proliferating compartment.

4) There is a decrease in the LI of the subependymal cell population, but this is not associated with a decrease in the number of mitoses after neon irradiation, as compared to the control population. This suggests that there is a proportionately higher number of mitoses in the proliferating population due to an increased birth rate of cells in the subependymal cell population one week after 10 Gy Ne irradiations. This is possible if there is a stimulation of slowly proliferating cells into a more rapidly proliferating 'stem cell' compartment.

5) The modified Barrett-Steel model applied to the experimental PLM curves indicates that there is stimulation of a subpopulation in the proliferating zone, and this cell population has a shorter cell cycle than the normal subependymal cell population. It is concluded that this rapidly dividing cell population is a stem cell population effecting recovery after radiation injury through mechanisms of compensatory cell proliferation.

6) The cell cycle and cell population kinetic parameters of the mixed cell population one week after irradiation are the same as those in the control population, though the population levels are profoundly reduced in number.

5.5 Comparison of the effects of irradiation with 10 Gy Ne and 25 Gy He

Comparison of the subependymal cell population kinetics after irradiation with 10 Gy Ne and 10 Gy He.

The cell cycle and cell population kinetic parameters derived from the PLM curves one week after irradiations with 10 Gy Ne and 10 Gy He are similar (Table 11): there appears to be a stimulation or triggering of the 'stem cell' population with a shortening of the cell cycle in the stem cell compartment in both instances. However, there is a prolonged G_1 phase in the mixed populaiton following irradiation with 10 Gy Ne, which is not seen after exposure to 10 Gy He ions. Comparing the effects of both these irradiations on the subependymal layer, the overall conclusions are:

1) There is a marked decrease in the total number of labeled cells one week after irradiation with 10 Gy Ne as compared to irradiation with 10 Gy He, indicating that Ne is much more effective in damaging DNA synthesis.

2) There is no difference in the number of mitoses seen after 1 week in both instances, suggesting that recovery of the surviving proliferating cells occurs within 1 week, and that increased cell production rate occurs to compensate for cell death and cell loss from the proliferating copartment.

3) 10 Gy Ne is much more effective in killing proliferating cells of the subependymal cell layer than is 10 Gy He, but those cells that survive showed little perturbation of the cell cycle and cell population kinetics.

Comparison of the subependymal cell population kinetics after irradiation with 10 Gy Ne and 25 Gy He

10 Gy Ne is more effective in decreasing the LI compared to 25 Gy He 1 week following irradiation (Figs. 32 and Table 12). However, again the mitotic indices are similar in both cases 1 week following irradiation. Comparison of the cell cycle kinetics in the subependymal cell populations one week after both the irradiations (Table 11), indicates that stimulation of a 'stem-cell' population 1 week after exposure to 25 Gy He does not appear to occur. There is also a prolonged G_1 phase in the mixed cell population after exposure to 25 Gy He. After 10 Gy Ne however there is a stimulation of the 'stem cell' population and not as much of a prolonged G_1 phase as is seen after the exposure to 25 Gy He (i.e., G_1=20 hr vs. G_1=40 hr).

The following conclusions from the results of the experments with 25 Gy He and 10 Gy Ne:

1) 10 Gy Ne is about 50% or more effective than 25 Gy He in decreasing the LI i.e., preventing cellls from entering DNA synthesis, and in inactivating or killing the proliferating cells as they progress through the cell cycle.

2) The similar mitotic indices indicate a similar birth rate of cells following both irradiations. The mitotic indices 1 week after the irradiations are similar to those seen in the control population, suggesting that recovery of the surviving proliferating cells occurs within 1 week, and that increased cell production rate occurs to compensate for cell death and cell loss from the proliferating compartment.

3) The analyses of the cell cycle and cell population kinetics indicate that no stimulation of the stem cell population occurs 1 week after irradiation with 25 Gy He but does occur following irradiation with 10 Gy Ne. This may mean that the biological effectiveness for preventing the triggering of stem cells into speeding up their cell cycle may be greater for 25 Gy He than 10 Gy Ne.

An estimate of the relative biological effectiveness of Ne ions as compared with He ions in the subependymal cell layer

The plateau region of the Bragg ionisation curve was used in the irradiation procedures. This was an unmodified beam and the physical doses absorbed in the irradiated cortices was 10 Gy and 25 Gy for the helium ions and 10 Gy for neon ions. The pulse thymidine labeling indices in the subependymal cell

populations of the irradiated cortices in the mice after the three irradiation experiments (Fig. 32) demonstrate that 10 Gy Ne is the most effective in decreasing the H^3-TdR labeling indices. Table 11 indicates considerable interanimal variation in LIs. The average LI 1 week following 10 Ne irradiation was about 1.4%; the average LI 1 week after irradiation with 25 Gy He was 11.3%. Taking into consideration that these are mean values for 3 animals per interval, then 10 Gy Ne is at least as biologically effective as 25 Gy He in decreasing the LI. From the data in Fig. 32 and Table 12, it is possible to put a minimum value of about 2.5 for an RBE for "plateau" beam irradiations with neon ions as compared helium ions, using the LI as the end point in the subependymal cell population 1 week after the irradiations. On average, the depressions of LI values for 10 Gy He were 30%; on average, the values for 25 Gy He were 62%; on average, the values for 10 Gy Ne were 92%. Therefore, an average value for RBE of 10 Gy Ne to 10 Gy He would be 3 for decrease in LI in subependymal cells.

5.6 Some explanations for the effects observed in the 'internal control' subependymal cell population

The cell population and the cell cycle kinetics of the unirradiated subependymal layer (internal control) in the irradiated animals are similar to those seen in the irradiated populations, although the brain was protected from radiation exposure during the irradiation procedures. This was a consistent finding in all the irradiation experiments. Histologically, the unirradiated population was nor-

mal (see Fig. 17) but with decreased labeled subependymal cells. The cell kinetic indices were consistently a little higher in the unirradiated subependymal population as compared to those on the contralateral irradiated cortex, but the overall temporal pattern of response was the same in both the unirradiated and irradiated cell populations of the irradiated animals.

The subependymal cells are capable of migration and this population is believed to contain a stem cell population for the neuroglial cells, even in the adult rodent (Patterson et al, 1973; Hubbard and Hopewell, 1980). This indirect radiation response of the contralateral unirradiated subependymal population has been observed by other investigators (Fabrikant, personal communication; Tobias, personal communication) and the underlying mechanism remains unknown. However, a number of explanations have been suggested; it could be: (1) a sympathetic response to the radiation injury in the irradiated population possibly mediated through some neurovascular mechanism, or (2) indirect (abscopal) radiation injury, or (3) a physiologic and metabolic response of the brain in order to maintain its homeostatic balance.

A review of the literature indicates that most of the comparisons in the two cortices, of the effects of irradiation of one hemisphere, are based on histological findings primarily in dogs (Tiller-Borcich et al, 1987) and in rabbits (Lindberg, 1958). Neither of these investigations demonstrated any change in the histological appearance of the unirradiated cortex in the irradiated animal. This also is the case in the present investigations reported here. However, Caverness (1977)

has observed similar changes in the CSF pressure in both the cortices following focal X-irradiation of the brain in monkeys. Zeeman (1960) has described an abscopal effect seen in the brain tissues following whole body irradiations. This was considered a physiological response of the brain to radiation injury.

This response of the contralateral subependymal population within 1 week after irradiation with helium and neon ions, may just be confined to this particular population because of its unique function, but this is not known. It may not be seen in later phases of the post-irradiation response, and this would be of interest. The post-irradiation response of stimulation of the stem cell population in both the subependymal layers, unirradiated and irradiated would give rise to a greater number of progeny to expand the proliferative compartments and, consequently increase the number of functional end cells (the glial cells) that may be required to repair the radiation damage, but the underlying mechanisms are not understood.

5.7 The stem cell compartment in the subependymal layer; a cell kinetic model and the response to irradiation

The SD cells in the subependymal cell population show the most number of mitoses and a more rapid grain count decrement than the SL and LL cellsin both the control and irradiated animals. This indicates that the SD cells proliferate more frequently and with a shorter cell cycle duration than do the SL and LL cells. It is possible that the SD cells comprise the stem cell compartment in the subependymal layer, and this conclusion is based on the cell cycle and cell

population kinetics of the SD cell compartment. This hypothesis has also been proposed before by Patterson et al. (1973) and, Hubbard and Hopewell (1980), but their conclusions were not based on differences in cell cycle and cell population kinetics, and their response to irradiation.

Analyzing the post-radiation response seen in the subependymal population 1 week after exposure to charged particle irradiation, two possible models among others that could explain these cell and tissue kinetic experimental observations can be described (Fig. 33):

Model A in Fig. 33 shows the unirradiated subependymal cell population with a stem cell compartment consisting of two types of SD cells, SD_1 is a slowly proliferating stem cell population and SD_2 is a rapidly proliferating one. These cells supply the proliferative compartment giving rise to the SL and LL cells; these latter cells divide and differentiate further into the neuroglial cells. In Model B the unirradiated subependymal cell population contains a population of noncycling G_0 cells as part of the stem cell compartment. The SD cells in this stem cell compartment are the rapidly proliferating type (SD_2), whereas the G_0 cells are unrecognized precursors. The G_0 cell has the characteristics of a quiescent SD cell which is capable of entering the proliferating SD pool upon demand conditions. The remaining cell renewal compartments, P, D, F are the same as in Model A.

After irradiation, the two possible cellular responses are illustrated in Model C and Model D. In Model C the SD_2 cell population increases its proliferation

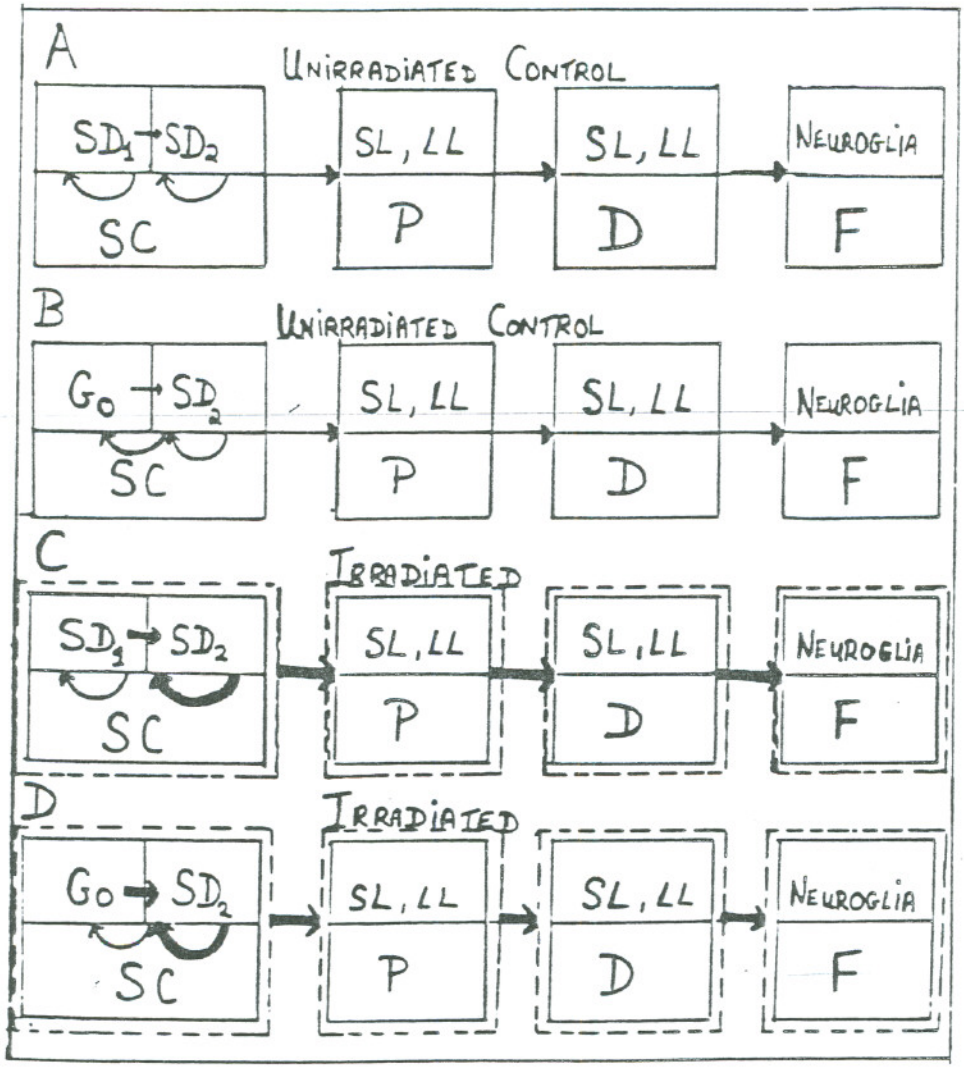

Figure.33 A schematic representation of the subependymal layer as a cell renewal system. The 3 morphologically distinct types of cells that make up the subependymal layer are SD (small dark nucleus), SL (small light nucleus), and LL (large light nucleus).

Models A and B in the unirradiated mouse illustrate the possible arrangements in the stem cell compartment. Models C and D represent the irradiated systems A and B respectively.

SD ---slowly proliferating SD cell, SD ---rapidly proliferating SD cell, SC---stem cell compartment, P---proliferating compartment, D---differentiating compartment, F---functional compartment.

rate, and the stem cell compartment is dominated by these rapidly proliferating SD_2 cells. This provides a high birth rate for the SD_1 cells that survive the radiation injury. There is an increase in the size of the proliferative compartment with time, and this compartment expands due to an increased birth rate as well, with increased progeny and an eventual increase in differentiation and the functional end compartments of the neuroglial cells to compensate for cell loss in the proliferating and stem cell compartments.

Model D illustrates one other possibile mechanism. Here, the G_0 cells enter the SD_2 cell compartment either directly, or through symmetrical or asymmetrical division and increase the size of this rapidly proliferating cell compartment. The other transitions of an increased proliferative compartment and an increased functional compartment follow. The concept of a two compartment stem cell population has been used to explain the cell kinetic stages of erythropoiesis and spermatogenesis (Alpen et al., 1960; Fabrikant, 1972; Lajtha, 1963).

5.8 Main conclusions of these investigations

1) The subependymal cell population in the mouse is a mixed cell population made up of SD, SL, and LL cells that may be characterized histologicaly and by their cell and tissue kinetics. These cells are in various stages of proliferation, migration and differentiation into mature functional end cells, the neuroglia.

2) It is an actively proliferating population with a moderately high labeling index(17.4%-26.4%), but a low mitotic index (0.5%-1.5%). It has a GF of 0.22 and a cell cycle duration of about 37-39 hr. The cell cycle phase durations are

estimated to be $T_{G1} = 8$ hr, $T_s = 20$ hr, $T_{G2} = 8$ hr.

3) This is an exponentially proliferating population with extensive cell loss through ineffective proliferation mainly resulting in cell death (pyknoses) and cell emigration. The cell birth rate and cell loss rate are balanced thereby maintaining a steady-state of cell renewal in the subependymal cell population.

4) Analysis of the cell cycle cell population kinetics indicates that the subependymal population is made up of at least two subpopulations that are proliferating with varying cell cycle times and phase durations. However, in the normal subependymal cell layer, there appears to be a recognizable stem cell compartment dominated by the SD cell population.

5) The cellular response 1 week after partial irradiations with heavy charged particles beams of one cerebral cortex of the mouse brain has been investigated; it appears that both the subependymal populations (unirradiated and irradiated) in the irradiated animal are affected similarly as regards the radiation perturbation of the cell and tissue kinetics and attempts to maintain homeostatic control.

6) The decrease in the H^3-TdR labeling indices 1 week after the charged particle irradiations is radiation dose-dependent and ion dependent: Neon ion (425 MeV/amu) irradiation is more effective in altering the cell and tissue kinetics in the subependymal cell than is helium ion (230 MeV/amu).

7) The mitotic indices 1 week after 10, 25 Gy He and 10 Gy Ne irradiation were similar to those seen in the control subependymal populations. This indicates that the birth rate of cells 1 week after these irradiations is maintained by the

surviving proliferating population, and can be explained on the basis of altered cell and tissue kinetics following irradiation.

8) Cell cycle analyses indicates that the capacity for stimulation of a rapidly proliferating subpopulation of cells in the stem cell compartment, 1 week after irradiation with helium ions, is dose-dependant. This was seen after exposure to 10 Gy He but not after 25 Gy He.

9) The triggering of a stimulated and rapidly proliferating stem cell population within the stem cell compartment was also seen 1 week after irradiation with 10 Gy Ne.

10) The cellular response of the subependymal cells to irradiation with 10 Gy Ne indicates that these ions are more effective in producing direct cell injury as compared to the He ions (10 and 25 Gy), but the surviving cells continue to proliferate and maintain the same birth rate as the normal cells.

11) There is a marked decrease in the GF of both the unirradiated and irradiated subependymal layers in the irradiated animals 24-48 hr after exposure to 45 Gy He; the GF is reduced from 0.22 to 0.8. This appears to be due to a combination of post-irradiation delays in the cell cycle phases and the killing of proliferating cells.

12) The cell kinetic parameters of the durations of the cell cycles and the component phases in unirradiated subependymal populations and following heavy charged particle He and Ne irradiation using techniques of analysis of cell population kinetics are listed in the following table (11).

Table 11: Cell Cycle Durations (hr) for the Control and Irradiated Subependymal Cell Populations

Unirradiated Control Mice‡	
Left Cortex	Right Cortex
$T_{G_1} = 8 \pm 4$ hr $T_S = 22 \pm 8.8$ hr $T_{G_2} = 8 \pm 4$ hr $T_M = 1$ hr $T_C = 39 \pm 16.8$ hr	$T_{G_1} = 8 \pm 4$ hr $T_S = 20 \pm 8$ hr $T_{G_2} = 8 \pm 4$ hr $T_M = 1$ hr $T_C = 37 \pm 16$ hr
1 week following 10 Gy He^+ (230 MeV/amu)	
Mixed cell population	Second cell population
$T_{G_1} = 8 \pm 3$ hr $T_S = 15 \pm 6$ hr $T_{G_2} = 8 \pm 3$ hr $T_M = 1$ hr $T_C = 32 \pm 12$ hr	$T_{G_1} = 8 \pm 3$ hr $T_S = 8 \pm 3$ hr $T_{G_2} = 8 \pm 3$ hr $T_M = 1$ hr $T_C = 25 \pm 9$ hr
1 week following 10 Gy Ne^+ (425 MeV/amu)	
Irradiated S.E. Cell Population	Unirradiated S.E. Cell Population
Mixed cell population / 2nd cell population	Mixed cell population / 2nd cell population
$T_{G_1} = 20 \pm 10$ hr $T_S = 10 \pm 5$ hr $T_{G_2} = 3 \pm 1.5$ hr $T_M = 1$ hr $T_C = 34 \pm 16.5$ hr	$T_{G_1} = 8 \pm 3$ hr $T_S = 8 \pm 3$ hr $T_{G_2} = 8 \pm 3$ hr $T_M = 1$ hr $T_C = 25 \pm 9$ hr
$T_{G_1} = 20 \pm 10$ hr $T_S = 12 \pm 6$ hr $T_{G_2} = 3 \pm 1.5$ hr $T_M = 1$ hr $T_C = 36 \pm 17.5$ hr	$T_{G_1} = 20 \pm 3$ hr $T_S = 8 \pm 3$ hr $T_{G_2} = 8 \pm 3$ hr $T_M = 1$ hr $T_C = 25 \pm 9$ hr
1 week following 25 Gy He^+ (230 MeV/amu)	
Mixed cell population	Second cell population
$T_{G_1} = 40 \pm 20$ hr $T_S = 8 \pm 6$ hr $T_{G_2} = 8 \pm 4$ hr $T_M = 1$ hr	same parameters, but start cycling 15 hrs later $T_C = 56 \pm 30$ hr

† Cell cycle phases obtained by using the Modified Barrett-Steel PLM Model for the "computer fit" to the experimental data points.

‡ Cell cycle phases obtained by using the Barrett-Steel PLM Model for the "computer fit" to the experimental data points.

13) The RBE for the neon "plateau beam" (425 MeV/amu) as compared to a similar helium beam (230 MeV/amu), using the depression in LI values in the subependymal layer 1 week post irradiation, is at least 2.5. This is based on comparison of the responses to 10 Gy He, 25 Gy He and 10 Gy Ne irradiation.

14) A model of the cell and tissue kinetics of the subependymal cell population in the mouse brain and the cellular response and cell population kinetics following heavy charged particle irradiation is proposed based on the experimental results of these investigations.

5.9 Summary

The subependymal layer in the CB6F1 four week old mouse brain is an actively proliferating cell population as evidenced by a moderately high H_3-TdR labeling (17.4%-26.4%). The labeling index varies with the sites in the brain. It is consistently highest at the level of the corpus callosum (about 26%), and lowest in the olfactory lobe (about 10%). Inspite of the high labeling index there is a low mitotic index in the subependymal cells, which indicates a low birth rate in this proliferating population. The growth fraction of about 22% indicates there is a nonproliferating population within the layer. Analyses of percent labeled mitoses (PLM) data indicates that the cell are cycling with a cell cycle time of about 37-39 hr with cell cycle phase durations of $T_{G1} = 8$ hr, $T_s = 20$ hr, and $T_{G2} = 8$ hr.

Morphologically the subependymal cell populations are made up of SD, SL, and LL cells in sequential stages of proliferation, differentiation and migration.

Analyses with high resolution autoradiography indicates that this layer is made up of subpopulations with varying cell cycle times and phase durations and, that the SD cells are probably the "stem cells" of this poplation. The cell populations are continually proliferating with cell loss due to migration and cell death through pyknoses, thus maintaining a steady-state of growth.

Following partial brain irradiations with helium and neon ions that were confined to one cortex of the brain, the subependymal layers in the unirradiated and the irradiated cortices show similar disturbances in the cell and tissue kinetics in the first post-irradiation week. This is probably an indirect radiation response of the brain which helps maintain the homeostatic balance.

The decrease in the LI one week after charged particle irradiations is radiation dose-dependent and ion-dependent. The mitotic indices 1 week after the irradiations indicates that the birth rate of cells is maintained by the surviving proliferating population. The cellular response of the subependymal cells to irradiation with neon and helium ions, indicates that the neon ions are more effective in producing direct cell injury as compared to the helium ions, but the stem cells continue to proliferate and maintain the same birth rate 1 week after exposure to 10 Gy Ne. An RBE of 2.5 for the neon 'plateau beam' (425 MeV/amu) as compared to a similar helium beam (230 MeV/amu) was estimated from the LI values in the subependymal layer 1 week post irradiation.

A model of the cell and tissue kinetics of the subependymal cell population in the mouse brain is proposed based on the experimental results of these

investigations. A stem cell compartment with 2 types of cells is proposed.

References

Alexander, P. (1961) Mouse lymphoma cells with different radiosensitivities. *Nature (London),* **192,** 572.

Alonso, J.R., Benton, E.V., Chu, W., Llacer, J., Richier, J., Tobias, C.A. (1980) Biological and medical research with accelerated heavy ions at the Bevalac, 1977-1980. (eds. M.C. Pirruccello and C.A. Tobias), Lawrence Berkeley Laboratories, Berkeley, CA., 21.

Alpen, E.L., Cranmore, D. (1959) Observations on the regulation of erythropoiesis and on cellular dynamics by Fe 59 autoradiography. *The Kinetics of Cellular Proliferation,* (ed. F. Stohlman Jr.), Grune & Stratton (New York), 290.

Arnold, A., Bailey, P., Harvey, R.A. (1954) Intolerance of the primate brainstem and hypothalamus to conventional and high energy radiations. *Neurology,* **4,** 575.

Bailey, O.T. (1962) Basic problems in the histopathology of radiation of the central nervous system. *Response of the Nervous System to Ionizing Radiation* (eds. T.S. Haley and R.S. Snider), 165.

Baker, C.P., Curtis, H.J., Zeman, W., Woodley, R.G. (1961) The design and calibration of a deuteron microbeam for biological studies. *Radiat. Res.,* **15,** 489.

Barrett, J.C. (1966) A mathematical model of the mitotic cycle and its application to the interpretation of percentage labeled mitoses data. *J. Natn. Cancer Inst.*, **37**, 443.

Baserga, R., Tyler, S.A., Kisieleski, W.E. (1963) The kinetics of growth of the Ehrlich tumor. *Archs. Path.*, **76**, 9.

Berg, N.O., Lindgren, M. (1958) Time-dose relationship and morphology of delayed radiation lesions of the brain in rabbits. *Acta Radiol. Suppl.*, 167.

Bichsel, H. (1968) Charged-particle interactions. In: *Radiation Dosimetry* (eds. F.H. Attix and W.C. Roesch), **I**, Academic Press (New York), 157.

Bird, R., Burki, J. (1975) Survival of synchronized Chinese hamster cells exposed to radiation of different linear-energy transfer. *Int. J. Radiat. Biol.*, **27**, 105.

Blakely, E.A., Tobias, C.A., Yang, T.C.H., Smith, K.C., Lyman, J.T. (1979) Inactivation of human kidney cells by high-energy monoenergetic heavy-ion beams. *Radiat. Res.*, **80**, 122.

Bronk, B.V., Dienes, G.J., Paskin, A. (1968) The stochastic theory of cell proliferation. *Biophys. J.*, **8**, 1353.

Brownson, R.H., Suter, D.B., Diller, D.A. (1963) Acute brain damage induced by low-dosage X-irradiation. *Neurology*, **13**, 181.

Cairnie, A.B., Lamerton, L.F., Steel, G.G. (1965a) Cell proliferation studies in the intestinal epithelium of the rat. *Exp. Cell. Res.*, **39**, 528.

Cairnie, A.B., Lamerton, L.F., Steel, G.G. (1965b) Cell proliferation studies in the intestinal epithelium of the rat. *Exp. Cell. Res.*, **39**, 539.

Cameron, I.L., Cleffman, G. (1964) Initiation of mitosis in relation to the cell cycle following feeding of starved chickens. *J. Cell Biol.*, **21**, 169.

Castro, J.R., Quivey, J.M. (1977) Clinical experience and expectations with helium and heavy-ion irradiation. *Int. J. Radiat. Biol.*, **29**, 127.

Cater, D.B., Holmes, B.E., Mee, L.K. (1956) Cell division and nucleic acid synthesis in the regenerating liver of the rat. *Acta Radiol. (Stockholm)*, **46**, 455.

Caveness, W.F. (1977) Pathology of radiation damage to the normal brain of the monkey. *Natl. Cancer Inst. Monogr.*, **46**, 57.

Chauser, B., Morris, C., Field, S.B., Lewis, P.D. (1977) The effects of fast neutrons and X-rays on the subependymal layer of the rat brain. *Radiology*, **122**, 821.

Cleaver, J.E. (1967), *Thymidine Metabolism and Cell Kinetics.* North-Holland, Amsterdam.

Collyn-d'Hooghe, M., Hemon, D., Gelet, R., Curtis, S.B., Valleron, A.J.,

Malaise, E.P. (1981) Comparative effects of Co^{60}-rays and neon and helium ions on cycle duration and division probability of EMT 6 cells. A time-lapse cinematography study. *Int. J. Radiat. Biol.*, **39**, 297.

Crowter, D.G., Evans, E.A., Lambert, W. (1960) Tritium-labeled thymidine. *Chem. Ind.*, 899.

Denekamp, J., Kallman, J.F. (1973) In vitro and in vivo labeling of animal tumours with tritiated thymidine. *Cell Tissue Kinet.*, **6**, 217.

Evans, E.A., Stanford, F.G. (1963) Stability of Thymidine Labelled with Tritium or Carbon-14. *Nature (London)*, **199**, 762.

Fabrikant, J.I. (1987) Adaptation of cell renewal systems under continuous irradiation. *Health Physics*, **52**, 561.

Fabrikant, J.I. (1971) The effects of continuous irradiation. *Pathology of Irradiation* (ed. C.C. Berdjis), Williams and Wilkins (Baltimore), 50.

Fabrikant, J.I. (1967) The effect of prior continuous irradiation on the G_2, M, and S phases of proliferating parenchymal cells in the regenerating liver. *Radiat. Res.* **31**, 304.

Fabrikant, J.I. (1964) Studies on cell proliferation in the regenerating liver and the effect of prior continuous irradiation. PhD Thesis, University of London, (London).

Fried, J. (1970) Mean, geometric mean, or median grain count in cell cycle studies. *Exp. Cell Res.*, **59**, 447.

Fried, J. (1968) Estimating the mean generation of proliferating cell systems in steady state. *Biophys. J.*, **8**, 710.

Gelfant, S. (1963) Patterns of epidermal cell division. I. Genetic behavior of the G_1 cell population. *Exp. Cell Res.*, **32**, 521.

Gelfant, S. (1962) Initiation of mitosis in relation to the cell division cycle. *Exp. Cell Res.*, **26**, 395.

Globus, J.H., Kuhlenbeck, H. (1944) Subependymal cell plate (matrix) and its relationship to brain tumors of ependymal type. *J. Neuropath.*, **3**, 1.

Gracheva, N.D. (1969) Autoradiographic investigation of proliferative activity of the rat brain subependymal cells. *Citologija (Leningrad)*, **11**, 1521.

Hall, E.J., Bird, R.P., Rossi, H.H., Coffey, R., Varga, J., Lam, Y.M. (1977) Biophysical studies with high-energy argon ions. 2. Determinations of the Relative Biological Effectiveness,the oxygen enhancement ratio, and the Cell Cycle Response. *Radiat. Res.*, **70**, 469.

Hartmann, N.R., Gilbert, G.W., Jansson, B., MacDonald, P.D.M., Steel, G.G., Valleron, A.J. (1975) A comparison of computer methods for the analysis of labeled mitoses curves. *Cell Tissue Kinet.*, **8**, 119.

Haymaker, W. (1969) Effects of ionizing radiation on nervous tissue. *The Structure and Function of Nervous Tissue* (ed. G. Bourne), **3,** 441.

Haymaker, W. (1962) Morphological changes in the nervous system following exposure of ionising radiation. *Effects of Ionising Radiation on the Nervous System, Vienna, IAEA,* 309.

Haymaker, W., Ibrahim, M.Z.M., Miguel, J., Call, N. (1968) Delayed radiation effects in the brains of monkeys exposed to X and γ-rays. *Exp. Neurol.,* **27,** 50.

Hicks, S.P., Wright, K.A. and Leigh, K.E. (1956) Time intensity factors in radiation response, 1. The acute effects of megavolts, electrons (cathode rays), and high- and low-energy X-rays; with special reference of the brain. *A.M.A. Arch. Pathol.,* **61,** 223.

Hicks, S.P., Montgomery, P.D. (1952) Effects of acute radiation on the adult mammalian central nervous system. *Proc. Soc. Exp. Biol. Med.,* **80,** 15.

Hommes, O.R., Leblond, C.P. (1967) Mitotic division of neuroglia in normal adult rat. *J. of Compar. Neurol.,* **129,** 269.

Hopewell, J.W. (1980) Late radiation damage to the central nervous system: a radiobiological interpretation. *Neuropath. and Applied Neurobio.,* **5,** 329.

Hopewell, J.W. (1971) A quantitative study of the mitotic activity in the

subependymal plate of adult rats. *Cell Tissue Kinet.*, **4**, 273.

Hopewell, J.W., Wright, E.A. (1970a) Modification of subsequent freezing damage to the rat spinal cord. *Exp. Neurol.*, **26**, 160.

Hopewell, J.W., Wright, E.A. (1970b) The nature of latent cerebral irradiation damage and its modification by hypertension. *Brit. J. Radiol.*, **43**, 161.

Hopewell, J.W., Wright, E.A. (1967) The effect of previous X-irradiation on the response of brain to injury. *Nature (London)*, **215**, 1405.

Hopewell, J.W., Cavanagh, J.B., (1972) Effects of X-irradiation on the mitotic activity of the subependymal plate of rats. *Brit. J. Radiol.*, **45**, 461.

Howard, A., Pelc, S.R. (1953) Synthesis of deoxyribonucleic acid in normal and irradiated cells and its relation to chromosome breakage. *Heredity (Suppl.)*, **6**, 261.

Hubbard, B.M., Hopewell, J.W., (1980) Quantitative changes in the cellularity of the rats subependymal plate after X-irradiation. *Cell and Tissue Kinet.* **13**, 403.

Kershman, J. (1938) The medulloblast and the medulloblastoma, *Arch. Neur.Psychiat.*, **40**, 937.

Killman, S.A., Cronkite, E.P., Fliedner, T.M., Bond, V.P. (1962) Cell

proliferation in multiple myeloma studied with tritiated thymidine in vivo. *Lab. Invest.*, **11**, 845.

Kimeldorf, D.J., Garcia J., Rubadeau, D.V. (1960) Radiation induced conditioned avoidance behaviour in rats, mice and cats. *Radiat. Res.* **12**, 710.

Koburg, E. (1963) The use of grain counts in the study of cell proliferation. *Cell Proliferation* (eds. L.F. Lamerton and R.J.M. Fry), Blackwell (Oxford), 63.

Kogel, A.J. van der, Barendsen, G.W. (1974) Late effects of spinal cord irradiation with 300 kV X-rays and 15 MeV neutrons. *Brit. J. Radiol.*, **47**, 393.

Korr, H. (1980) Proliferation of different cell types in the brain. *Adv. Anat. Embryol. Cell Biol.*, **61.**

Korr, H. (1978) Autoradiographische Untersuchungen zur Proliferation Verschiedener Zellelemente in Gehirn von Nagern waehrend der prae- und postnatalen Ontogenese, (Habilitationsscchrift), Univ. of Wuerzburg.

Korr, H., Schultze B. Maurer, W. (1975) Autoradiographic investigations of glial proliferation in the brain of adult mice. II. Cycle time and mode of proliferation of neuroglia and endothelial cells, *J. Comp. Neurol.*, **160**, 477.

Kraft, L.M., D'Amelio, F.E., Benton E.V. (1980) HZE particle effects in the mammalian brain: Relevance to manned space flight. *Biological and Medical Research with Accelerated Heavy Ions at the Bevalac,* 1977-1980. (eds.M.C. Pirruccello and C.A. Tobias), 287. Lawrence Berkeley Laboratories CA.

Lajtha, L.J. (1963) The Use of Radiation in Studies of Cell Proliferation. *Cell Proliferation* (eds. L.F. Lamerton and R.J.M. Fry), Blackwell (Oxford), 80.

Lajtha, L.G., Oliver, R. (1962) Cell population kinetics following different regimes of irradiation. *Brit. J. Radiol.,* **35,** 131.

Lajtha, L.G., Oliver, R., Kumatori, T., Ellis, F. (1958) On the mechanism of DNA synthesis. *Radiat. Res.,* **8,** 1.

Lamerton, L.F., Steel, G.G. (1965a) Cell proliferation studies in the intestinal epithelium of the rat, I. Determination of the kinetic parameters. *Exp. Cell Res.,* **39,** 528.

Lamerton, L.F., Steel, G.G. (1965b) Cell proliferation studies in the intestinal epithelium of the rat, II. Theoretical aspects. *Exp. Cell Res.,* **39,** 539.

Leith, J.T., Schilling, W.A., Lyman, J.T., Howard, J., Baker, D.G. (1975)

Comparison of skin responses of mice after single or fractionated exposure to cyclotron-accelerated helium ions and 230 kV X-irradiation *Radiat. Res.*, **62**, 195.

Lesher, S., Fry, R.J.M., Kohn, H.I. (1961) Aging and the generation cycle of intestinal epitheliel cells in the mouse. *Gerontologia*, **5**, 176.

Lewis, P.D. (1975) Cell death in the germinal layers of the postnatal rat brain. *Neuropathol. Appl. Neurobiol.*, **4**, 191.

Lewis, P.D. (1968) A quantitative study of cell proliferation in the subependymal layer of the adult rat brain. *Exp. Neurol.*, **20**, 203.

Lewis, P.D., Patel, A.J., Balazs, R. (1977) Effect of undernutrition on cell generation in the adult rat brain. *Brain Res.*, **138**, 511.

Luecke-Huhle, C., Blakely, E.A., Chang, P.Y., Tobias, C.A. (1979) Drastic G_2 arrest in mammalian cells after irradiation with heavy-ion beams *Radiat. Res.* **79**, 97.

Lyman, J.T., Kanstein, L., Yeater, F., Fabrikant, J.I., Frankel, K.A. (1986) A helium-ion beam for sterotactic radiosurgery of central nervous system disorders. *Med. Phys.*, **13**(5), 695.

Lyman, J.T., Howard, J. (1977) Dosimetry and instrumentation for helium and heavy ions. *Int. J. Radiat. Oncol. Biol. Phys.*, **3**, 81.

Lyman, R.S., Kupalov, R.S., Scholz, W., (1933) Effects of roentgen rays on the CNS. *Arch. Neurol. Psychiat.*, **29,** 56.

Macdonald, P.D.M. (1970) Statistical inferences from the fraction labeled mitoses curve. *Biometrika,* **57,** 489-503.

Manz, H.J., Woolley, V., Ornitz, R.D. (1979) Intolerance of primate brainstem to fast neutron beam irradiation. *Cancer,* **44,** 473.

Mendelsohn, M.L. (1965) The kinetics of tumour cell proliferation. *Cellular Radiation Biology,* Williams and Wilkins (Baltimore).

Mendelsohn, M.L. (1962) Autoradiographic analysis of cell proliferation in spontaneous breast cancer of C3H mouse, III. The growth fraction. *J. Nat. Cancer Inst.*, **28,** 1015.

Mendelsohn, M.L. (1960) The growth fraction: A new concept applied to tumors. *Science,* **132,** 1496.

Ngo, F.Q.H., Han, A., Utsumi, H., Elkind, M.M. (1977) Comparative radiobiology of fast neutrons: Relevance to radiotherapy and basic studies. *Int. J. Radiat. Oncol. Biol. Phys.*, **3,** 187.

Noetzel, H., Rox, J. (1964) Autoradiographische Untersuchungen ueber Zellteilung und Zellentwicklung in Gehirn der erwachsenen Maus und des erwachsenen Rhesus-Affen nach Injecktion von radioaktivem Thymidin.

Akta Neuropathol. (Berlin), **3,** 326.

O'Connel, J.F.A., Brunschwig, A., (1937) Observations on the roentgen treatment of intracranial gliomata with special reference to the effects of irradiation upon the surrounding brain. *Brain,* **60,** 230.

Opalski, A. (1933) Ueber lokale Unterschiede im Bau der Ventrikelwaende beim Menschen. *Ges. Neurol. Psychiat.,* **149,** 221.

Paterson, J.A, Privan, A., Ling, E.A., Leblond, C.P. (1973) Investigation of glial cells in semithin sections. III. Transformation of subependymal cells into glial cells as shown by radio-autography after H^3-thymidine injection into the lateral ventricle of the brain of young rats. *J. Comp. Neurol.,* **149,** 83.

Pelc, S.R. (1964) Labeling of DNA and cell division in so-called non-dividing tissues. *J. Cell Biol.,* **22,** 21.

Pendergrass, E.P., Hodes, P.J. Groff, R.A. (1940) Intercranial complications following irradiation for carcinoma of scalp. *Am. J. Roentgenol. Radium* **60,** 230.

Quastler, H. (1963) The analysis of cell population kinetics. *Cell Proliferation* (eds. L.F. Lamerton and R.J.M. Fry), Blackwell (Oxford), 18.

Quastler, H. (1960) cell population kinetics. *Ann. N.Y. Acad. Sci.*

90, 580.

Quastler, H., Sherman, F.G. (1959) Cell population kinetics in the intestinal epithelium of the mouse. *Exp. Cell Res.,* **17,** 420.

Rajewsky, M.F. (1965) In vitro studies of cell proliferation in tumours. *Eur. J. Cancer,* **1,** 281.

Raju, M.R., Johnson, T.S., Tokita, N., Carpenter, S., Jett, J.H. (1980) Differences in cell-cycle progression delays after exposure to 238 Pu Particles compared to X Rays. *Radiat. Res.,* **84,** 16.

Reichard, P. (1962) Enzymatic synthesis of deoxyribonucleotides. I. Formation of deoxycytidine diphosphate from cytidine diphosphate with enzymes from escherichia coli. *J. Biol Chem.,* **237,** 3513.

Richmond, C.R., Langham, W.H., Trujillo, T.T. (1962) Comparative metabolism of triated water by mammals. *J. cell comp. Physiol.,* **59,** 45.

Rosenthal, F., Timiras, P.S. (1961) Changes in brain excitability after whole-body X-irradiation in the rat. *Radiat. Res.,* **12,** 710.

Rubin, P., Casarett, G.W. (1968) Haemopoietic tissues and blood. *Clinical Radiation Pathology,* II Saunders and Company (Philadelphia), 778.

Rydberg, E. (1932) Cerebral injury in newborn children consequent on birth trauma; with an enquiry into the normal and pathological anatomy of the

neuroglia. *Acta Path. Microbiol. Scan., Suppl.*, **10,** 1.

Schlag, H., Luecke-Huhle, C. (1981) The influence of ionization density on the DNA synthetic phase and survival of irradiated mammalian cells *Int. J. Radiat. Biol.*, **40,** 75.

Schneider, D.O., and Whitmore, GF (1963) Comparative effects of neutrons and X-rays on mammalian cells. *Radiat. Res.*, **18,** 286.

Scholz, W., Hsu, Y.K., (1938) Late damage from roentgen irradiation of human brain. *Arch. Neurol. Psychiat.*, **40,** 928.

Schultze, B., Korr, H. (1981) Cell kinetic studies of different cell types in the developing and adult brain of the rat and the mouse: A review. *Cell Tissue Kinet.*, **14,** 309.

Shimada, M. (1966) Cytokinetics and histogenesis of early postnatal mouse brain and its cell production as studied by H^3-thymidine autoradiography. *Arch. Histol. Japan,* **26,** 413.

Smart, I. (1961) The subependymal layer of the mouse brain and its cell production as shown by radioautography after H^3-thymidine injection. *J. Comp. Neur.*, **16,** 325.

Smart, I., Leblond, C.P. (1961) Evidence for division and transformations of neuroglia cells in the mouse brain as derived from autoradiography after

injection of H^3-thymidine. *J. Comp. Neur.*, **116,** 349.

Steel, G.G. (1977) *Growth Kinetics of Tumours,* Oxford Univ. Press, Oxford.

Steel, G.G. (1966) Delayed uptake by tumours of tritium from thymidine. *Nature (London),* **210,** 806.

Steel, G.G., Hanes, S. (1971) The technique of labeled mitoses: Analysis by automatic curve-fitting. *Cell Tissue Kinet.*, **4,** 93.

Storer, J.B., Harris, P.S., Furchner, J.E., Langham, W.H. (1957) The relative biological effectiveness of various ionizing radiations in mammalian systems. *Radiat. Res.*, **6,** 188.

Takahashi, M. (1968) Theoretical basis for cell cycle analysis: Further studies on labeled mitosis wave method. *J. Theor. Biol.*, **18,** 195.

Takahashi, M., Hogg, G.D., Mendelsohn, M.L. (1971) The automatic analysis of PLM curves *Cell Tissue Kinet.*, **11,** 119.

Taylor, J.H., Woods, P.S., Hughes, W.L. (1957) The organization and duplication of chromosomes using tritium-labeled thymidine. *Proc. Natn. Acad, Sci.*, **43,** 122.

Terasima, T., Tolmach, L.J. (1963) Variations in several responses of HeLa cells to X-irradiation during the division cycle. *Biophys. J.*, **3,** 11.

Tiller-Borcich, J., Fike, J.R., Phillips, T.L., Davis, R.L. (1987) Pathology of

delayed radiation brain damage: An experimental canine model. *Radiat. Res.*, **110,** 161.

Tobias, C.A. (1973) Pretherapeutic investigations with accelerated heavy ions. *Radiology (Easton, Pa.),* **108,** 145.

Tobias, C.A., Todd, P.W. (1967) Heavy charged particles in cancer therapy. *Natl. Cancer Inst. Monogr.*, **24,** 1.

Tobias, C.A., Lyman, J.T., Lawrence, J.H. (1971) Some considerations of physical and biological factors in radiotherapy with high-LET radiations including heavy particles, Pi mesons, and fast neutrons. *Prog. At. Med.*, **3,** 167.

Tobias, C.A., Alpen, E.L., Blakely, E.A., Castro, J.R., Chatterjee, A., Chen, G.T.Y., Curtis, S.B., Howard, J., Lyman, J.T., Ngo, F.Q.H. (1979) Radiobiological basis for heavy ion therapy. In: *Treatment of Radioresistant Cancers* (eds. R.A. Meyn and H.R. Withers), Am. Elsevier (New York), 195.

Trucco, E., Brockwell, P.J. (1968) Percentage labelled mitoses curves in exponentially growing cell populations. *J. theor. Biol.*, **20,** 321.

Vogel, F.S., Hoak, C.G., Sloper, J.C., Haymaker, W., (1958) The induction of acute morphological changes in the central nervous system and pituitary body of macaque monkeys by cobalt 60 (gamma) radiation. *J. Neuropathol.*

Exptl. Neurol., **17**, 138.

Wender, M., Kozik, M., Mialarek, O., Ozarzewska, E. (1974) Incorporation of H_3-thymidine into neuroglial cells in the course of myelinogenesis. *Folia Histochem. Cytochem.*, **12**, 115.

Willis, P., Berry, M., Riches, A.C. (1976) Effects of trauma on cell production in the subependymal layer of the rat neocortex. *Neuropath. Applied Neurobiol.*, **2**, 337.

Wilson, R.R. (1946) Radiological use of fast protons. *Radiology*, **47**, 487.

Zeman, W. (1965) Pathogenesis of radiolesions in the mature cns. *Excerpta Med. Int. Congress*, **100**, 302.

Zeman, W., Samorajski, T. (1971) Effects of irradiation on the nervous system. *Pathology of Irradiation* (ed. C.C. Berdjis), Williams and Wilkins (Baltimore), 213.

Zeman, W., Curtis, H.J., Baker, C.P. (1961) Histopathologic effect of high-energy-particle microbeams on the visual cortex of the mouse brain. *Radiat. Res.*, **15**, 496.

Zeman, W,. Curtis, J.H., Gebhard, K.L., Haymaker, W. (1959) Tolerance of mouse brain tissue to high-energy deuterons. *Science*, **130**, 1760.

Appendix A

Characteristics of Heavy Charged Particle Radiation

A.1 Rationale for the use of heavy charged particle irradiations in radiotherapy

A fundamental understanding of the effects of high-energy heavy ions on normal tissues is critical to the intention of using accelerated heavy ions in radiotherapy. Normal tissues are necessarily, always, included in the radiation treatment volume, and so an understanding of the early and late effects of high linear energy transfer (LET) radiations on these tissues is clearly important. Different cellular populations may be involved in these responses, and it is the late sequelae which may ultimately determine the clinical effeciency of these particles.

The rationale for the use of accelerated heavy charged particles, first proposed by Wilson (1946) is similar to that proposed for other types of high LET radiations (Tobias and Todd, 1967; Tobias, 1973 ; Tobias et al., 1979). The physical and biological considerations are summarized below:

1) Physical characteristics of heavy particles are unique by virtue of their depth-dose profiles. An increased physical dose is deposited at depth in the tissue as compared to the plateau region of ionization. The tumor volume can thus be located at the Bragg Peak, and the normal tissues located in the plateau region would receive a smaller physical dose of irradiation.

2) Biological advantages provided by the increase in the relative biological effectiveness (RBE) of the heavy ion beam (Tobias et al., 1971, 1979).

3) The additional advantage of enhanced biological killing of hypoxic cells by high linear energy transfer (LET) particle beams was suggested by Tobias and Todd (1967).

3) Reduction in the influence of cell age in responses (Bird and Burki, 1975; Hall et al., 1977), and production of potentially exploitable perturbations in cellular kinetics (Lucke-Huhle et al., 1979).

5) The possibility that some tumor systems which are aneuploid and hyperploid may be more sensitive than normal diploid cells to high LET particle irradiation (Tobias et al., 1979).

There are important additional physical factors which must be assessed as these factors modulate the nature of the biological responses (Castro and Quivey, 1977). These are; 1) The incident energy of the heavy ion beam (i.e., 425 versus 557 MeV/amu) which will determine the total range in tissue and also be of importance in the contribution to the total dose in terms of secondary fragments. 2) The heavy ion beams are not used as pristine beams (Blakely et al., 1979). The width of these spread beams will vary and as a result, the dose, LET distributions, and RBE values will vary across these peaks. 3) Position of the target in the heavy ion beam. The biological responses must be evaluated both in the plateau ionization region of the heavy ion beam, and in the spread Bragg peak region of ionization. The description of the peak-to-plateau RBE

ratios are of importance, as this ratio will define the biological response of the tumor tissue to the response of the intervening normal tissues, which may be dose limiting. Thus, the biological response is complicated by, and dependent on, the choice of heavy ion, energy, extent of spreading of the Bragg peak, and the position of the target in the depth dose pattern of the heavy ion beam. These effects will all modulate the effective LET at the target and will all be reflected in the observed RBE values.

A.2 Relative biological effectiveness (RBE)

When living cells and tissues are exposed to different types of ionizing radiations, the absorbed dose of each type which is required to produce an equal biological response usually differs. The differences encountered are considered characteristic of the radiations and are an indication of their relative biological effectiveness, or RBE. In practice, the RBE is a measure of the extent to which one type of radiation is more or less effective compared to another type which is chosen as a reference (usually 250 kVp X-rays). The RBE is an experimental value and may be defined as the ratio of the dose of the reference radiation required to produce a specific biological effect to the dose of the experimental radiation required to produce the same effect. In other words:

$$\text{RBE} = \frac{\text{Dose of reference radiation required for effect}}{\text{Dose of experimental radiation required for equal effect}} \quad (5\text{-}1)$$

In experimental determinations of RBE of a given radiation, orthovoltage X-rays or Co^{60} gamma rays are used as the reference radiation; 250 kVp is usually

assigned a value of unity.

A.3 Linear energy transfer (LET)

Linear energy transfer (LET) is a physical parameter characteristic of the ionizing radiation under study. LET is a measure of the mean rate of energy deposited locally along the linear track of a charged particle by electromagnetic interactions. The parameter is refered to as LET_{∞} when all energy transfers up to the highest energy δ rays or knock-on electrons that are kinematically possible are included.

LET values increase as charged particles are slowed down in matter. Because at any depth of particle range there is a mixture of primary and secondary particles with different energies, the spectrum of LET can be quite broad and does not necessarily follow a Gaussian distribution. This is most significant at the Bragg ionization peak. The function D(L), where L is the LET, can be defined such that the absorbed dose, D, is given by:

$$D = D(L)dL = 2.3 \quad LD(L)d(\log L) \qquad (5\text{-}2)$$

D is measured in Gray (Gy). D(L) has the units of 0.01 Gy.g/MeV cm^2 with L in units of MeV cm^2/g.

A.4 Heavy-ion beam geometry

Four heavy-ion beams at the Lawrence Berkeley Laboratory's 184-inch Synchrocyclotron and the Bevalac which are being used in biomedical research, are those of helium (230 MeV/amu),carbon (400 MeV/amu), neon (425 MeV/amu

and 557 MeV/amu) and argon (570 MeV/amu)ions. The helium and neon (425 MeV/amu) ion beams were used for these studies on the subependymal cell population in the mouse brain.

The pattern of energy deposition as the charged particles pass through matter, produces a characteristic pattern of energy or dose distribution within the matter which is called the Bragg ionization curve. The most important energy loss process occurring in a beam of charged particles is caused by electromagnetic interaction with the target molecules (Bichsel, 1968). This energy loss phenomenon is quantitatively described by the well known Bethe stopping power formula (1930). The Bragg curves for the unmodified helium, neon, carbon and argon ion beams (Lyman and Howard, 1977b) are illustrated in Fig. 34. The plateau region of the Bragg ionization curve was used for all the irradiations in this study. Beam monitoring of data for biological and medical heavy-ion irradiations is based on thin-foiled parallel-plate ion chambers filled with pure nitrogen gas. Bragg curve ionization measurements are made with a pair of ion chambers using an interposed variable absorber (Lyman and Howard, 1977; Alonso et al., 1980). In this study the dose was determined by calibration of the transmission chambers with a tissue-equivalent (TE) ionization chamber located at the isocenter of the patient positioner (Lyman et. al., 1986). The 184-inch Synchrocyclotron at LBL has been used extensively for investigation of effects of helium ions on various normal tissues (Leith et al. 1975a).

Mean grain count decrements in the subependymal layer of the unirradiated and irradiated mice (48 hr after exposure to 45 Gy He (230 Me/amu))

```
 MOUSE 1; LEFT CORTEX IRRADIATED 45 GY HE
 SRS> ass file11.dat for001   IRRADIATED CORTEX
 SRS> run avh1
 enter animal number
 1
   n=          45 av=    29.51111      var=    216.3010     sigma=
   14.70718
  file no. = 1
   20  29  16  16  35  16  20  89  13  30  40  10  24  27  39  10  17  23
   30  20  15  17  23  36  27  49  40  25  11  17  48  46  41  40  52  32
   24  34  38  35  36  51  25  22  20
SRS> ass file1r.dat for001 UNIRRADIATED CORTEX
SRS> run avh1
enter animal number
1
  n=          76 av=    34.26316      var=    189.7166     sigma=
  13.77376
 file no. = 1
   65  31  25  35  57  35  25  28  16  20  12  30  57  25  44  33  39  41
   63  31  54  33  39  40  28  57  59  26  60  37  59  44  47  20  19  27
   37  50  36  27  27  29  38  53  39  11  25  26  23  20  18  30  32  34
   48  27  49  48  30  16  17  11  16  17  20  24  26  32  12  28  41  51
   45  43  46  41
MOUSE 5; CONTROL
SRS> ass file51.dat for001
SRS> run avh1
enter animal number
5
  n=         538 av=    23.88662      var=    72.27572     sigma=
  8.501513
 file no. = 5
   20  12   9  33  29  15  34  29  35  18  10  16  18  20  37  24  29  20
   18  19  25  11  15  23  12  13  22  16   8  10  14  33  15  21  17  12
   10  23  21  17   8  24  25  26  31  17   7  16  13  24  12  20  16  16
   22  19  16  12  11  16  18  14  19  18  19  17  46  21   9  17  24  23
   17  15  20  23  22  11  22  16  18   8  22  24  27  16  18  23  25  16
   16  15  23  13  17  17  13   9  13  12  23  11  17  21  13  12  19  12
   10  15  14  13  15  12  16  16  13  26  20  18  13  15  18  19  11  17
   14  15  30  16  14  18  16  17  16  21   9  14   8  22  16  20  12  35
   28  23  28  18   9  18  24  19  16  20  27  18  11  24  18  17  18  24
   25  20  36  28  25  26  23  36  14  14  21  23  17  19  15  35  19  23
   29  17  17  18  15  27  30  26  22  17  30  24  18  35  19  51  28  20
   27  22  18  23  30  21  16  19  12  24  20  16  24  14  17  25  33  21
   24  24  24  17  19  43  26  24  22  23  21  24  28  26  26  28  22  24
   19  16  20  17  25  26  24  26  40  31  23  32  43  28  21  17  20  25
   16  18  19  16  20  17  20  19  24  28  23  20  20  22  13  19  20  25
   16  23  22  19  37  28  22  24  22  28  23  24  21  19  19  22  23  23
   26  21  29  22  20  24  23  29  26  22  27  17  26  22  16  20  21  25
   28  23  24  15  29  18  22  24  35  24  14  18  24  29  35  40  22  26
   25  15  28  16  26  30  21  16  29  30  21  16  29  30  48  39  37  59
   42  31  39  40  23  39  16  28  42  27  32  26  18  49  23  22  23  17
   30  25  40  38  37  39  42  30  23  24  16  25  15  19  20  28  21  18
   20  26  37  36  31  20  19  28  21  25  21  21  13  41  29  26  27  33
   37  41  37  22  23  26  39  35  31  29  35  34  34  25  42  31  28  27
   19  27  29  29  21  28  19  17  37  16  25  24  32  25  23  46  23  50
```

```
   27  17  26  20  15  40  47  20  18  37  16  16  16  31  17  32  47  28
   20  15  43  42  33  38  31  29  27  31  32  31  34  39  37  30  27  33
   34  31  30  42  42  25  26  12  21  27  32  25  18  38  14  38  28  25
   40  37  42  30  27  27  39  43  31  30  26  18  25  29  33  22  26  20
   30  32  24  37  29  31  32  23  29  24  20  25  27  45  28  17  21  28
   28  46  30  31  14  13  24  23  27  22  23  25  21  37  40  34
MOUSE 8; LEFT CORTEX IRRADIATED 45 GY HE
SRS> ass file8l.dat for001 IRRADIATED CORTEX
SRS> run avh1
enter animal number
8
  n=           6 av=    27.16667      var=    70.96670     sigma=
  8.424173
 file no. = 8
   18  23  33  41  22  26
SRS> ass file8r.dat for001 UNIRRADIATED CORTEX
SRS> run avh1
enter animal number
8
  n=         263 av=    23.90114      var=    68.15047     sigma=
  8.255329
 file no. = 8
   17  15  22  31  17  31  33  30  28  32  30  25  29  32  39  34  33  15
   31  32  26  29  29  17  40  26  19  20  28  30  25  27  20  19  20  18
   15  14  18  36  31  24  20  27  17  16  18  29  32  18  16  23  21  23
   19  22  33  18  28  25  30  16  16  21  18  18  20  18  16  43  36  20
   22  51  31  13  14  21  20  18  25  20  40  27  10  22  20  16  13  20
   24  15  17  36  23  41  27  17  35  23  29  24  27  13  15  19  24  18
   26  22  23  46  44  38  16  29  12  36  22  27  29  18  26  24  27  27
   22  21  37  54  23  25  16  33  33  61  25  38  17  27  32  33  18  16
   19  18  39  20  28  24  27  26  21  30  23  39  30  19  32  14  18  10
   13  26  22   9  26  23  21  26  26  26  24  26   9  17  23  16  39  14
   24  28  28  25  31  32  20  27  19  26  17  22  17  16  13  11  23  18
   21  31  26  24  12  12  13  27  18  22  20  16  26  16  18  15  21  33
   17  29  16  12  31  25  26  20  24  17  24  20  19  19  13  27  16  34
   26  21  22  43  24  17  14  17  15  17  14  14  33  28  25  26  50  21
   40  21  22  15  23  23  15  34  27  25  17
MOUSE 7; LEFT CORTEX IRRADIATED 45 GY HE
SRS> ass file7l.dat for001 IRRADIATED CORTEX
SRS> ass file7l.dat for001
SRS> run avh1
enter animal number
7
  n=          21 av=    26.90476      var=    55.29048     sigma=
  7.435757
 file no. = 7
   45  33  16  35  23  23  34  27  21  23  18  24  26  20  34  29  26  32
   29  14  33
SRS> ass file7r.dat for001 UNIRRADIATED CORTEX
SRS> ass file7r.dat for001
SRS> run avh1
enter animal number
7
  n=         155 av=    29.10323      var=    124.5737     sigma=
  11.16126
```

```
 file no. = 7
   21  30  21  30  23  29  32  34  34  33  21  27  25  24  27  24  20  24
   47  32  32  25  23  27  20  28  16  20  15  31  31  22  22  15  17  23
   25  43  31  30  22  19  16  17  20  21  31  28  27  31  25  19  18  38
   19  35  39  14  31  40  11  16  26  34  17  15  21  36  32  31  36  47
   59  33  81  25  21  45  15  31  42  31  27  11  45  21  27  44  22  39
   26  39  15  82  47  19  36  30  34  36  31  25  25  42  29  26  29  34
   27  32  39  46  28  44  31  31  30  26  27  16  21  37  61  31  38  26
   29  15  28  18  19  13  20  28  38  28  33  25  29  18  25  42  57  17
   53  29  29  29  22  23  22  32  25  30  34
MOUSE 10; CONTROL
SRS> ass file10l.dat for001
SRS> run avh1
enter animal number
10
  n=          169 av=    17.76923      var=    29.90479      sigma=
  5.468527
 file no. = 10
   21  13  11  22  14  16  13   8  19  14  23  21  26  10  16  17  12  11
   15  27  13  18  17  10  17  13  14  14  23  13  13  13  10  13  20  13
   14  10  21  18  24  31  29  19  17  28   9  20  16  27  31  20  14  16
   19  21  20  14  13  12   9  14  16  12  15  16  13  33   9  19  17  20
   20  20  17  21  27  18  12  20  28  21  20  17  14  17  13  22  16  20
   21  13  22  16  20  21  18  19  12  22  21  27  26  16  23  23  30  25
   16  16  26  30  13  23  21  24  23  26  18  14   9  26  12  22  25  19
   11  19  22  31  25  20  20  10  21  20  14  17  14  31  15  10  11  11
   12  14  15  13  20  17  21  16  19  14  11  16  13  16  18  18  10  15
   14  15  15  13  17  14  15
SRS> ass file10r.dat for001
SRS> run avh1
enter animal number
10
  n=          170 av=    17.95882      var=    30.00418      sigma=
  5.477607
 file no. = 10
   26  16  19  28  20  18  14  21  14  17  25  19  15  22  15  17  15  17
   19  19  23  13  22  21  18  29  26  18  25  26  21  20  25  15  17  15
   13  18  22  14  26  19  15  15  20  15  20  20  14  20  33  21  12  33
   16  20  14  13  11  35  14  17  15  20  11  23   9  17  16  20  15  15
   16  13  14  29  12   9  17  15  14  18  14  22  17  18  21  32  16  17
   16  17  29  13  14  35  10  20  19  11  18  14  19  12   8  14   8  12
   18  12  16  16  36  18  14  14  15  21  18  19  16  19  20  15  14  22
   28  12  18  15  18  27  18  27  19  16  32  20  18  15  22  22  19  15
   12  11  10  17  10  17  12  15  17  16  17  17  16  21  13  13  23  21
   16  23  15  11  13   9  19  21
MOUSE 13; RIGHT CORTEX IRRADIATED 45 GY HE
SRS> ass file13l.dat for001 UNIRRADIATED CORTEX
SRS> run avh1
enter animal number
13
  n=          195 av=    19.24615      var=    47.74319      sigma=
  6.909645
 file no. = 13
   21  13  19  22  15  21  12  11  17  18  19  14  11  25  17  19  37  20
   13  17  18  13  15  20  24  28  19  11  21  13  19  20  23  16  10  17
```

```
  11  13  13  37  26  13  10  10  12  19  25  21  21  19  13  16  22  18
  12  20  26  29  15  24  13  24  12  18  15  24  16  12  15  11  13  31
  25  19  21  17  24  25  11  21  16  17  16  18  22  10  20  16  26  16
  17  47  21  17  37  18  12  20  23  15  12  17  29  13  18  29  12  13
  14  30  24  21  13  24  24  23  16  22  20  10  21  21  30  23  24  26
  17  14  19  17  14  14  17  38  25  28  19  25  13  14  30  22  26  19
  17  31   9  23  38  15  27  13  32  26  26  12  15  14   9  12  10   7
  28  12  26  14  11  20  19  24  21  25  23  39  14  17  14  16  33  33
  13  21  21  25  25   6  12  15  18  29  22  10  20  15  12
SRS> ass file13r.dat for001 IRRADIATED CORTEX
SRS> run avh1
enter animal number
13
  n=          24 av=    15.45833      var=    73.65037     sigma=
  8.581979
 file no. = 13
  16  22  10  29  38  20  13  20  11   9  34  21  10  12  11  11  20  10
  16   7   8   9   6   8
MOUSE 17; CONTROL
SRS> ass file17l.dat for001
SRS> run avh1
enter animal number
17
  n=         307 av=    17.81759      var=    43.84901     sigma=
  6.621859
 file no. = 17
  31  33  27  16  25  15  22  26  20  11  11  15  19  14  17  15  24  16
  27  25  24  21  15  18  16  13  20  17  12  14  26  11  15  15  16  28
  28  16  11  12  24  18  32  17  23  16  10  17  24  20  16  20  12   9
  13  17  22  20  24  27  25  30  18  19   8  12  19  17  31  19  18  15
  11  12  16  16  25  22  18  13  13  12  14  16  12  22  20  23  25  13
  15  14  11  18  17   7   8  14  14  12  17  11  12   9  12  14  21  13
  15  14  15  22  22  13  12  19  19  22  18  21  17  16  13  12  24  11
  15  14  24  13  12  13  12  14  11  14  13  20  24  13  16  11  22  21
  22  22  18  14  13  16  16  15  32  26  15  16  17  13  16  21   8  14
  14  12  12  11  28  11   9  37  15  17  27  14  15  18  18   9  12  18
  17  11  17  21  10  14  14  17  15  10  21  16  17  14  14  16  11  17
  26  13  12  29  23  16  18  27  19  17  11   8  14   7  17  14  12  12
  14  27  25  19  14  18  13  11  18   9  13  21  11  17  13  13  19  22
  15  12  18  36  42  21  25  31  10  11  11  28  16  18  17  28  25  34
  21  30  16  17  16  11  14  12   9  11  10  22  13  14  17  17   9  16
  25  16  16  18  20  13  23  21  17  28  25  44  17  18  20  21  31  26
   9  18  13  17  20  14  17  33  22  20  29  13  20  17  49  45  17  24
  28
SRS> ass file17r.dat for001
SRS> run avh1
enter animal number
17
  n=         172 av=    20.84884      var=    62.53842     sigma=
  7.908124
 file no. = 17
  17  17  17  21  33  17  19  16  20  14  18  20   9   9  15  22  15  19
  17  17  18  32  16  39  20  15  29  13  29  12  34  28  38  41  22  29
  27  20  17  17  12  33  24  15  12   9  23  40  14  18  18  32  18  17
  22  34  18  17  12  10  16  35  35  22  27  33  13  26  15  27  11  42
```

```
   20  19   9  16  21  21  25  15  16  17  31  34  32  15  29  14  19  15
   15  15  29  23  23  14  26  24  14  14  25  26  23  13  19  12  21  19
   19  13  24  19  19  19  18  19  29  20  15  18  21  27  20  23  29  31
   14  32  21  20  15  32  19  22  21  13  49  15  38  27  25  29  11  19
   21  18  10  13  15  26  16  14  16  15  15  21  26  19  25   9  21  22
   33  12  15  13  11   7   7  36  36  18
MOUSE 20; RIGHT CORTEX IRRADIATED
SRS> ass file201.dat for001 UNIRRADIATED CORTEX
SRS> run avh1
enter animal number
20
  n=          359 av=    23.19499      var=    207.8166     sigma=
  14.41585
 file no. = 20
   44  15  54  14  25  18  43  13  16  15  29  30   6  27  96  38  11  27
   18  37  10  17  35  20  74  10  17  14  16  45  13  29  94  40  25  29
   24  23  11  43  28   9  14  77  21  20  12  10  24  13  15   6  14  13
    7   9   9   8  11   7   7   3  11   9  27  14  10   6   8  18  20  19
   12   7  12  13  35  31  14  15   8  11  11  22  47  25  21  11  10  35
   23  16  25  18  20  15  24  15  17   5  17  25  52  49  43  14  14  26
   18  55  45  29  13  17  38  23  12  32  12  12  11  39  57  31  10  25
   35  29  39  25  20  19  10  13  26  12  19  19  13  12  47  11  14  23
   14  16  20  19  16   9  16  11   8  19  27  26  10  16  25  17  14   8
   13  11  10   8  18  14  19   8  24  29   6  15  10  13   8  10  20  33
   15  17  60  13  14  11  12   9  36  11  20  21  15  17  20  19  62  20
   24  37  29  34  12  25  15  46  26  12  11  16  18  19  13  19  28  15
   30  34  46  20  19  18  12   7  21  20  10  20  22  13  24  27  25  20
   35  31  31   8  14  24  30  27  37  91  29  35  23  30  22  17  18  20
   15  23  33  16  16  10  17  12  15  23  14  18  25  22  34  21  21  19
   25  18  16  74  13  73  30  23  23  26  25  71  18  23  15  49  34  18
   19  39  20  46  59  27  37  36  17  50  24  19  18  75  40  51  21  17
   14  16  19  17  36  19  19  31  26  42  17  12  29  20  27  11  14  33
   30  29  32  22  19  22  30  32  21  36  29  32  17  19  33  12  13  32
   34  18  26  20  25  38  18  56  31  18  13  15  17  14  13  18  20
SRS> ass file20r.dat for001 IRRADIATED CORTEX
SRS> run avh1
enter animal number
20
  n=           25 av=    27.76000      var=    471.0233     sigma=
  21.70307
 file no. = 20
   38  32  16   5  28  42  41  27  28  35  59  25  17  14  18  11  10  16
   40  14  66  96   6   7   3
MOUSE 23; CONTROL
SRS> ass file231.dat for001
SRS> run avh1
enter animal number
23
  n=          519 av=    18.97881      var=    45.96673     sigma=
  6.779877
 file no. = 23
   25  17   8  26  13  15  13  25  20  14  14  17  16  13  18   8  19  12
   16  32  18  17  27  13  20  14  18  17  23  21  15  14  17  20  18  17
   35  14  23  26  12  20  36  24  22  13  33  23  30  16  17  25  11  14
   21  17  16  23  18  15  18  19  16  16  10  27  10  19  16  12  25  39
```

```
   11  20  13  19   8  12  25   8  14  16  24  10  11  15  22  24  13  14
   17  15  13  19  23  26  19  10  25  17  27  20  18  14  14  19  12  12
   12  11  12  16  18  14   9  12  10  13  24  16  20  21  13  12  18  15
   27  18  39  20  40  36  39  28  13  22  38  16  41  16  18  16  20  18
   23  21  13  16  14  13  12  22  11  32  25  23  19  39  50  22  23  38
   27  20  21  33  28  15  23  31  14  17  15  14  22  29  25  24  15  11
   20  11  17  20  21  15  23  32  29  15  17  16  10  20  21  17  22  23
   16  28  43  10  19  20  18  29  18  14  19  17  17  22  11  30  12  14
   19  13  14  13  33  21  20  11   9  12  22  19  20  30  12  23  13  14
   12  14  12  19  12  16  17  25  14  18  11  10  23  24  18  15  10  15
   10  15  25  28  25  16  39  24  21  16  15  16  25  21  18  19  12  21
   25  12  15  15  20  22  11  11  13  26  12  16  17  34  18  16  17  34
   18  16  17  20  22  19  11  16  16  15  17  16  12  38  17  18  16  27
   20  18  10  15  26  36  21  22  20  23  15  17  26  33  15  34  16  12
   11  14  11  18  10  14  14  21  27  13  16  18  16  16  31  12  16  23
   18  26  11  12  16  15  23  23  28  27  24  25  12  13  18  17  16  35
   11  13  20  21  10  12  10  16  16  15  17  13  28  15  20  18  12  21
   15  15  16  19  24  19  14  18  18  17  18  12  17  25  22  16  16  23
   20  14  12  12  21  17  21  19  15  16  25  17  22  20  16  12  14  12
   22  27  16  15  16  28  21  16  16  30  37  22  17  40  17  20  11  22
   25  15  17  19  16  21  16  22  19  21  14  27  20  14  18  14  16  16
   14  16  12  24  22  14  37  19  26  26  20   8   9  28  17  19  15  20
   16  12  25  14  15  26  15  42  25  15  22  23  21  27  11  35  21  20
   13  16  18  42  19  16  18  22  17  17  24  15  20  16  18  14  26  15
   15  17  28  14  15  20  16  16  14  19  17  16  16  23  17
MOUSE 27; LEFT CORTEX IRRADIATED 45 GY HE
SRS> ass file27l.dat for001 IRRADIATED CORTEX
SRS> run avh1
enter animal number
27
  n=          20 av=    16.20000      var=    216.1684      sigma=
  14.70267
 file no. = 27
   11  10  11  11  10  11  16  13  14  30  10  11   7  16   7   6  11   7
   49  63
SRS> ass file27r.dat for001 UNIRRADIATED CORTEX
SRS> run avh1
enter animal number
27
  n=          80 av=    17.01250      var=    81.32894      sigma=
  9.018256
 file no. = 27
   14  15  12  13  17  22  15   7  20  10  22  18   8   6   7  21  11  16
   22  15   8   7  12  11   8  40  24  28  10  11  11  15  15  20  14   9
   11  11  10  11  15  14  11  19  34  12  12  15  14  13  27  13  16  13
   21  25   9  10  22  11   7  12  48  16  23  16  31  29  18  27  10  24
   18  32  10  13  21  51  14  38
MOUSE 30; CONTROL
SRS> ass file30l.dat for001
SRS> run avh1
enter animal number
30
  n=         475 av=    20.42947      var=    59.49871      sigma=
  7.713541
 file no. = 30
```